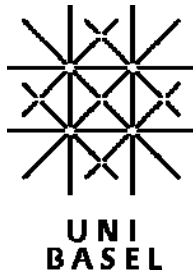


Template directed synthesis of highly organized functional biomimetic silica nanostructures



Inauguraldissertation

zur

Erlangung der Würde eines Doktors der Philosophie

vorgelegt der

Philosophisch-Naturwissenschaftlichen Fakultät

der Universität Basel

von

Lucy Kind

aus Duisburg/ Deutschland

Basel/ 2009

Genehmigt von der Philosophisch-Naturwissenschaftlichen Fakultät
auf Antrag von

Prof. Dr. Wolfgang Meier
Prof. Dr. Uwe Pieles
Prof. Dr. Andreas Taubert

Basel, den 24. März 2009

Prof. Dr. Eberhard Parlow
Dekan

to André

Table of Content

1	Abstract	5
2	Introduction	7
3	Objectives	11
4	General Synthetic Strategy	14
4.1	Polymeric templates	16
4.1.1	Basic principles of polymers and self-assembled structures.....	16
4.1.2	Functional requirements of the polymeric templates	19
4.1.2.1	<i>Polyamine / silica systems</i>	19
4.1.3	Star-shaped PDMAEMA and PMETAI polymers	21
4.1.3.1	<i>Synthesis of star-shaped polymers</i>	23
4.1.4	Block copolymers PEI-b-PEG.....	24
4.2	Silica shell formation process	25
4.2.1	Sol-gel synthesis	27
4.2.2	Sol-gel process in microemulsions	28
4.3	Potential compounds for encapsulating and entrapping in polymer/silica systems .	29
4.4	Chemically functionalized silica matrix	30
4.4.1	Non-functionalized silica shell surface.....	30
5	Results and Discussion	32
5.1	Polymeric templates	32
5.1.1	Star shaped polymers (PDMAEMA and PMETAI).....	32
5.1.1.1	<i>Structure and characteristics of the star shaped polymers</i>	32
5.1.2	Self-assembled structures from linear PEI-b-PEG block copolymer	34
5.2	Silica shell	36
5.2.1	PDMAEMA / and PMETAI / silica system.....	36
5.2.1.1	<i>Structure of the polymer/silica systems after silicification</i>	36
5.2.1.2	<i>Formation mechanism and growth process of the particles</i>	42
5.2.2	PEI-b-PEG / silica system	47

5.3	Star-shaped polymer/silica nanoparticles as trapping and carrier systems.....	48
5.3.1	PDMAEMA / and PMETA / silica systems	48
5.3.1.1	<i>Encapsulation of the fluorescent dye sulforhodamine G</i>	<i>48</i>
5.3.1.2	<i>Trapping of metal complexes in the polymer/silica nanoparticles.....</i>	<i>52</i>
5.3.1.3	<i>Trapping of hemoglobin in the polymer/silica nanoparticles</i>	<i>58</i>
5.3.1.4	<i>Activity test of the trapped hemoglobin in polymer/silica nanoparticles</i>	<i>63</i>
5.4	Silica surface functionalization	68
6	Conclusion and Outlook.....	70
7	Materials and Methods.....	72
7.1	Materials.....	72
7.2	Methods.....	73
7.2.1	Nanoparticle synthesis	73
7.2.1.1	<i>PDMAEMA and PMETA/silica nanoparticles.....</i>	<i>73</i>
7.2.1.2	<i>PEG-b-PEI/silica nanoparticles</i>	<i>74</i>
7.2.1.3	<i>SiO₂ nanoparticles from inverse microemulsion</i>	<i>74</i>
7.2.2	pH measurements.....	75
7.2.3	ζ-potential and size measurements.....	75
7.2.4	Atomic force microscopy (AFM)	75
7.2.5	Scanning electron microscopy (SEM)	75
7.2.6	Transmission electron microscopy (TEM)	76
7.2.7	Cryogenic transmission electron microscopy (cryo-TEM).....	76
7.2.8	3D transmission electron microscopy (3D-TEM)	76
7.2.9	Small angle X-ray scattering (SAXS).....	77
7.2.10	Fluorescence correlation spectroscopy (FCS).....	77
7.2.11	Electron paramagnetic resonance (EPR)	77
7.2.12	UV-Vis spectroscopy	78
8	Annex.....	79
8.1	Materials.....	79
8.1.1	Chemicals	79
9	References	80
10	Curriculum vitae.....	88

Abbreviations

AFM	atomic force microscopy
APTMS	(3-aminopropyl)-trimethoxysilane
ATRP	atom transfer radical polymerization
Cryo-TEM	cryogenic transmission electron microscopy
DLS	dynamic lightscattering
DMAEMA	2-(<i>N,N</i> -dimethylaminoethyl)methacrylate
DNA	deoxyribonucleic acid
EPR	electron paramagnetic resonance
6-FAM	5(6)-carboxyfluorescein N-hydroxysuccinimide ester
FCS	fluorescence correlation spectroscopy
Hem	hemoglobin
Hem-(6-FAM)	fluorescein-labeled hemoglobin
HEP	formerly denoted cell wall proteins of diatoms including frustulins and pleuralins
IEP	isoelectric point
IR	infrared spectroscopy
mPEG- <i>b</i> -PLA	methylether poly(ethylene glycol)- <i>block</i> -poly(lactic acid)
NMR	nuclear magnetic resonance spectroscopy
PDI	polydispersity index
PDMAEMA	poly(<i>N,N</i> -dimethylaminoethyl) methacrylate
PEG	poly(ethylene glycol)
PEI	poly(ethyleneimine)
PEI- <i>b</i> -PEG	poly(ethyleneimine)- <i>block</i> -poly(ethylene glycol)
PMEI	poly(<i>N</i> -methylethyleneimine)
PMETAI	poly[2-(methacryloyloxy)ethyl]trimethylammonium iodide
PMOXA	poly(2-methyl-2-oxazoline)
PMPI	poly(<i>N</i> -methylpropyleneimine)
PPI	poly(propyleneimine)
PS-PVP-PEO	poly(styrene- <i>block</i> -2-vinyl pyridine- <i>b</i> -ethylene oxide)
R_g	radius of gyration
RNA	ribonucleic acid
SAXS	small angle X-ray scattering
SDV	silica deposition vesicles
SEM	scanning electron microscopy
SLS	static lightscattering
STV	silica transport vesicles
TEM	transmission electron microscopy
TEOS	tetraethyl orthosilicate
TMOS	tertamethyl orthosilicate
UV-Vis	ultraviolet-visible spectroscopy

Acknowledgments

I would like to thank **Prof. Wolfgang Meier** for supervising my thesis and for giving me the encouragement, patience and freedom to find my way in research.

I thank **Prof. Uwe Piele**s for his trust in me and his engagement to support my work professionally and personally. He believed in me from the very beginning and I enjoyed the professional discussions as well as the reflections about my ideas and future plans.

I am also thankful to **Prof. Andreas Taubert** for guiding me during my thesis and for all his suggestions, criticisms and advices giving me the opportunity to develop creativity, strategies and ideas, which strengthened my ability to solve questions and difficulties.

I thank **Dr. Cornelia Palivan** for the fruitful discussions and help in the hemoglobin project.

Dr. Katarzyna Kita I would like to thank for the corrections and the tuning of my thesis. She was always present to help. (Thanks also to the coffee machine!)

I thank also **Dr. Alexandre Manton** for the instructive discussions and the good time in Berlin.

A big “thank you” also goes to **Elisabeth Barna**, who worked with me together in the collaboration with EMPA and became a very good friend.

I would like to thank **Prof. Axel Müller** and **Dr. Felix Plamper** for the material supply and the inspiration to follow this thesis.

I greatly benefited from the suggestion, support and assistance from my colleagues and the enjoyable atmosphere in the lab. Many thanks to all of you! This work would not have been possible without many previous and current lab members.

I would like to thank **Dr. Diana Sebök**, **Serena Belegri**nou and **Dr. Caroline Ailhas** for the girls-club-chats and for being real friends during snowy and sunny days inside and outside the lab; **Sven Kasper**, for his technical and personal support and the always present helping hand; **Thomas Schuster**, for the funny time and good handmade Bavarian dumplings. **Dr. Rainer Nehring**, for inspiring discussions in art and other topics; **Dr. Fabian Axthelm**, for always helping out; **Stefan Egli**, for being U.; **Dr. Ekaterina Rakhmatullina**, for helpful advice and the funny excursion to Alsace; **Mariusz Grzelakowski**, for always helping out like a gentleman.

It was also a pleasure to work with **Dr. Markus Dürrenberger**, **Vesna Olivieri** and **Ursula Sauter**, the good souls of the microscopy center.

Especially I would like to thank my family, **Ernst**, **Christel**, **Melanie**, **Matthias**, **Amélie** and my husband **André Kind**, for never ending patience and personal support they gave me during my PhD time and beyond it.

1 Abstract

Silica is an important mineral in technological and biological applications. Many protocols have been developed for the synthesis of complex silica architectures. Most prominent is the silicification approach, where polymers build up the templates for the revealed polymer/silica structures.

The current thesis demonstrates that star-shaped polymers and block copolymers are efficient templates for the fabrication of silica particles with spherical or raspberry-like morphology. The shape of the resulting particles depends on the pre-formed or self-assembled polymer structure and on the polymer chemistry.

In this work, we used two different templates: Star-shaped polymers were synthesized by polymerizing individual arms via ATRP from a silsesquioxane core (2–2.5 nm) as the connecting point. Those polymers build up star-like structures in solution. On the other hand, a linear diblock copolymer poly(ethyleneimine)-*b*-poly(ethylene glycol) (PEI-*b*-PEG) self-assembles into simple spherical aggregates.

PEI-*b*-PEG as well as the star-shaped polymer poly(*N,N*-dimethylaminoethyl methacrylate) (PDMAEMA), results in rather small spherical particles ($d = 20\text{--}30\text{nm}$) after silicification. The PDMAEMA/silica nanoparticles appear to have low electron density interior domains, resulting from the silsesquioxane core in a polymer-rich region. Furthermore, the silica particles synthesized using the star-shaped polymer template poly[2-(methacryloyloxy)ethyl] trimethylammonium iodide (PMETA) result in raspberry-like structures also with a low electron density core embedded in a silica layer and an average diameter of 50 nm. The external raspberry-bulbs investigated by electron microscopy and small-angle X-ray scattering (SAXS) exhibit the length of 10 nm. This leads to the assumption of individual polymer arms encapsulated in silica, since the number of bulbs is roughly related to the number of polymer chains connected to the silsesquioxane core.

As the amino groups of the polymers catalyze the hydrolysis and condensation reaction of the silicon alkoxide precursor TEOS, no additional catalysts are required e.g. ammonium hydroxide solution. The reaction can take place under ambient conditions compared to other silica nanoparticles production methods (Stöber method or microemulsion method), where solvents or surfactants are required. Time-resolved ζ -potential and pH measurements, dynamic light scattering, and electron

microscopy reveal that silica shell formation proceeds differently if PDMAEMA or PMETA are used as templates.

The ability to trap compounds by electrostatic interactions is an advantage of the star-shaped polymers. The encapsulation and trapping of the fluorescent dye sulforhodamine G can be monitored by fluorescence correlation spectroscopy (FCS) and confocal microscopy. Electron paramagnetic resonance spectroscopy (EPR) proves the trapping of the paramagnetic copper species $\text{Cu}(\text{OTf})_2$.

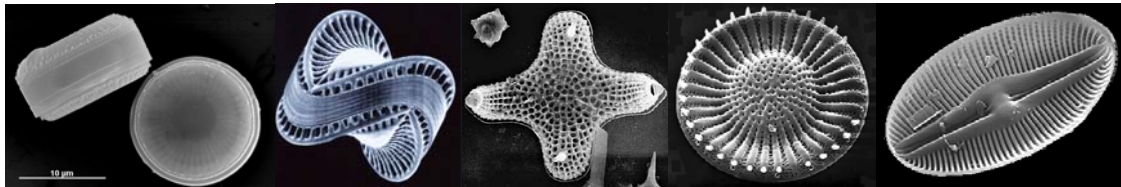
The process of encapsulating the protein hemoglobin can be monitored by FCS, after labeling with the fluorescent dye 5(6)-carboxyfluorescein N-hydroxysuccinimide ester (6-FAM). The UV-Vis measurements of hemoglobin trapped in the silica shell confirm that the activity of the protein towards CN^- and CO remains intact.

The definite encapsulation of hemoglobin and the protective shielding by the silica shell against digesting-enzymes can be monitored by UV-Vis spectroscopy. The enzyme trypsin digests only the accessible proteins, which are free in solution, on the silica surface, or not completely encapsulated.

To complete the multifunctional template-directed polymer/silica nanoparticles, surface functionalization of the silica shell can be performed by a post-synthetic step in a one-pot synthesis. This procedure implicates a facile approach to functionalize silica with amine groups, without any previous washing steps, which avoid unnecessary aggregation of particles before the functionalization step.

Jules Henri Poincaré (French mathematician 1854–1912)

The scientist does not study nature because it is useful; he studies it because he delights in it, and he delights in it because it is beautiful. If nature were not beautiful, it would not be worth knowing, and if nature were not worth knowing, life would not be worth living. Of course I do not here speak of that beauty which strikes the senses, the beauty of qualities and of appearance; not that I undervalue such beauty, far from it, but it has nothing to do with science; I mean that profounder beauty which comes from the harmonious order of the parts and which a pure intelligence can grasp.



*Cyclotella piltvicensis*¹

*Cyclotella*²

*Odontella*¹

*Cyclostephanus muelleri*³ *Diploneis puella*⁴

2 Introduction

Complex structures with a high degree of organization and symmetry are very common in nature from a macroscopic level to the molecular scale. Particularly beautiful examples of these organized structures are the silicified cell walls of diatoms (~1–500 μm in length).

Diatoms are unicellular algae that have the extraordinary capability to produce an enormous variety of intricate and ornate silicified structures. Their frustules consist of highly ordered amorphous hydrated silicon dioxide (biosilica) $[(\text{SiO}_2)_n (\text{H}_2\text{O})]$. There are more than 100,000 extant species estimated⁵ and each diatom species is characterized by its specific biosilica cell wall that contains regularly arranged slits or pores in the size range between 10 and 1000 nm. Diatoms can be split into two main groups depending on the symmetry of their frustules. Centric diatoms (Centrales) tend to be radially symmetric while pennate diatoms (Pennales) are bilaterally symmetric and tend to be elongated and generally have parallel striae arranged to the long axis (Figure 1). Therefore diatom frustules are one of the most outstanding examples of nanoscale-structured materials in nature.

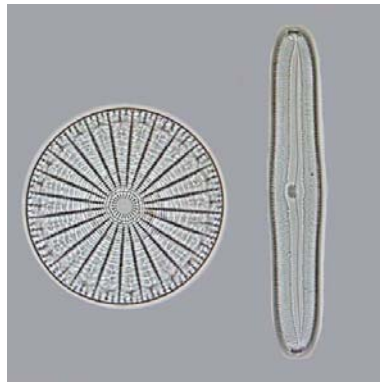


Figure 1: Centric and pennate diatoms ⁶

Apart from the representation of fascinating organized frustules, diatoms perform the task of providing a dominant fraction of biosilica to the environmental cycle. Biosilica is the second common mineral on earth (ca. 24×10^{12} mol per year) ⁷. Furthermore, as the most important group of eukaryotic phytoplankton, diatoms serve as the major source of nutrients for marine organisms. One important characteristic is that they are estimated to contribute to 20% of global CO₂ fixation which counts as a great ecological impact. Therefore they have been dubbed the “lungs of the earth” ^{8,9}.

Despite their beauty, usefulness, and environmental importance, their basic biology and the mechanism of building up their highly organized structure is still poorly understood. Biosilicification proceeds at ambient temperature and pressures, producing a diversity of nanostructured frameworks unlike the chemical synthesis of silica-based materials (resins, molecular sieves, and catalysts) which requires extremes of temperature, pressure and pH. Therefore the natural ornately-patterned silica structures are a source of inspiration for nanotechnologists, who dream of replicating artificially similar formations ¹⁰⁻¹³.

Researchers try to disclose the secret and suspect that the process of diatomic frustules formation is accompanied by the diffusion-limited precipitation of silica. Relatively small amorphous silica particles (~ 1 -10 nm in diameter) are carried by silica transport vesicles (STVs) to the periphery of the silica deposition vesicles (SDVs), where the particles diffuse until they adhere to the growing aggregates ¹⁴. These precipitating silica aggregates are precisely controlled by organic components within the diatom cell. It is known that organic molecules, that have been hypothesized to act as regulating molecules in biosilicification, are associated to amorphous silica in the diatom cell walls. Kröger et al. characterized this protein

composition of cell walls from the diatom *Cylindrotheca fusiformis* and extracted two main protein fractions: a high molecular mass protein family (HEPs) and a low molecular mass fraction with affinity to silica (silaffins)¹⁵. Silaffins are able to precipitate silica within seconds when added to freshly prepared solution of metastable silicic acid. As pointed out by Iler¹⁶, silica precipitation is caused by cationic and hydrogen-bonding polymers which is exactly the case in silaffins. They are polycationic molecules with a high proportion of hydroxylamino acids. Additionally, silaffins are covalently modified by oligo-*N*-methyl-propylamine units, found to catalyze silicic acid polymerization and silica flocculation¹⁷.

Based on this analysis, major research activities have started world wide, to investigate the mechanism of the formation of distinct frustules structures with the aim to mimic this process in laboratory^{18,19}.

The progress is still in its infancy, despite the first results showing the successful synthesis of simple spherical silica particles utilizing the silica depositing peptide silaffin 1A₁ and 1A₂ from *Cylindrotheca fusiformis*²⁰⁻²² or the modification of these silica deposition peptides²³ and involving the identification and application in model systems²⁴.

A significant breakthrough was achieved by Hildebrand and colleagues, when they cloned, characterized, and identified the cDNA encoding the first silicic acid [Si(OH)₄] transporter²⁵. Kröger and colleagues cloned and characterized cDNAs encoding completely the two protein families (HEPs and silaffins) that contribute to the organic sheath surrounding the silica walls of a diatom^{15,26}.

The peptide-directed synthesis of the versatile, highly complex and ordered diatom frustules structures is still impossible or rather aligned with elaborated methods like e.g. direct ink writing¹⁰. The precision of these nanoscale architectures is far beyond the capabilities of present-day material science engineering. However, the process will one day be exploitable in nanotechnological applications.

In general, fabrication of two-dimensional (2D) structures and devices have been done either by top-down (lithography based)²⁷⁻³¹ or by bottom up (self-assembly)³²⁻³⁵ microfabrication approaches. However, there is still a need for low-cost methods to produce complex micro to nanostructures on a large scale. Thereby, a variety of precise and reproducible 3D morphologies can be obtained for the application of new functional materials in nanotechnology.

Because nature provides these fine and intricate 3D inorganic structures, several approaches for altering the diatom frustules chemistry, while preserving the 3D frustules shapes, have been reported in recent years. Gas-silica displacement, hydrothermal reactions³⁶⁻⁴¹, and wet chemical coating or impregnation methods⁴²⁻⁴⁸ have generated 3D frustules replicas fully or partially from silicates (e.g., Zn_2SiO_4), non-silica-based oxides (e.g., MgO , TiO_2 , ZrO_2 or BaTiO_3), polymers, carbon^{49,50} or metals (e.g., Au)⁵¹ by using the diatom frustules as templates.

These advanced nanocrystalline materials have been of interest in different fields e.g., environmental (gas sensing^{52,53}), chemical/physical (adsorbents^{54,55}, filtration (diatomaceous earth (DE)⁵⁶⁻⁵⁸), catalytic (N_2O decomposition⁵⁹), electronic (semiconductors), optical (photonic devices¹⁸ photonic crystals⁶⁰ and medical applications (drug delivery systems) because of well-defined and controllable micro- and nanoscale features^{11,61,62}.

Such obtained 3D structures open a wide field of possible applications, but their production methods require, in most cases, strong reaction conditions, e.g. high temperature, high pressure, extreme pH or organic solvents. Furthermore, scale-up is rather limited and the chemical functionality would be only provided by the inorganic material like silica.

In order to achieve structures with a higher degree of complexity, our approach utilizes flexible polymer templates with additional functional moieties e.g., amino-groups, carboxyl groups, etc. These groups can either add further functionality to the final core-shell particulate structure for trapping of biomolecules, pH responsive release and/or can actively participate in the shell formation process (Scheme 1).

A variety of different methods to obtain these silica core-shell structures have been published⁶³⁻⁶⁶. In contradiction to the Stöber^{67,68} or microemulsion-approach^{63,69} the template directed method offers a very promising alternative route because only a little or no surfactant or organic solvent is needed. Moreover, this template based technology can utilize polymers as scaffold to build up three dimensional structures by covalent linkage or self assembly of different polymer chains. The resulting morphology will be preserved after the silicification process.

The use of polymers as templates offers a high degree of flexibility with respect to, e.g., their three-dimensional structures or their functionality^{70,71}.

3 Objectives

In order to study complex three-dimensional silica structures, polymer template directed synthesis has been established. Because of the complexity of the systems used in this thesis, the objectives can be subdivided into the following three parts.

1. Choice of suitable polymer templates

For a universally applicable polymer/silica core-shell assembly, the system will be integrated into a LEGOTM type tool box approach, which allows the flexible combination of various polymers and silica precursors.

The following general types of polymers have been considered and studied as templates in the silica shell formation process:

- i. Covalently pre-formed star-shaped polymers comprising tertiary or quaternary amino groups
- ii. Self-assembling linear diblock copolymer

2. Shell formation process under ambient conditions

Due to the functional potential of the polymers in this template directed synthesis of polymer/silica structures, the approach offers also the possibility to encapsulate compounds within the silica shell. For encapsulation of sensitive compounds e.g. biomolecules, the whole procedure has to be performed under ambient conditions.

- i. Establishment of silica shell formation under ambient and biocompatible conditions without additional catalysts

3. Encapsulation of various compounds into the silica shell by entrapping into the polymeric structure

In order to demonstrate the versatility of the approach presented in the thesis, the following range of different compounds have been investigated as potential active compounds for encapsulation and trapping in the polymer silica system

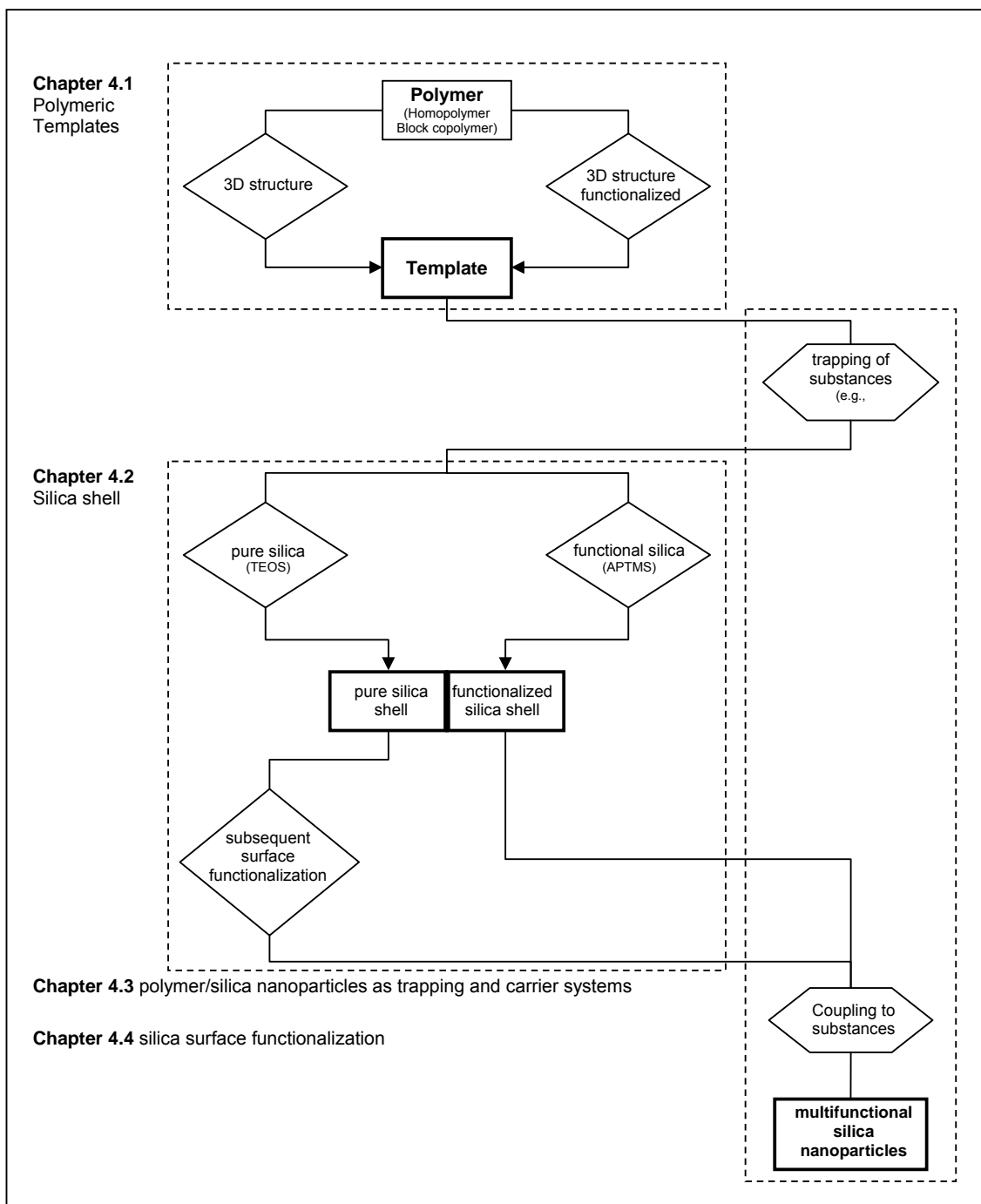
- i. Fluorescent dyes
- ii. Catalytically active metals and transition metal complexes
- iii. Biomolecules

4. Functionalization of the silica shell

To further functionalize the particles the silica shell is chemically modified to offer the possibility of coupling additional functional group or molecules e.g. receptors to the surface, or in order to avoid aggregation by covering the silica surface with e.g. PEG.

- i. Amino functionalization via a post-synthetic functionalization step in a one-pot approach

The flow chart (Scheme 1) illustrates the workflow followed in this thesis by comprising all the above possibilities.



Scheme 1: Scheme of the synthetic strategy

4 General Synthetic Strategy

The LEGO™ approach

In general, the entire system exhibits a high degree of flexibility concerning the choice of polymeric templates and silica shell structures. The polymer structures can be selected and synthesized from synthetically or commercially available compounds, e.g. homopolymers or block copolymers.

Various compounds can be encapsulated into the particle core depending on the polymer chemistry. In addition, the silica surface easily allows the further chemical modification by functional trialkoxysilanes in a post-synthetic step, to result in multifunctional silica nanoparticles. By this procedure, the particles can carry chemical moieties, like amines, perfluorinated alkyl chains or more complex molecules e.g. biomolecules and polymer chains (PEG for protection against immune response). These highly sophisticated, complex particulate structures offer a great variety of potential applications in catalysis, drug delivery, medical sensing and imaging. This approach compares best to the well known LEGO™ brick system (Figure 2).

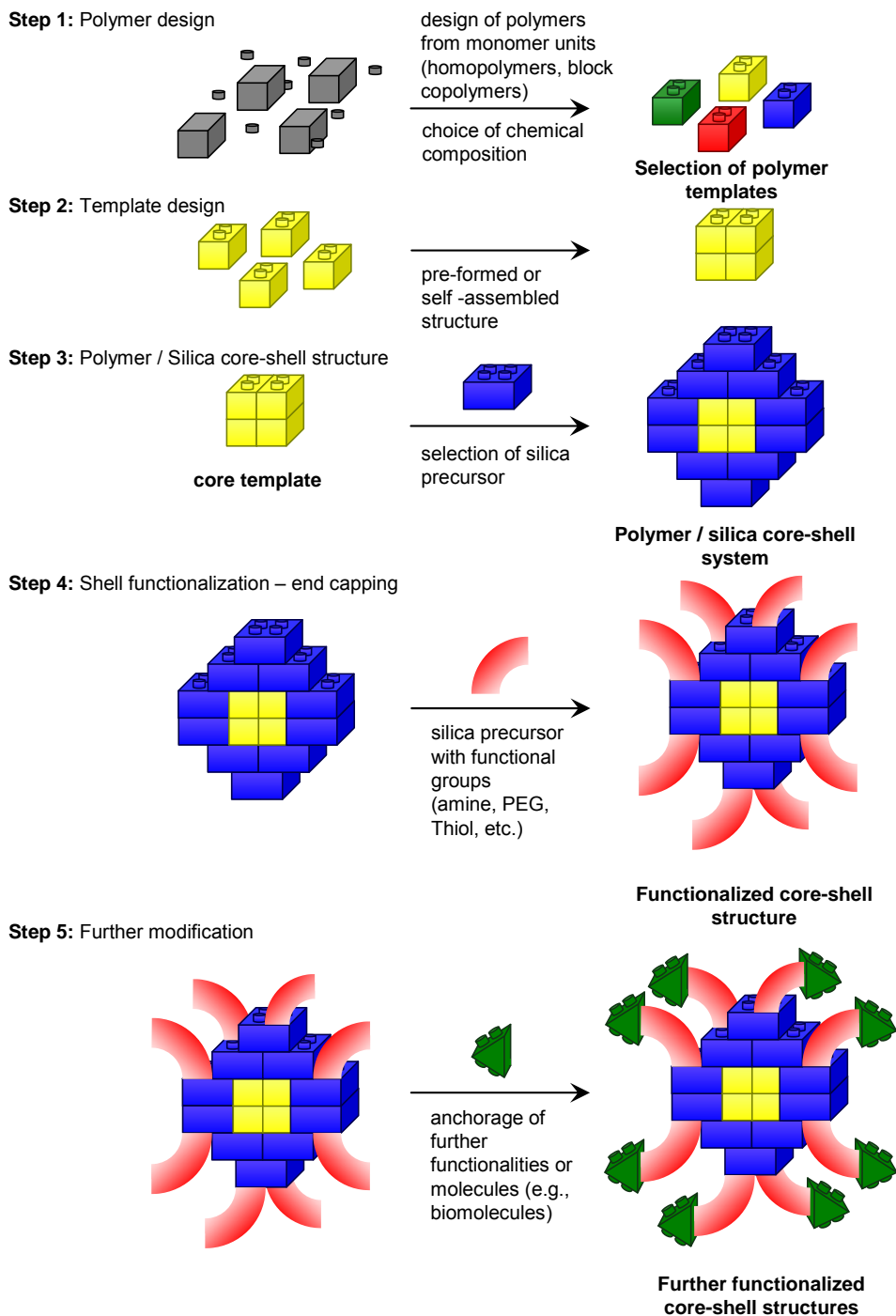


Figure 2: Scheme of the LEGO™ approach to produce core-shell structures with the desired functionalization and features. The scheme shows cross-sections of spherical structures

4.1 Polymeric templates

There are different models to obtain silica core-shell arrangements. Contrary to the implementation of Stöber chemistry^{67,68} or the microemulsion approach^{63,69}, the template method offers a very promising alternative route to circumvent the disadvantage of elevated temperatures, large amount of surfactants and/or organic solvents. Moreover the template based particle formation process utilizes polymeric templates as scaffolds to form three dimensional structures by silicification. The polymeric three dimensional templates form either by covalent bonding or by self assembly.

In addition, the polymeric superstructures can also possess further chemical properties, e.g. for stimuli responsive release or entrapping of molecules.

4.1.1 Basic principles of polymers and self-assembled structures

A polymer which consists of only one type of structural repeating unit (monomer) is called “homopolymer”. If two or more different monomers are interconnected, the polymeric molecule is called “copolymer”. A block copolymer contains at least two chemically different polymer chains that are covalently bound to each other (Figure 3).

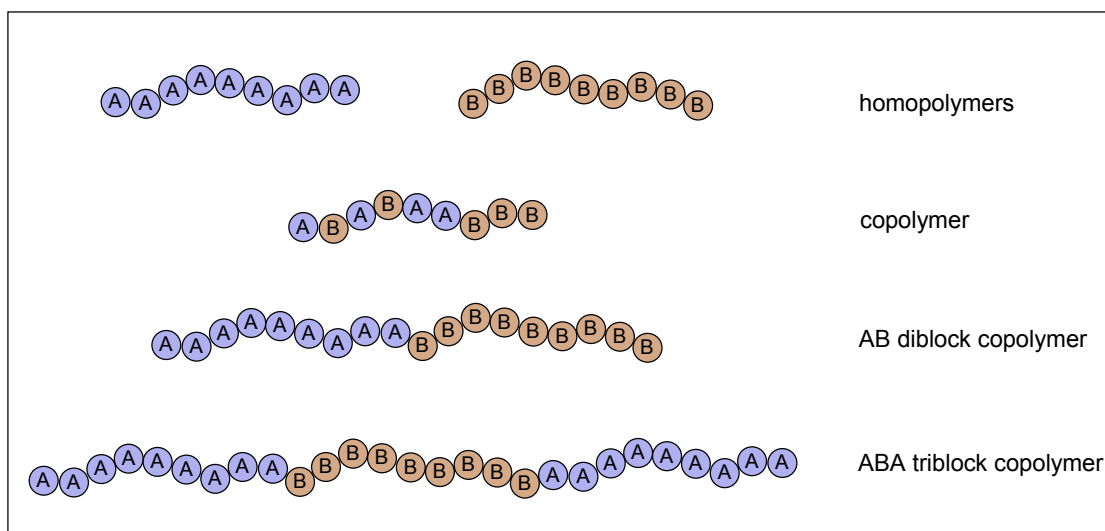


Figure 3: Types of polymers

Linear block copolymers comprise two or more polymer chains in a sequence, whereas a star block copolymer is composed of more linear block copolymers attached at a common branching point. In a polymer brush, individual polymer chains are connected to a linear polymer backbone (Figure 4). Individual block copolymer molecules can be also integrated into larger functional units by self-organizing to result in higher organized structural assemblies ⁷².

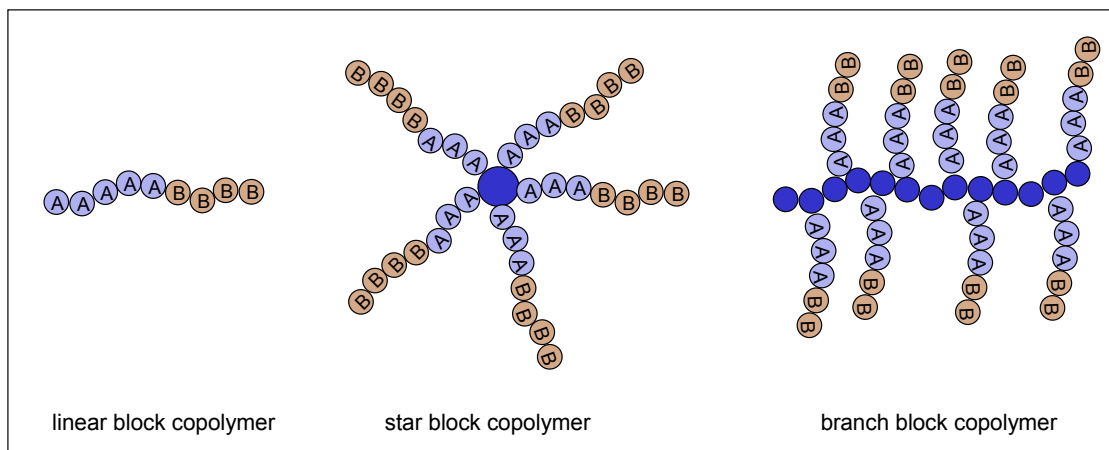


Figure 4: Types of block copolymers

In general, self-assembly in the classic sense is described as the spontaneous and reversible process of generating structures or patterns of a higher degree of organization from disordered systems or pre-existing components by non-covalent interactions ⁷³. Amphiphilic block copolymers can self-assemble into spherical micelles, worm-like micelles or vesicular structures ⁷² (Figure 5), dependent on the chemical composition of the blocks, the block length, ratio (molecular weight), arrangement, and experimental conditions like polymer concentration and temperature etc.

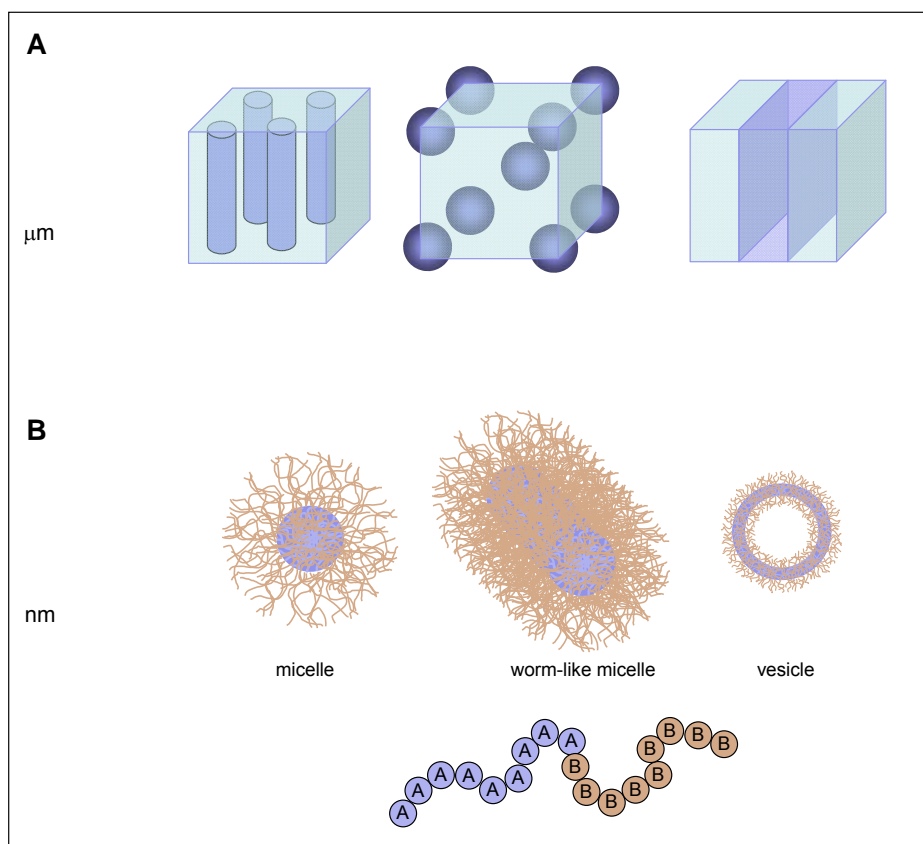


Figure 5: Structural hierarchies of self-organizing polymers

The above mentioned factors strongly influence the polymer properties (solubility) and therefore also have impact on the shape of self organized superstructures (Figure 5). For instance, amphiphilic block copolymers, as well as surfactants, can form micelles in dilute aqueous solutions. In polar solvents the hydrophilic polymer blocks will coordinate to the polar solution by building the micellar outer part (corona), whereas the hydrophobic polymer blocks coordinate to the interior of the micelle by building the core. The capability of micelle formation is also present in non-polar media with the core/shell hydrophobic/hydrophilic structure is oppositely directed.

Many reviews and featured articles were published with regard to the variety in sizes and topologies of self-assembled block copolymer structures^{74,75}, illustrating the possibility to produce nano- and microstructures by hierarchical self-organizing⁷⁰.

4.1.2 Functional requirements of the polymeric templates

Core-shell polymer/silica structures are usually prepared by adsorption or grafting of polymers on a pre-formed silica core⁷⁶⁻⁸⁰. Interestingly, examples of the reverse approach to use a polymer template as core surrounded by a silica shell are scarce. In order to achieve core-shell synthesis under ambient conditions, the templates have to comprise cationic and hydrogen-bonding polymers because they can cause silica precipitation¹⁶ without any further catalysts.

The amphiphilic block copolymer template, methyl ether-poly-(ethylene glycol)-*block*-poly(lactic acid) (mPEG-*b*-PLA), has been synthesized by ring-opening polymerization, with systematic variation of the chain lengths of the hydrophilic and hydrophobic blocks⁸¹. This allows the control of size and shape of the spontaneously formed micelles resulting in ordered nanoporous silica structures with specific surface area and tunable pore sizes after silicification and subsequent calcination.

In our approach, we focus on cationic polyamine-based polymers as templates in polymer/silica systems.

4.1.2.1 Polyamine / silica systems

Silaffins¹⁵ are proteins essential in the shell formation process of diatoms. They appear to be the model compounds in the template-directed silicification and thus formation of three dimensional complex core-shell silica structures. Silaffins are predominantly composed of polycationic molecules and a high proportion of hydroxylamino acids, known to be responsible for the formation of ornate silica structures¹⁷.

In 1950, important investigations concerning the influence of organic amines and ammonium ions on silicification processes were published⁸². Further on, the flocculation of silica particles with polyethyleneimine was investigated in 1976⁸³ and the formation of mesoporous materials using alkyltrimethylammonium ions was discovered in 1992⁸⁴. There are many examples of different polyamine structures published (Figure 6)⁶⁴.

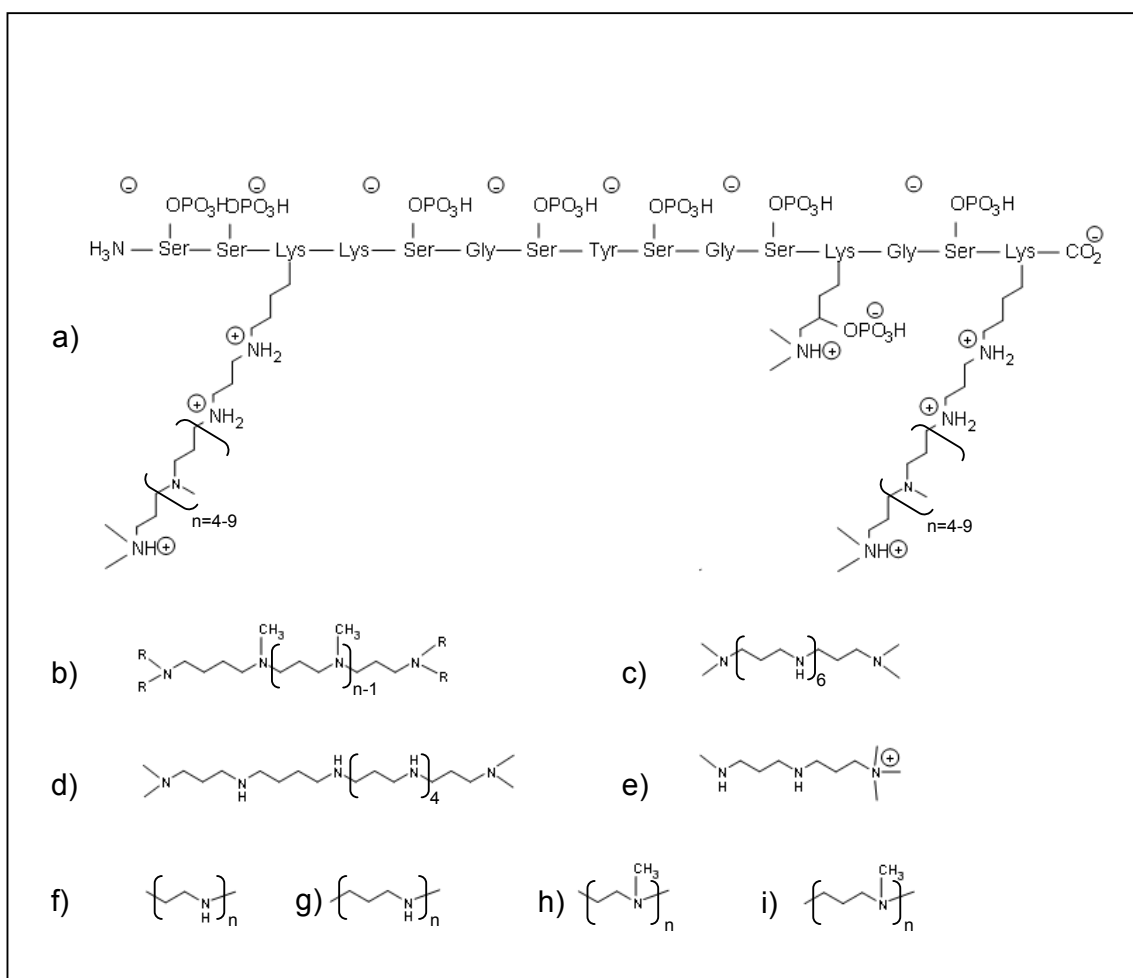


Figure 6: Chemical formulae of molecules involved in the biomineralization of silica in diatoms (a-e) and of model compounds (f-i). (a) native silaffin 1A. (b) Polyamines from diatoms of the *Genus Coscinodiscus*. (c-e) Amine compounds of the diatom *Thalassiosira Pseudonana*. Synthetic linear polyamines used as model compounds: (f) poly(ethyleneimine) (PEI); (g) poly(propyleneimine) (PPI); (h) poly(*N*-methylethyleneimine) (PMEI); (i) poly(*N*-methylpropyleneimine) (PMPI)⁶⁴

The more intricate template-directed systems can be obtained by the synthesis and self-assembly of amine-based block copolymers. In the case of block copolymers the self-assembled morphologies can be employed (Figure 7). Covalently bound 3D structures (e.g., stars or brushes) from homopolymers can also be utilized as template systems. The advantage of amine-based polymers is that they can act as *in situ* catalysts for silica hydrolysis and condensation¹⁷, leading to silica shells with polymer cores. These polymers have been used under biocompatible conditions for the controlled synthesis of silica/polymer hybrids¹⁷. Some examples are polymers which contain blocks of positively charged aliphatic tertiary amines⁸⁵, pyridine, imidazole⁸⁶, or dendrimers⁸⁷⁻⁸⁹. Khanal et al.⁹⁰ reported on ABC triblock copolymer of poly(styrene-*b*-2-vinyl pyridine-*b*-ethylene oxide) (PS-PVP-PEO) which

self-assembles into micelles. At low pH, PVP is protonated and causes the selective deposition of the silica precursor. The resulting particles have a diameter of 30 nm and the PEO block prevents further aggregation. It is also possible to reveal a final hollow structure of the silica particles by calcination. The main problem of this approach is that the synthesis and modification of block copolymers is tedious. Moreover, if the polymer/silica hybrid material is used for, e.g., drug delivery, the encapsulation of a small molecule needs to be controlled by the polymer. As a result, polymers that

- (i) are easy to manufacture in large quantities,
- (ii) support encapsulation of appropriate cargo compounds, and
- (iii) catalyze the hydrolysis and condensation reaction of silica alkoxide precursor

are interesting candidates for the synthesis of responsive and biocompatible polymer/cargo/silica nanoparticles.

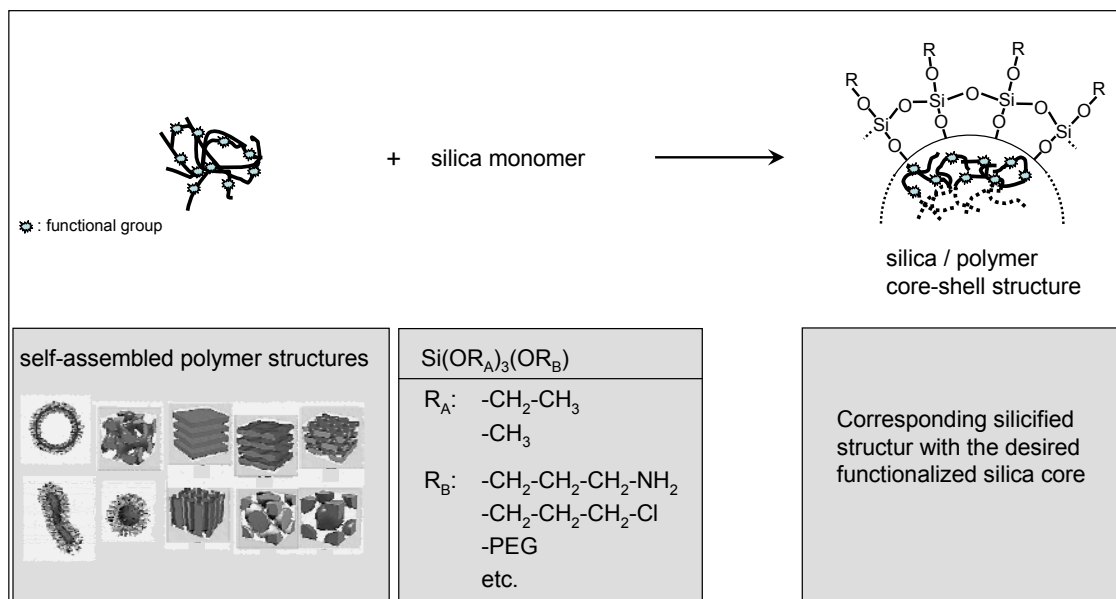
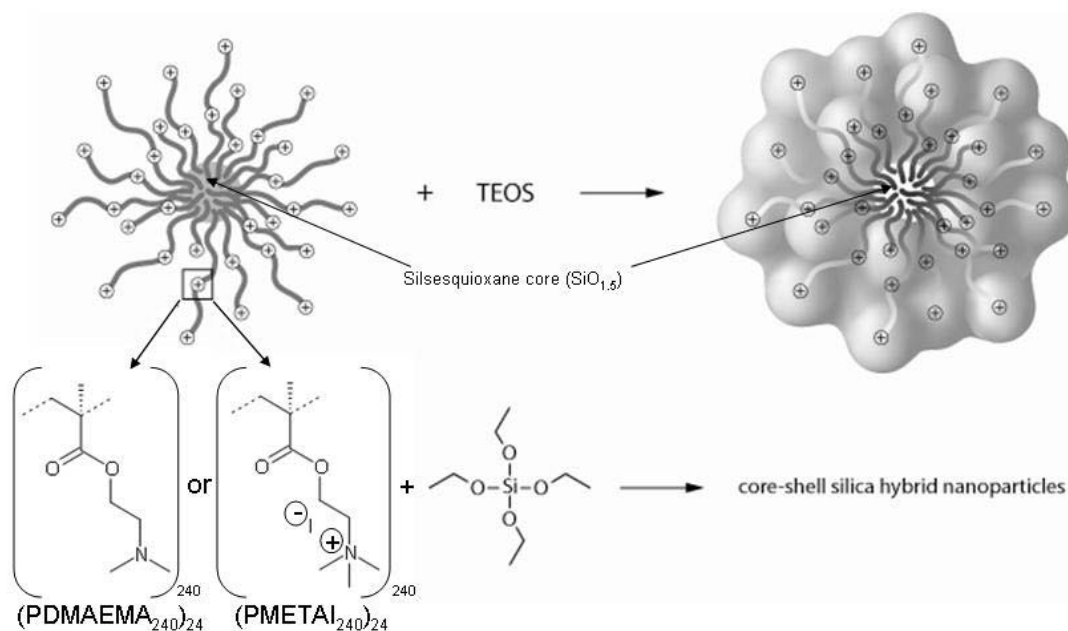


Figure 7: Scheme of the composition of silica/polymer core-shell structures. Bottom right corner: Structures of self-assembled block copolymers.

4.1.3 Star-shaped PDMAEMA and PMETA polymers

The current work shows that for the synthesis of unique, raspberry-like, polymer/silica hybrid particles, only a rather simple, star-shaped, polyelectrolyte is necessary. The polycation poly(*N,N*-dimethylaminoethyl) methacrylate (PDMAEMA)

or its quaternized equivalent poly[2-(methacryloyloxy)ethyl] trimethylammonium iodide (PMETAI) are attached to a silsesquioxane core⁹¹, yielding a template with 24 polymer arms, which catalyzes the silicification only by its basic nature. Depending on the tertiary or quaternary amine groups of the polymer (PDMAEMA or PMETAI), either spherical particles with a low density core or raspberry-like particles, which are rare in the literature so far^{86,92-94} form (Scheme 2). The main advantage of the silsesquioxane/polymer template is that it is pre-organized and, because all bonds within the template are covalent, is not prone to decomposition or internal rearrangements. It therefore enables the investigation of the silicification without additional complications due to a changing template⁹⁵.



Scheme 2: Sketch of the star-shaped polymer (24 polymer chains covalently connected to a silsesquioxane core) and the mineralization reaction. Magnified view of the square region shows the structure of poly(N,N-dimethylaminoethyl) methacrylate (PDMAEMA) and poly[2-(methacryloyloxy)ethyl] trimethylammonium iodide (PMETAI).

One should distinguish between a weak (annealed) polyelectrolyte like PDMAEMA and a strong (quenched) polyelectrolyte like PMETAI. Strong polyelectrolytes are made of monomers, which are strong acids or bases and their salts. The number of charges in this class of polyelectrolytes is independent of changes in pH, whereas the number of charges for weak polyelectrolytes can be easily modified by adjusting the pH.

4.1.3.1 Synthesis of star-shaped polymers

Star-shaped PDMAEMA and its quaternized analogue PMETA1, with a moderate arm number, arm size distribution and low polydispersity, can be achieved by the polymerization of 2-(*N,N*-dimethylamino)ethyl methacrylate (DMAEMA) on the basis of atom transfer radical polymerization (ATRP) employing the core-first method⁹⁵ (Figure 8). Besides other methods, ATRP^{96,97} is the preferred polymerization technique for advanced polymer architectures not only because of its simplicity to obtain suitable multifunctional initiators, but also for the impassiveness towards other functional groups. The principle is the reduction of the radical concentration in the polymerization mixture compared to concentrations used in conventional radical polymerization methods. By masking the majority of the radicals the probability for the encounter of two radicals, leading to the termination reactions like recombination or disproportionation, will be reduced compared to the feasibility of the propagation reaction. The modality to introduce the initiators to the system is different depending on each requirement. In the case of star-shaped polymers, in general two approaches can be followed: The core-first and the arm-first method.

In the arm-first method, the individual polymer chains are synthesized first and subsequently crosslinked to the connection point. However, this method includes the drawback of a rather broad distribution in arm number. Further on, unattached remaining arms need to be separated from the star-shaped molecules by tedious purification steps. Therefore, the convenient method for PDMAEMA and PMETA1 stars is the core-first method. This method presents a system to obtain well defined polymers with precise number of arms based on multifunctional initiators for the ATRP. As possible core scaffolds, sugar-based initiators or small inorganic nanoparticles can be utilized. If an increasing number of arms per star is desired, a high number of initiation sites are required. Therefore silsesquioxane nanoparticles bearing a high number of hydroxyl functions can be considered as the most versatile core templates⁹⁸. These particles exhibit moderate polydispersity in molecular weight ($PDI \sim 1.2$) and have been therefore utilized in the synthesis of star-shaped polymers.

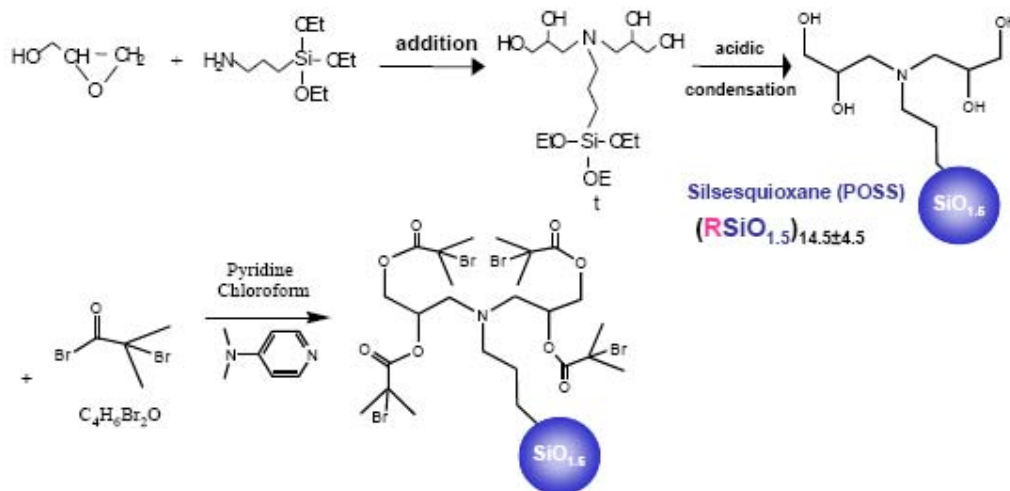


Figure 8: Synthesis of hybrid nanoparticle initiators for ATRP ⁹⁵

4.1.4 Block copolymers PEI-b-PEG

Linear and branched poly(ethylenimine)s, (PEI)s, are attractive and well-known polymers that have been commonly used for various industrial applications e.g. wastewater treatment, shampoo and in paper industry (Epomin[®], Polymin[®]). Due to its cationic character the polymer is utilized for gene delivery because it combines excellent transfection efficiency with high complex stability under in vitro and in vivo conditions ⁹⁹⁻¹⁰². These cationic carriers bind spontaneously to negatively charged oligonucleotides and also enhance their stability and uptake in vitro ^{103,104}. However, in vivo performance of these systems appears more problematic. The major problem of most cationic carriers is poor solubility and the tendency to aggregate in aqueous solution when complexed to polynucleotides or other anionic molecules ¹⁰⁵. To overcome these problems certain hydrophilic polymers can be employed, which can bind or conjugate to particles or conglomerate surfaces and therefore offer sterical stabilization ¹⁰⁶⁻¹⁰⁸. Poly(ethylene glycol), PEG, is one of the most versatile polymers used for this purpose and in combination with PEI it produces block copolymers consisting of the cationic block, PEI, and the nonionic block, PEG (Figure 9). This combination reduces the polymer toxicity and improves its biocompatibility ¹⁰⁹⁻¹¹¹. The outstanding steric protection provided by PEG is related to its molecular properties, such as low interfacial energy, conformation, hydrophilicity and high flexibility.

Concerning the application of PEI-*b*-PEG block copolymers in biological systems a consideration between the potential of PEI to take part in the transgene expression and the cytotoxicity, in dependence of the molecular weight has to be performed. Low molecular weight PEI (~2000 g/mol) has shown no toxicity but in contradiction a poor transfection activity, whereas in the case of high molecular weight PEI (~25000 g/mol) the situation is contrarywise ^{110,112}.

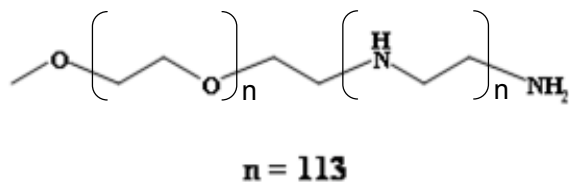


Figure 9: Formula of the block copolymer PEI-*b*-PEG

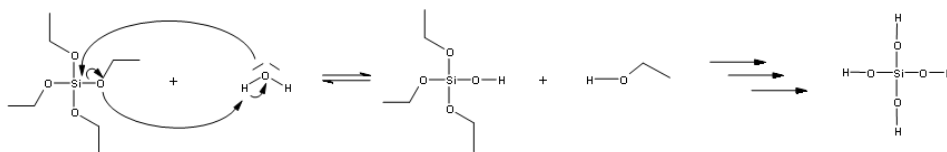
4.2 Silica shell formation process

The silicification process of silicon alkoxide precursors is a complex multi-step reaction. This involves hydrolysis, condensation, aggregation, agglomeration, gelation or flocculation processes, each following different reaction pathways and chemical intermediates ¹⁶.

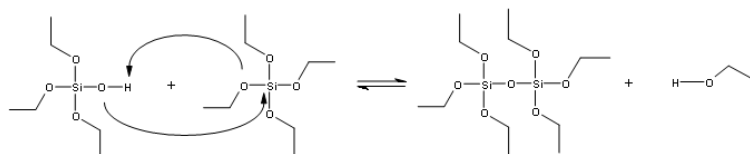
The hydrolysis of silicon alkoxides leads to the formation of monosilicic acid, which further on condensates via the intermediate steps of disilicic, oligosilicic and polysilicic acid, to primary particles (Scheme 3 and Scheme 4).

The hydrolysis and condensation result in a colloidal solution (silica sol) and their rates depend on many factors such as temperature, ionic strength and pH. A so-called sol (colloid) is normally stable under ambient conditions for an infinite time unless flocculation or gel formation is induced by a variation of the ionic strength, temperature or pH, as mentioned above.

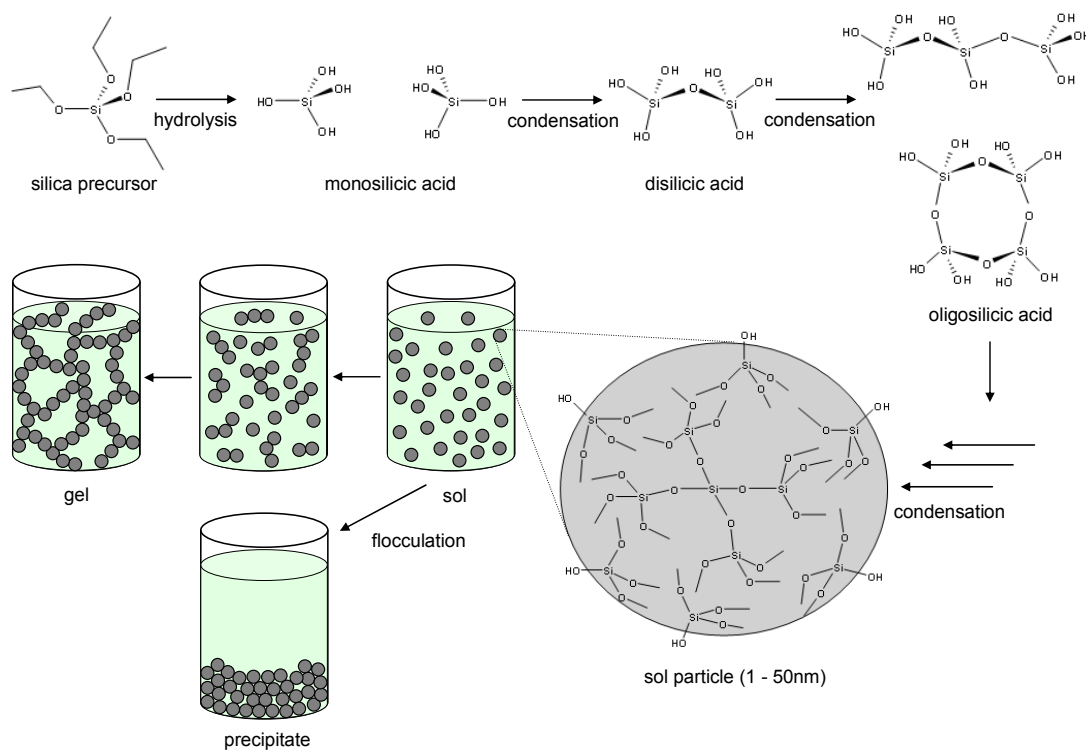
1)Hydrolysis reaction:



2)Condensation reaction:



Scheme 3: Hydrolysis and condensation reaction of the organosilane TEOS. The condensation reaction could take place at every step of the hydrolysis but preferentially at the stage of completely hydrolyzed monosilicic acid



Scheme 4: Schematic representation of the silica sol-gel process

4.2.1 Sol-gel synthesis

Sol-gel techniques are widely applied in the synthesis of ceramic powders, transparent glass coatings and composite materials based on silicon or other metal alkoxides (e.g., titanium isopropoxide (TTIP), tetraethyl orthosilicate (TEOS)). This process has been well known since the 19th century and is continuously improved. Major advantages of the sol-gel process are:

- i. ambient temperature of sol preparation and gel processing;
- ii. high purity of precursors;
- iii. product homogeneity;
- iv. low temperature of sintering;
- v. ease of production of multicomponent materials;
- vi. good control of powder particle size and distribution.

Possible drawbacks of the sol-gel method are the high expenses for some precursors, the often very long reaction times and the sensitivity of the reactions towards many influencing factors (e.g., pH, temperature, reaction time, reagent concentrations, catalyst constitution and concentration, H₂O/Si molar ratio and aging temperature/time). By careful control of these factors, the structure and properties of the sol-gel derived inorganic network can be influenced and tailored^{113,114}. Stöber et al. described in the late 60s the influence of pH on the morphology and the size of emerging particles in the sol-gel process⁶⁸.

Besides purely inorganic materials, the process also allows the synthesis of inorganic-organic composite materials via a similar hydrolysis and condensation process (Scheme 3).

4.2.2 Sol-gel process in microemulsions

Microemulsions are mixtures of water, oil, and surfactant, often in combination with a co-surfactant, e.g. long-chain alcohols. Opposite to the classical emulsions which are inherently colloiddally unstable and require shear forces for their preparation, microemulsions form upon simple mixing of the components to result in thermodynamically stable, transparent solutions.

Two types of microemulsions can be distinguished, oil-in-water (O/W) microemulsion or water-in-oil (W/O) microemulsion, known as reverse microemulsion.

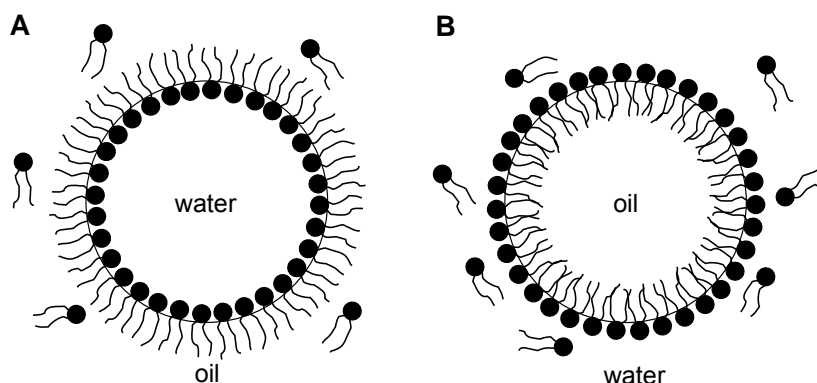


Figure 10: (A) Water in Oil microemulsion; (B) Oil in Water microemulsion

Monodisperse spherical silica nanoparticles in nanometer size range can be conveniently synthesized by the addition of silicon alkoxide, typically tetraethylorthosilicate (TEOS), to a reverse water-in-oil microemulsion. Particles in the size range of 20 to 500 nm can be obtained, depending on the reaction conditions. The silicon alkoxide diffuses preferentially into the water droplets. Upon hydrolysis and condensation, spherical silica nanoparticles form. The reaction is catalyzed by pH adjustment. The accretion of the primary silica particles is favored by the aqueous nano-environment¹¹⁵⁻¹¹⁷. A disadvantage of this method is the rather small yield (wt product / wt solution) because most microemulsion systems contain less than 20 % (v/v) of aqueous domains. In addition the workup procedures result in further yield decrease because of the particle removal from the oil phase and carryover of surfactants, which require extensive washing steps.

4.3 Potential compounds for encapsulating and entrapping in polymer/silica systems

As described above, the polymers used as templates for the silica shell formation exhibit positive charge due to the amine groups. This property offers the unique opportunity to entrap various components into the polymeric-silica aggregate especially that pH changes do not lead to swelling and porosity changes of the silica.

The mechanism of the interaction between the compound and the polymer depends on the nature and charge of the components. In the case of positively charged amine groups present in the polymer, a negatively charged compound is preferred to strongly interact by electrostatic forces.

Examples of potential classes of compounds are listed below:

- i. Fluorescent dyes e.g. sulforhodamine, fluorescein, Alexa dyes
- ii. Metal nanoparticles and transition metal complexes
- iii. Proteins and enzymes e.g. hemoglobin, superoxide dismutase

Fluorescent nanoparticles are highly attractive for imaging, especially for a versatile visualization modality for biological research, medical diagnosis, drug discovery, and clinical practice^{118,119}. Fluorescence microscopy benefits from the increasing availability of imaging techniques and fluorescent probes which enable the noninvasive studies of gene, protein, and cellular processes, at high spatial resolutions with single molecule sensitivity^{120,121}.

The brightness of the fluorescence signal from such imaging probes can be controlled by the number of dye molecules per nanoparticle, with the maximum dye density limited only by self-quenching. Therefore, dye-doped nanoparticles can be quite photostable without showing fluorescence intensity fluctuations (blinking), enhanced due to the better protection of the dye inside the nanoparticle.

Silica shows various properties which are beneficial for optical imaging applications in biological systems. This includes chemical inertness, transparency, and the ability to protect the encapsulated dyes from the outside environment^{122,123}.

Regarding the transition metal complexes, which usually exhibit positive charge, complexation is considered as the predominant mode of interaction. The incorporated metals and transition metal complexes can be utilized for e.g. catalysis.

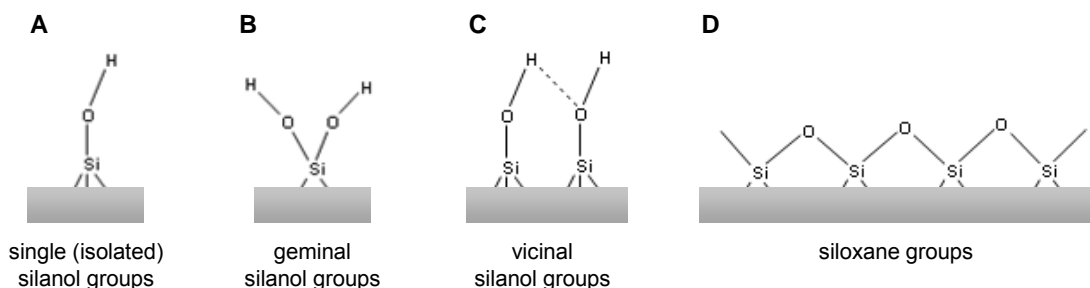
Besides different biomolecules, nucleic acids and proteins are the most prominent classes of molecules suitable for encapsulation. In particular, hemoglobin, myoglobin and neuroglobin, which are involved in oxygen transfer reactions, offer potential medical applications. In addition to that, these proteins can serve as model compounds to verify the native activity of proteins after the encapsulation process, because the oxygen or carbon monoxide binding process can be followed easily by spectroscopy.

4.4 Chemically functionalized silica matrix

4.4.1 Non-functionalized silica shell surface

Many of the adsorption, adhesion, chemical, and catalytic properties of silica depend on the surface chemistry and geometry. The silica surface displays different types of Si-O bonds, either silanols ($\equiv\text{Si}-\text{OH}$) or siloxanes ($\equiv\text{Si}-\text{O}-\text{Si}\equiv$), which have important influence on the particle properties. This offers a great potential for further functionalization¹⁷. The types of Si-O bonds on a silica surface can be identified as:

- (i) single silanol groups, also known as free or isolated silanols (Scheme 5 A)
- (ii) silanediol groups, also called geminal silanols (Scheme 5 B)
- (iii) hydrogen-bonded vicinal or bridged silanols (Scheme 5 C)
- (iv) siloxane groups (Scheme 5 D)



Scheme 5: Silanol groups and siloxane bridges on the surface of colloidal silica.

Pristine silica surfaces are negatively charged in the pH range of 4 – 7, also found in most biological systems. The isoelectric point (IEP) is around 2 – 3. The surface charge of silica can be influenced by chemical functionalization, depending on the nature and concentration of the functional groups. The functionalization of the

silica surface is relevant in many material applications. Functional groups are usually attached to the silica surface by the reaction of the surface hydroxyl groups¹²⁴ with functionalized trialkoxysilanes. Most common functionalized trialkoxysilanes compounds used are (3-aminopropyl)-triethoxysilane (APTMS) or (3-aminopropyl)-trimethoxysilane (APTES). The primary amine is a good ligand for metal ions and can therefore serve as sorbent in waste water treatment^{125,126} or can immobilize catalytically active transition metal ions^{127,128}. Furthermore the nucleophilic primary amine can be used as linker between the silica surface and any organic species with a leaving group for a nucleophilic substitution reaction^{129,130} or serve as a solid base catalyst^{131,132}. A preferred field of investigation is the coupling of bio- or dye molecules to the amine modified silica surface^{113,133}. Mesoporous materials functionalized with 3-aminopropyl groups can either be prepared by co-condensation of (3-aminopropyl) trialkoxysilane with a silica precursor (typically TEOS) or by post-synthetic grafting on the surface of a mesoporous silica support¹³⁴. However, there is a variety of functional groups available, e.g. thiol groups, epoxy groups or even polymers to tailor the desired particle surfaces.

5 Results and Discussion

The template directed synthesis of highly functional 3D core-shell structures is very complex, because of a great variety of templates, precursors and conditions which can be applied. Therefore, the synthetic procedure used in this work will be described in the form of separate steps, as displayed in Scheme 1.

5.1 Polymeric templates

Within the scheme of the experimental setup, three representative kinds of polymers were selected. The star shaped polymers (PDMAEMA and PMETAI) are thought to serve as a simple model for more complex structures to mimic the sophisticated diatoms. The PEI-*b*-PEG block copolymer represents a typical example of a self assembling material, building up simple aggregates like spherical particles and represents a model with the potential for more structural freedom with respect to the shape of the final silica structure.

5.1.1 Star shaped polymers (PDMAEMA and PMETAI)

5.1.1.1 *Structure and characteristics of the star shaped polymers*

The star polymers (PDMAEMA and PMETAI) were synthesized by ATRP based on a core-first approach (silsesquioxane core⁹⁸) and characterized by F. Plamper (University of Bayreuth)^{91,95,135} (Materials and Methods (Table 7)).

To visualize both star polymers (Scheme 2) without the addition of silicon alkoxide, atomic force microscopy (AFM) images were obtained (Figure 11). The silsesquioxane cores of the stars have the height and diameter of 2 to 2.5 nm. All cores are surrounded by polymer arms. The average size of the PDMAEMA polymer stars (core plus polymer chains) determined by AFM is about 70 nm in diameter. This is in good agreement with literature⁹¹ where the root of the z-average of mean squared radius of gyration $\langle R_g^2 \rangle_z^{0.5}$ is 29 nm, as determined by static light scattering (SLS) in acetone. For the PMETAI polymer star (diameter ~ 80 nm) no reference value is available. However, the PMETAI stars were prepared by quaternization of

PDMAEMA polymer stars with methyl iodide. Therefore, a similar diameter can be expected. Overall, AFM shows that the silsesquioxane/polymer stars are uniform and have a narrow size distribution. This is consistent with an earlier solution study on these stars^{91,135}.

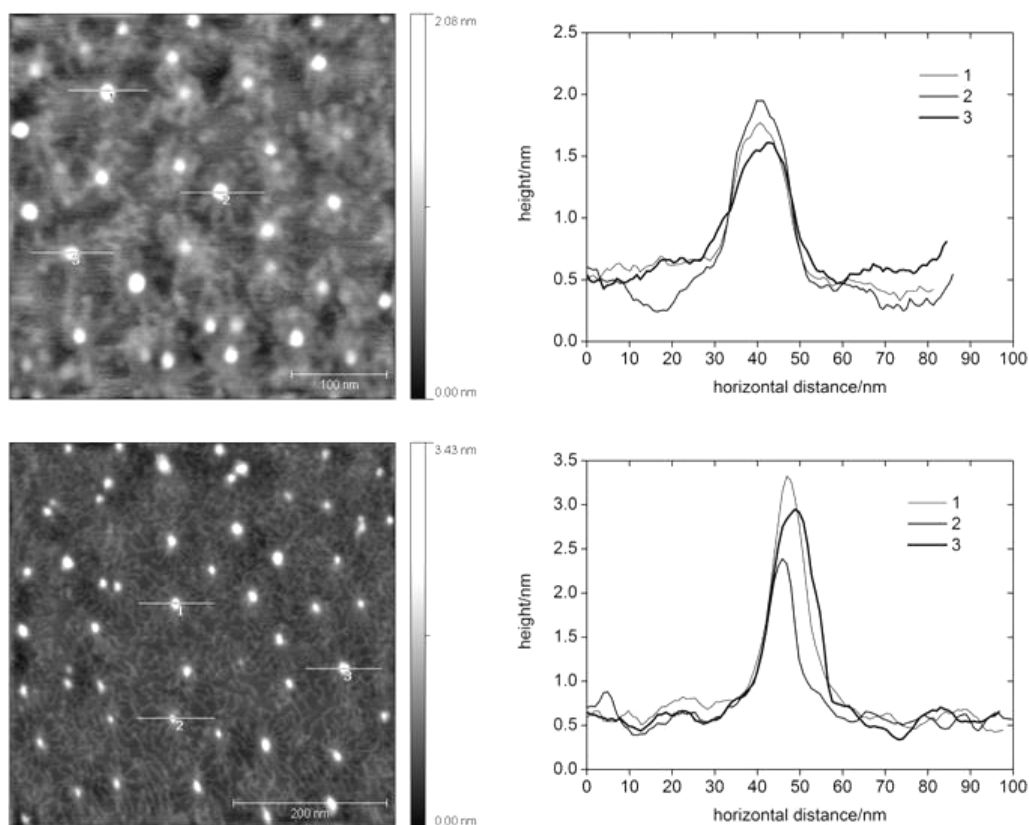


Figure 11: AFM images of PDMAEMA (top) and PMETAI (bottom) polymers with the respective height profiles (right) without the addition of silicon alkoxide.

The two star polymers were used as a simple template model due to the simplicity of the polymer (homopolymer) and the morphology (star-shaped). Further on, the features show either a pH induced response (PDMAEMA) or its absence (PMETAI). The pH-dependent behavior of both polymers, PDMAEMA and PMETAI, is determined by measuring the ζ -potential. Figure 12 shows the ζ -potential of the neat stars in aqueous solution at different pH. The ζ -potential of the PMETAI stars is pH-independent. In contrary, the ζ -potential of the PDMAEMA polymer stars decreases with increasing pH. This behavior can be assigned to the different states of charging in the two stars: While PDMAEMA can take up or release protons via its amine groups, the quaternary ammonium groups in PMETAI cannot. The tertiary

amino groups in PDMAEMA have an average pK_a of 7.5. In strong acidic media, PDMAEMA units are highly protonated and the ζ -potential is positive. With increasing pH the ζ -potential decreases. This is due to the deprotonation of the amine groups, leading to ζ -potential of zero at pH 9.5 (isoelectric point) and to a negative z-potential at $pH > 9.5$. The ζ -potential indicates also that the system tend to aggregate with increasing pH.

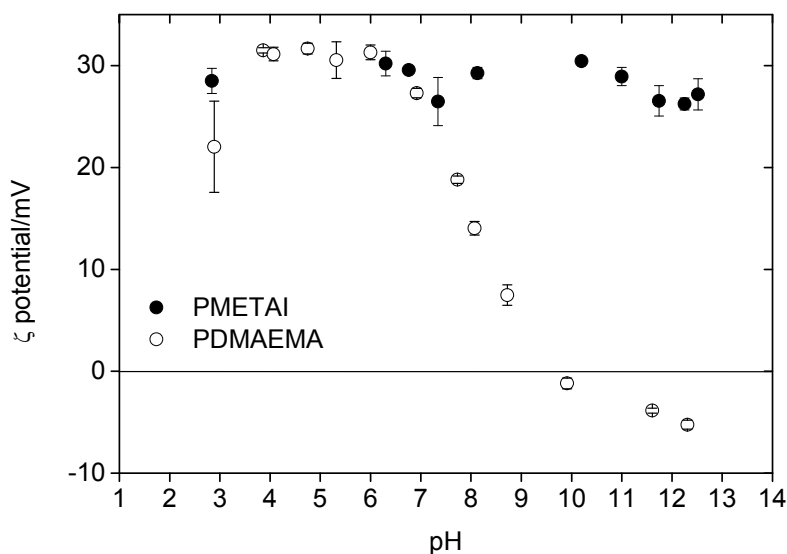


Figure 12: ζ -potential vs. solution pH for both (PDMAEMA and PMETA1) polymer stars (1 mg/mL). The horizontal line indicates the 0 mV potential.

5.1.2 Self-assembled structures from linear PEI-*b*-PEG block copolymer

As the self-assembled entities consisting of PEI-*b*-PEG block copolymers bear also charges induced by the imine groups, ζ -potential and size measurements were done in dependence of the pH. Since PEI does not contain quaternary amines, cationic charges are generated by protonation of the amine groups thus leading to a correlation between environmental pH and cationic charge density. The pK_a value of PEI is 7.9 and the polymer leads to a system with an effective buffer capacity.

The ζ -potential in Figure 13 (A) shows values around 15 mV in the acidic area (pH 2-3) and increasing to 36 mV at pH 3.5. ζ -potential slightly decreases with further pH increase. Figure 13 (B) shows a bubble point plot, representing the hydrodynamic diameters D_h of PEI-*b*-PEG aggregates versus pH. The bubble size is proportional to the intensity-weighted fraction of particles with the respective D_h . There are multiple points for most pH values. This is due to the fact that in most cases more than one

D_h population was observed, leading to the assumption that single and aggregated polymeric structures are coexistent in the solution.

Despite the predicted model that the PEI blocks build up a micelle core and the PEG blocks shield the charges and act as a corona, the ζ -potential is in the positive range, but shows a transition at pH 3.5. In the acidic environment, the amino groups of the PEI are protonated and should reveal electrostatic repulsion. However, the PEG block has an influence on the assembled system as shown by the low ζ -potential values. It would be expected to obtain more neutral ζ -potential and a small hydrodynamic diameter, if PEG was arranged as a fully shielding protection shell on the outer part of the aggregates¹³⁶. Since the particle size measurements (Figure 13 (B)) demonstrates prominent agglomerates ($D_h = \sim 500$ nm) in the pH range of 2-3, the presence of single chains or small aggregates can be excluded. The following increase in the ζ -potential at pH 3.5 could be an indication for a single chain transition, but the hydrodynamic diameter at that point is surprisingly large (200 nm). By the means of this relatively large diameter the presumption to achieve micelle structures is also excluded. As mentioned already, the ζ -potential decrease with increasing pH is due to the approximation of the pK_a value of PEI. In this region the dominant size fraction is present in the range of D_h 200nm. This leads to the conclusion that defined aggregates are built and the PEG block is not fully able to decrease the aggregate size. Analogous observations were also made with the block copolymer systems poly(ethylene glycole)-*block*- poly(2-methyl-2-oxazoline) (PEG-*b*-PMOXA), where well-defined aggregates in the range of 200 nm were detected. These aggregates perform a dynamic exchange of block copolymers with the environment¹³⁷. The DLS measurements are not essentially exact because qualitative analyses of polyelectrolytes are difficult due to the strongly charged system.

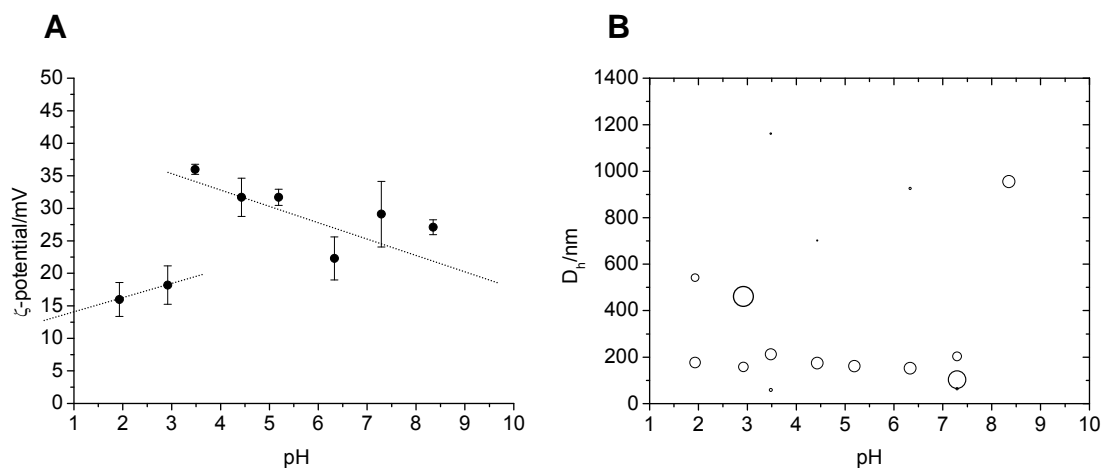


Figure 13: **A)** ζ -potential vs. pH for PEI-*b*-PEG structures. **B)** Hydrodynamic diameters D_h of the PEI-*b*-PEG structures vs. pH. Bubble diameters are proportional to the percentage of structures (weighted by intensity) with the respective D_h values.

5.2 Silica shell

5.2.1 PDMAEMA / and PMETA / silica system

5.2.1.1 Structure of the polymer/silica systems after silicification

The star polymers (PDMAEMA and PMETA) exhibit ideal preconditions for the successful assembly of silica shell structures surrounding the polymer template.

Figure 14 shows representative scanning (SEM) and transmission electron microscopy (TEM) images and Figure 15 represent AFM images (PMETA) of the silica particles obtained after mineralization of the stars with TEOS (Scheme 2). SEM, TEM and AFM show that relatively uniform nanoparticles form. The average diameter of the silica particles is 25 nm and 50 nm for the PDMAEMA and the PMETA stars, respectively.

TEM also shows that the particles grown with the PDMAEMA stars have a bright core in the center. The bright area is assigned to regions with smaller electron density. A less electron dense region is most likely due to the silsesquioxane core and probably some polymer. The diameter of the bright spot (2 to 3 nm) is consistent with a silsesquioxane core of 2 to 2.5 nm, measured by AFM, in a polymer corona. Given the rather small diameter of the bright center, the polymer corona is most likely

not entirely located in the bright dot, but partly encapsulated in the surrounding silica sphere obtained through the TEOS condensation reaction.

The particles grown in the presence of PMETA1 show a less common morphology in that they consist of a central, spherical particle carrying short arms. Depending on the sample preparation, different morphologies are observed. In cryo-TEM, without drying after the mineralization reaction, the particles exhibit long arms. In regular SEM and TEM, where samples are dried before imaging, the particles exhibit bulges rather than real arms. As a result, we suspect that the arms on the particle surface retain some flexibility even after mineralization, but this hypothesis will need to be confirmed in the future.

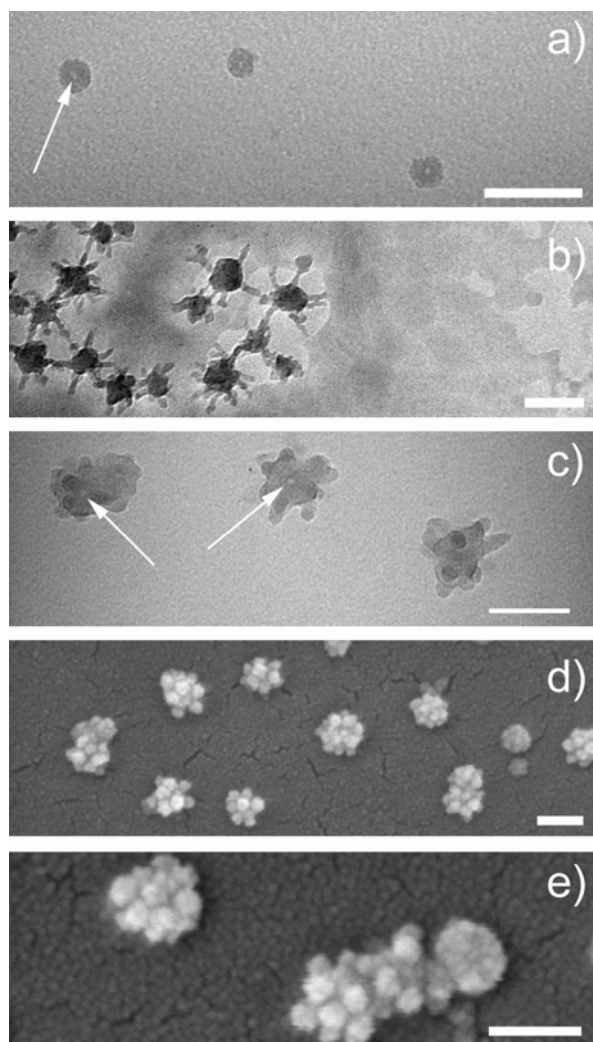


Figure 14: (a) TEM image of silica core-shell nanoparticles based on PDMAEMA. (b) Cryo-TEM, (c) TEM, and (d, e) SEM images of silica core-shell nanoparticles based on PMETA1. All scale bars are 50 nm. Arrows point to less electron dense particle interior.

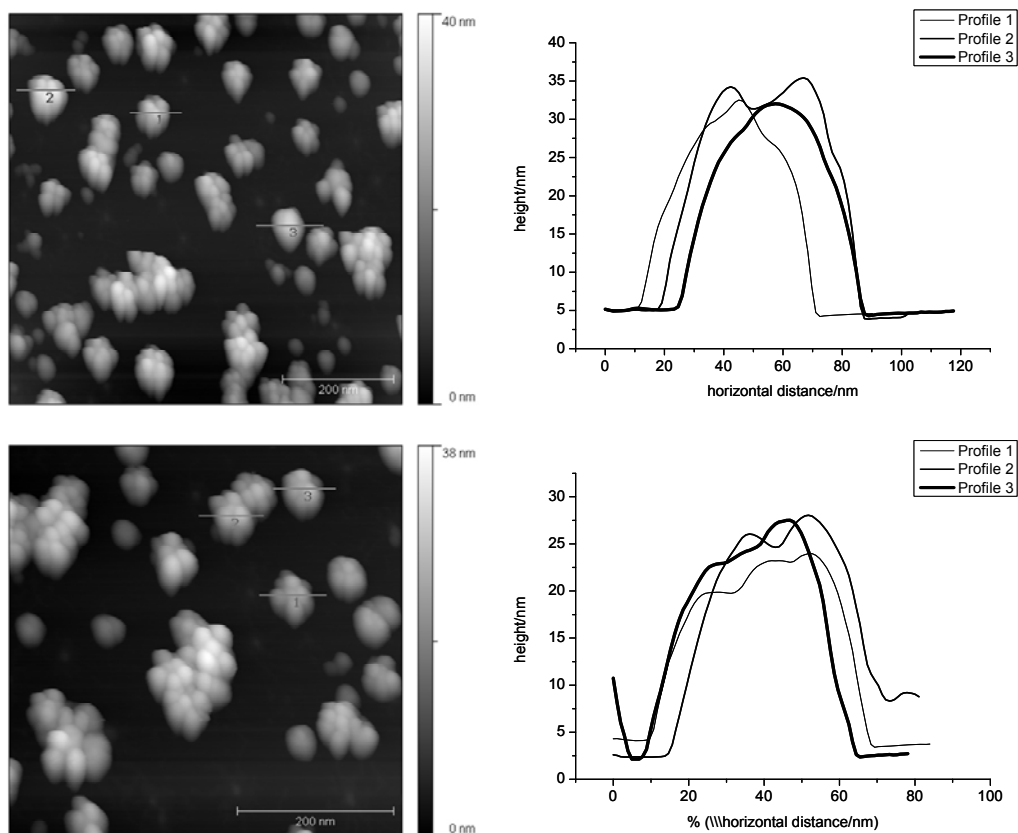


Figure 15: AFM images of PMETA/silica nanoparticles with the respective height profiles

For detailed analysis and in order to verify the construction (silsesquioxane core – bright center in TEM) of the silica/polymer nanoparticles, further data were obtained on the PMETA-based particles using 3D-TEM tomography (Figure 16). 3D-TEM tomography provides evidence that all particles have a less electron-dense core, although sometimes it is not clearly visible in conventional TEM images. The diameter of the central, low-electron-density region is 5 to 7 nm, which is slightly larger than the diameters obtained from conventional TEM. The diameter of the silsesquioxane core particles is 2 to 3 nm⁹¹. As a result, electron tomography shows that there is a gap of ca. 1 to 2 nm, which is presumably filled by the polymer, before the outer silica shell builds.

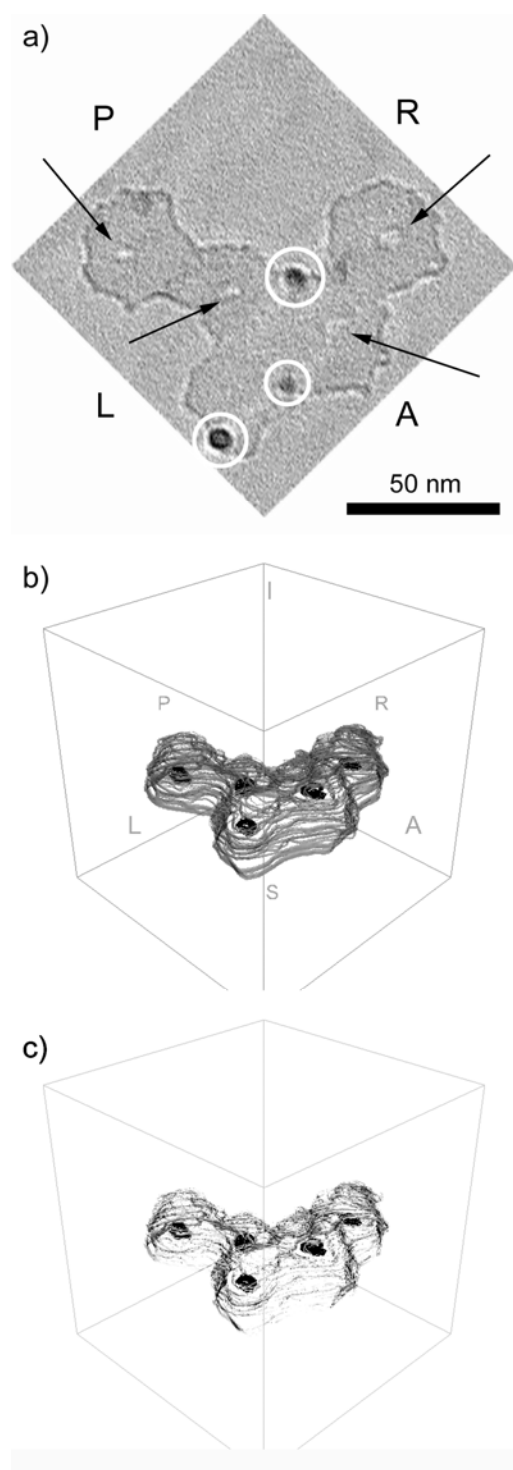


Figure 16: (a) A representative TEM image from a tilt series of silica core-shell nanoparticles with PMETAL cores. The brighter inner parts (arrows) show regions of less electron density. The dark dots (circles) are 5 nm gold particles used to match the single images for 3D reconstruction. The sample is aggregated due to drying on the TEM grid. (b, c) Surface renderings of the sample shown in (a). Panel (b) shows the silica particle surface. Panel (c) is the same tomogram as panel (b), but contrast was adjusted to better show the less electron dense core. Gold dots have been removed from the reconstruction in panels (b, c). Labels (L, R, A, P, I, S) are guides for the eye to simplify navigation in 3D. Panel (a) has been rotated such that all panels (a-c) have the same orientation.

Figure 17 shows small angle X-ray scattering (SAXS) patterns of the silica/polymer nanoparticles. Both samples show s^{-4} decay. Patterns of samples grown with PDMEAMA show an additional $s^{-0.5}$ and samples grown with PMETAI cores, an additional s^{-1} decay. The latter can be assigned to the presence of rod-like features. Closer inspection of the $s^{-0.5}$ decay suggests that it is in fact s^{-1} decay with a small plateau. However as the signal is weak and broad, we cannot unambiguously distinguish between the two. The s^{-4} and s^{-1} decays can be assigned to a two-phase system such as particles in suspension (s^{-4}) and rod-like features (s^{-1}). The reason for the $s^{-0.5}$ decay is unclear at the moment, but the fact that it could also be s^{-1} behavior, suggests that also the samples grown with PDMAEMA contain protrusions and possibly, that the surface of the particles is not perfectly flat.

Moreover, as TEM shows that the particles contain cores with lower electron density, interpretation of the SAXS patterns is not straightforward. The complex composition of the sample could lead to an overlap from hollow spheres and other features and it is therefore not possible to extract more information from the SAXS data. Nevertheless, electron microscopy and SAXS show that the chemistry of the polymer chains on the silsesquioxane cores has a strong influence on the structure of the particles formed after silicification.

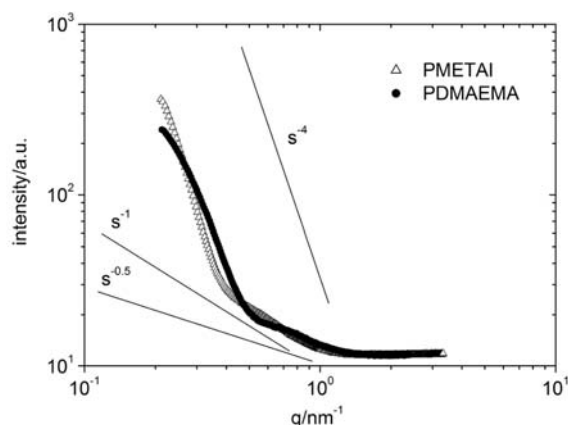


Figure 17: SAXS data of particles grown with the PDMAEMA and the PMETAI core particles.

The different morphologies obtained with the two polymers can be explained as follows. Tertiary or quaternary amine or ammonium groups can act as an “inner” catalyst in the condensation of silica monomers^{63,64,69,138}. In the current study, the initial solution containing the PDMAEMA star polymers is basic (pH 8.7) showing that the PDMAEMA ($pK_a = 7.6$) chains are weakly protonated. As a consequence, the

PDMAEMA chains are less extended but rather collapsed around the silsesquioxane core. In this case spherical particles form upon silicification. The brighter region observed in TEM is assigned to a less electron dense region caused by the silsesquioxane core and parts of the (collapsed) polymer chains. The diameter of the core of ca. 5 to 7 nm suggests that the polymer chains are partially buried in the outer silica shell, leading to a [silsesquioxane/polymer/SiO₂+polymer] trilayer structure of the particles. The reason for the lower density of the core lies in the fact that we do not directly observe the silsesquioxane core (which should have the same density as the other silica), but rather a “composite” central region, where the polymer arms also contribute to the overall electron density. This yields a central region with a density between that of the polymer and the silsesquioxane.

With PMETA1, the striking difference is the presence of the approximately 10 nm rods on the central sphere. The reason for the formation of these rods can be found in the high charge density of the PMETA1 chains, which are (unlike in PDMAEMA) pH-independent. Due to the high number of charges on each chain, the polymer chains are not collapsed onto the silsesquioxane cores, but extend into the solution. A fully extended chain is ca. 60 nm long. As a result, a silsesquioxane with fully extended PMETA1 chains should have a diameter of ca. 120 nm. However, fully extended chains are physically unrealistic. The rods observed in TEM and SAXS, which are only ca. 10 nm long, can therefore be explained by partly extended chains being mineralized. Due to the charge-charge repulsion, in ideal cases, each chain is mineralized individually. Overall, the silicified particles have a [silsesquioxane/polymer/SiO₂ + (partly extended) polymer] trilayer structure.

Overall, AFM, SEM, TEM, and SAXS show that the star-shaped polymers are efficient templates for the synthesis of polymer/silica nanoparticles, containing a central region with a lower electron density. Depending on the chemistry of the polymer surface and the sample treatment, spheres or raspberry-like particles form. This reflects the potential to form complex structures based on the polymers described here.

In order to better understand the formation of these different species, time-resolved pH, ζ -potential, and TEM experiments were performed.

5.2.1.2 *Formation mechanism and growth process of the particles*

Since it is known that amino groups in polymers and therefore also the charges and pH play an important role in the silicification process, time-resolved pH and ζ -potential data for the mineralization of PDMAEMA and PMETA1 stars for three different TEOS concentrations were recorded (Figure 18). With PDMAEMA, the pH of the initial polymer star solution is 8.7 and the ζ -potential rather low (ca. 15 mV) compared to the initial PMETA1 solution (ca. 28 mV with a pH 7.2). This finding supports the above hypothesis of collapsed PDMAEMA and extended PMETA1 chains.

The increase of the ζ -potential could be due to the fact that with the PDMAEMA arms, the pH of the reaction mixture reaches the pK_a value of PDMAEMA, which could result in a more pronounced protonation of the amino groups of the PDMAEMA. In contrast, the PMETA1 is insensitive to protonation. Possibly, there is an additional effect of the iodide counterions, but the details of the initial increase are not clear at the moment.

With the proceeding reaction in the starting period the pH of PDMAEMA decreases to ca. 7.7 which is roughly identical to the pK_a value (7.6) and ζ -potential increases to ca. 30 mV and subsequently decreases again. In contrast to the pH, the ζ -potential shows a strong dependence of the TEOS concentration versus reaction time. We explain this observation with the fact that the solution is buffered at ca. pH 7.7 by the PDMAEMA, which leads to deprotonation of surface silanol groups on the silica particles and hence lower or even negative ζ -potential. Indeed, Pham et al. reported ζ -potential of -20 mV for silica particles at pH 6.67¹³⁹, which is reasonably close to our measurements. The more TEOS is present in the solution, the more silanol groups are present and the more negative the overall potential becomes.

The corresponding data for the PMETA1 stars show that the pH rapidly decreases between 20 and 30 hours from ca. 7.2 to 3-4. Hereabout silica has an isoelectric point (around pH 2.6 to 3)¹³⁹. The decrease is followed by a very slow increase up to 170 hours of reaction. The corresponding ζ -potential increases from an initial value of 28 mV to 40 and 50 mV, followed by a TEOS concentration-dependent decrease. The strongest decrease, to ca. 18 mV is observed for the highest TEOS concentration.

We explain this behavior with an exchange of iodide ions against silicic acid, SiO_4^{4-} (active silica)¹⁷. As a result, iodide is released into the solution and the silicic acid species rapidly react to form SiO_2 . The resulting particles carry a number of positive charges, which are more and more obscured by the growing SiO_2 shell and thus the lowest positive potentials are observed for the highest TEOS concentrations.

Time-resolved TEM experiments (Figure 18) show that the decrease in the pH and ζ -potential is not necessarily correlated with the particle shape. The main result of these experiments is that the rod-like features in the PMETAI samples develop relatively late in the process, suggesting that the PMETAI chains extend throughout the entire spherical shell and are able to template the rods later on, whereas the PDMAEMA is collapsed and may not extend throughout the whole silica shell. The hypothesis of PMETAI chains sticking out of the silica shells even late in the reaction is further supported by the fact that the particles grown with PMETAI show a much lower aggregation tendency than the samples grown with PDMAEMA.

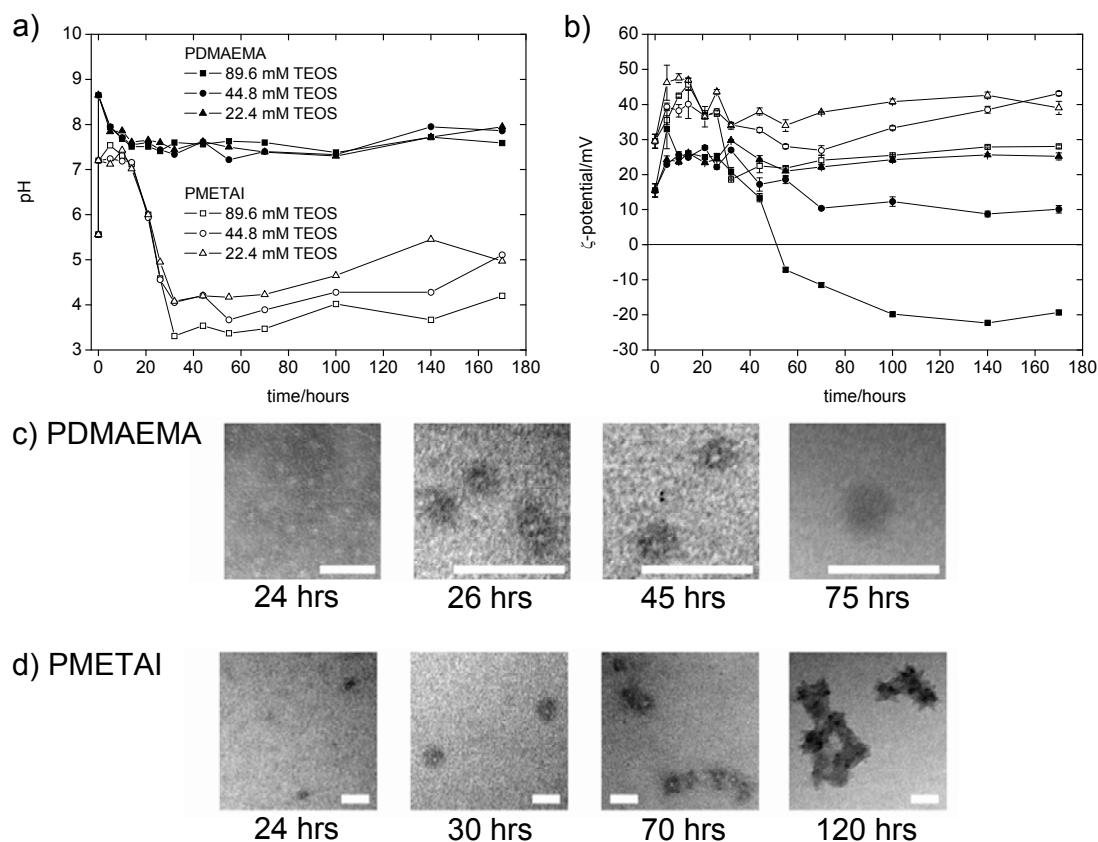


Figure 18: pH and ζ -potential vs. reaction time for PDMAEMA and PMETAI cores at different TEOS concentrations. (a) pH vs. reaction time, (b) ζ -potential vs. reaction time, (c, d) TEM images of samples isolated after different reaction times for both polymer stars. All scale bars are 50 nm.

Figure 19 shows results from time-resolved dynamic light scattering investigations of particle growth. The bubble plots represent the hydrodynamic diameters D_h of samples grown in the presence of PDMAEMA and PMETAI stars versus reaction time. The bubble size is proportional to the intensity-weighted fraction of particles with the respective D_h . There are multiple bubbles for most time values. This is due to the fact that in most cases more than one D_h population was observed, which is in agreement with TEM data. The vertical line in panel (a) highlights the case at 55 hours of reaction time where two populations with different D_h values are observed. Figure 19 indicates that there are significant differences between the two polymer stars. The particle growth with PDMAEMA stars as templates can be divided in three stages. During the first growth period up to 20 hours, the average particle sizes are on the order of 50 to 100 nm. After the reaction time of 20 hours, D_h increases and the most dominant D_h populations are in the range of 500 and 1000 nm. After ca. 55 hours the solution becomes turbid and a large D_h increase is observed. Here, the largest D_h populations are in the range of 3000 and 5500 nm (upper limit of the Malvern Zetasizer Nano ZS). In contrast, with PMETAI stars, D_h increases from ca. 20 nm to approximately 200 – 300 nm at 55 hours. Thereafter bimodal distributions with D_{h1} around 100 nm and D_{h2} between 250 and 380 nm are observed. Typically, D_{h1} is the dominant population, although the populations are quite similar in size.

In summary, with PDMAEMA particles we observe aggregate sizes up to a few micron in diameter and in the case of PMETAI the largest aggregates have a diameter of around 400 nm (Figure 19). In conjunction with TEM, we can also conclude that the features observed in DLS are indeed aggregates and not large single silica particles. Finally, the idea of a single polymer star template per particle is further supported by the fact that AFM shows star diameters of D_{PDMAEMA} of ca. 80 nm and D_{PMETAI} of ca. 100 nm. This is close to the sizes of the mineralized particles with D_{PDMAEMA} of ca. 25 nm and D_{PMETAI} of ca. 50 nm (Figure 14)

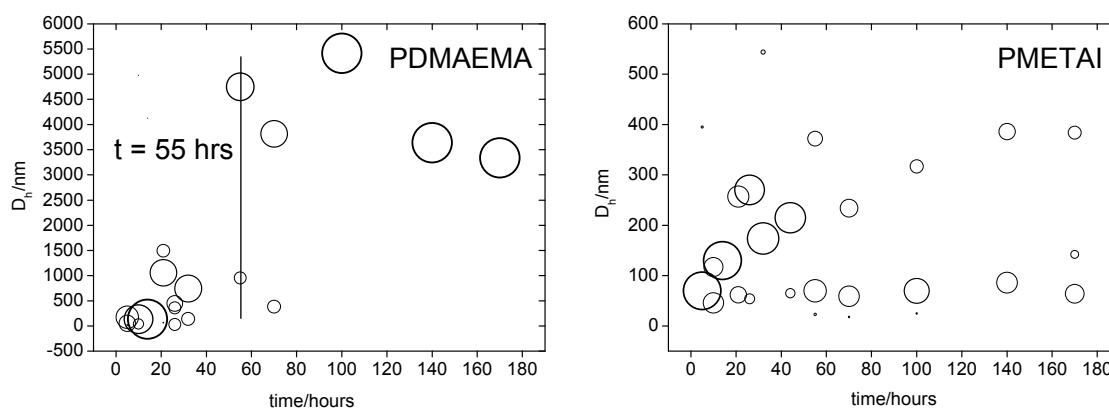


Figure 19: Hydrodynamic diameters D_h of samples grown in the presence of PDMAEMA and PMETAI stars vs. reaction time. Bubble diameters are proportional to the percentage of particles (weighted by intensity) with the respective D_h values. Vertical line in the top panel highlights the transition mentioned in the text. The data shown in the figure are for TEOS concentrations of 44.8 mM.

As aggregation behavior is also influenced by polymer concentration, supplemental DLS studies with respect to a broader range of different polymer concentrations at constant TEOS concentration (44.8mM) were performed, documented by TEM micrographs for the PMETAI polymer system. Figure 20 shows a histogram with R_h of the different polymer starting concentrations resulting either in silica/PDMAEMA nanoparticles or in silica/PMETAI nanoparticles. The form of the histogram was chosen for better visualization of the single data points (each top of the histogram represents a data point and therefore a fixed value for R_h). The data points calculated in mass-weighted fraction by the Kohlrausch-Williams-Watts model (KWW)^{140,141} concerning the silica/PMETAI system, represent a dominant fraction of R_h in the polymer concentration range from 0.05 to 0.5 mg/mL. This development is imaged also by TEM, where particles resulting from a polymer solution of 5mg/ml aggregates significantly (in this case no DLS measurements are presented). The solution of 1mg/ml polymer shows single particles and less aggregates, whereas the aggregation behavior increases again in the range of 0.05 to 0.5 mg/mL. The development follows via a network assembly (0.1 mg/mL - Figure 20: D) and back to aggregated spherical particles with no further bulb structures (0.05 mg/ml - Figure 20: E), and again quite monodisperse spherical particles at the concentration of 0.01 mg/ml. There seem to be two ranges of critical concentrations, above and below 1 mg/mL polymer (untill 0.01 mg/mL), where aggregation is dominant.

The above observations confirm our previous assumption that the silicification of PMETAI arms takes place in the last reaction time step. Depending on the

polymer/silica ratio, large, undefined aggregates, networks or spherical particle aggregates are built. In conclusion, the optimal concentration for the PMETAI/silica system accounts for 1 mg/ml polymer and 44.8 mM silica precursor.

Similar observations were done on the PDMAEMA/silica system where the dominant state of aggregation behavior was determined at the concentration of 0.1 mg/mL polymer and 44.8 mM TEOS (no TEM micrograph data were taken).

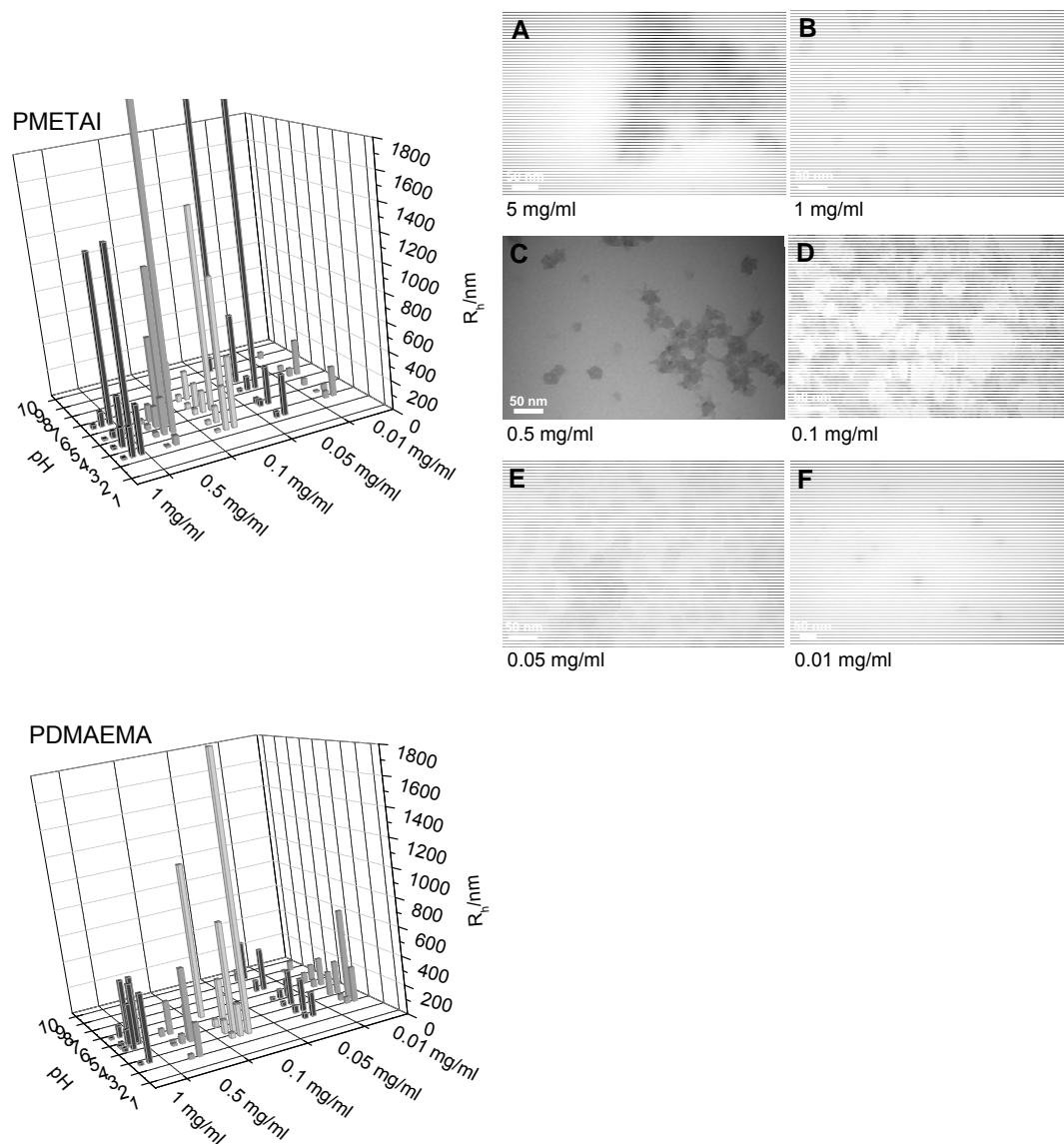


Figure 20: Hydrodynamic radius (R_h) of silica-PDMAEMA and PMETAI particles. At constant silica monomer concentration (44.8 mM) the polymer concentration changes from 0.01mg/mL to 1mg/mL TEM pictures (A-F) were taken for different concentrations of PMETAI particles. The histogram was chosen for better visualizing the data points (each top point of the histogram represents a data point and therefore a fixed value for R_h)

5.2.2 PEI-*b*-PEG / silica system

The PEI-*b*-PEG polymer aggregates offer also a good platform as a suitable template, as shown in the TEM micrographs (Figure 21). The particles, in general, are uniform and small (around 30 nm) but tend to build aggregates. After silicification, ζ -potential and size measurements versus pH were done on this particle system, as shown in Figure 22.

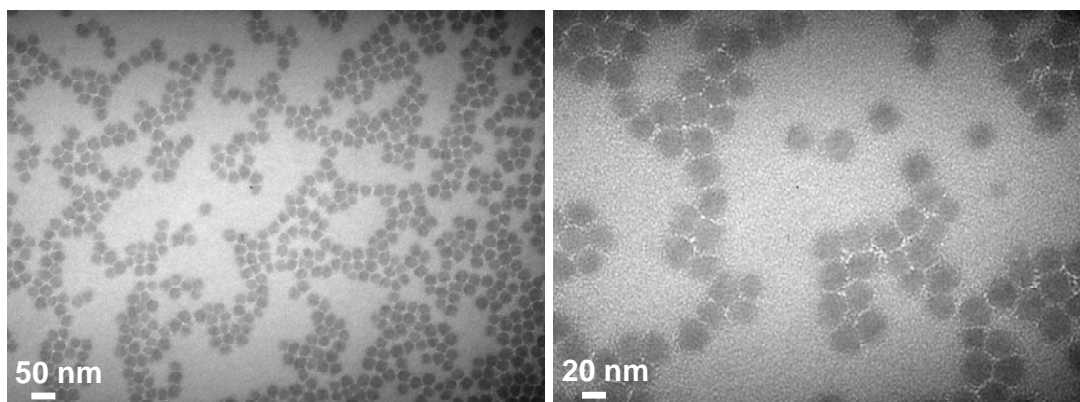


Figure 21: TEM micrographs of PEI-*b*-PEG silica nanoparticles

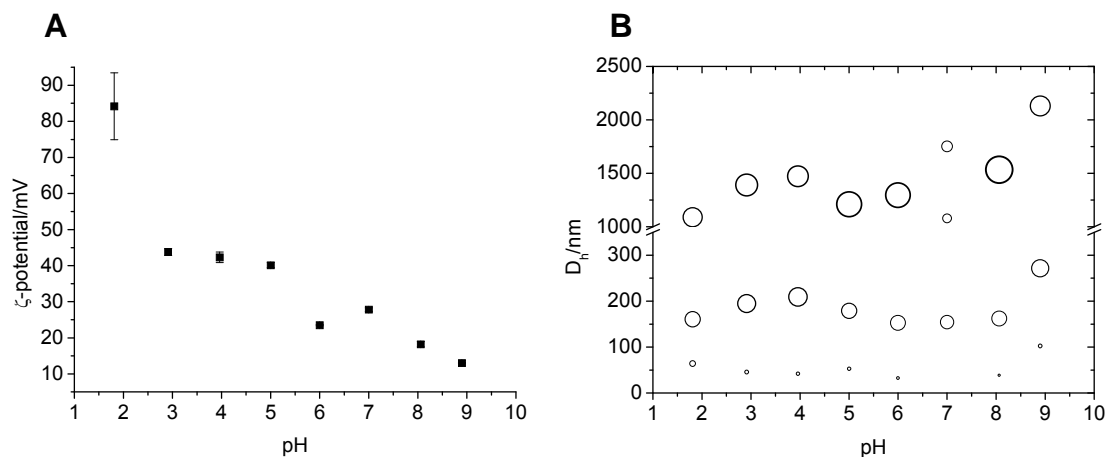


Figure 22: ζ -potential and size measurements on the PEI-*b*-PEG/silica particle system. Bubble diameters are proportional to the percentage of particles (weighted by intensity) with the respective D_h values.

The ζ -potential shows a decrease with increasing pH (Figure 22) comparable to the silica-free PEI-*b*-PEG micelles (Figure 13). Figure 22 B presents the results of aggregate size measurements versus pH. The bubble points represent the

hydrodynamic diameters D_h of PEI-*b*-PEG/silica particles. The bubble size is proportional to the intensity-weighted fraction of particles with the respective D_h . There are multiple points for most pH values. It can be clearly distinguished between three different populations present in the solution. The smallest population represents most likely the single polymer/silica particles in the range of 30 nm, whereas the others either show a size population with the mean value of 200 nm and 1500 nm. That means DLS measurements show that aggregates of defined sizes form. The particle solution appears turbid but no sedimentation could be observed.

In conclusion PEI-*b*-PEG copolymers are suitable templates for the formation of silica nanoparticles, and due to PEI charges may have the potential to encapsulate compounds like biomolecules (DNA, RNA).

5.3 Star-shaped polymer/silica nanoparticles as trapping and carrier systems

In this work, we investigated potential of star-shaped silica nanoparticles to encapsulate (trap) other molecules to evaluate their application possibilities as a carrier system. We applied first a simple, small fluorescent dye, and further increased the system complexity to include metal complexes and bigger molecules, like proteins (hemoglobin). In the case of fluorescent dye, the trapping potential was tested by subsequently changing the pH of the dye/polymer/silica nanoparticles solution. To analyze the polymer/silica particles doped with substances, fluorescence correlation spectroscopy (FCS) and electron paramagnetic resonance spectroscopy (EPR) were employed. Ultraviolet visible spectroscopy (UV-Vis) measurements were done to validate the trapping and activity of hemoglobin in the silica/polymer system.

5.3.1 PDMAEMA / and PMETA / silica systems

5.3.1.1 *Encapsulation of the fluorescent dye sulforhodamine G*

In order to confirm the potential of the star-shaped polymers/silica system to encapsulate substances, studies were performed including the fluorescent dye sulforhodamine G (Figure 23). Sulforhodamine G has the potential to dope the particles on the basis of charge interactions, and additionally the dye is stable in a

broad pH range (2-10). The anionic dye sulforhodamine G electrostatically interacts with the positively charged star-shaped polymers when mixed before silicification. Consequently, the proof whether the polymer is encapsulated in the silica shell, is obtained by the detection of fluorescent nanoparticles. Non-encapsulated polymer can easily be discriminated from the encapsulated one by measuring the characteristic diffusion time by FCS. It has to be mentioned that the dye/PDMAEMA/silica system tends to aggregate less in acidic environments.

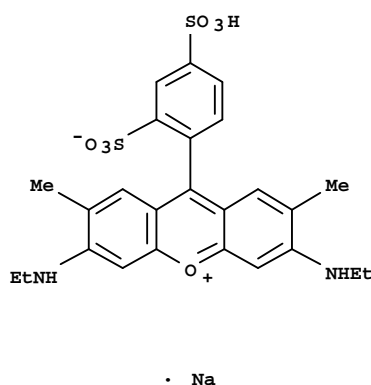


Figure 23: Chemical structure of a water soluble dye, sulforhodamine G

It is known that buffer salts can influence the system because of the ionic strength dependence which will attribute beside pH an additional unknown factor for the investigation of the system which we want to exclude. Therefore, the particles prepared by PDMAEMA star-shaped polymer were produced in a non-buffered acidified aqueous solution (pH 3). The synthesis of dye/polymer/silica nanoparticles with the pH independent star polymer PMETA1 was done in untreated deionized water (pH 5.5). The dye/polymer/silica particles were prepared by mixing first the polymer with sulforhodamine G and the addition of TEOS after a short equilibration time.

For interpretation of the system, the free dye (reference system 1), the dye with addition of TEOS (reference system 2) and consequently the dye/silica/polymer system in the respective solution were investigated. In Figure 24; panels 3 and 6 respectively, show the FCS autocorrelation curve of the two different dye/polymer/silica nanoparticles and the respective reference systems 1 and 2. As distinguished from the curves, the diffusion time of the free dye is 30 μ s. Since silica represents a negatively charged surface in solution, the interaction with

sulforhodamine G is nearly zero and the diffusion time is similar to that of the free dye. By measuring the star-shaped polymer alone with sulforhodamine G the deviation of the correlation time is small compared to that of the free dye. This is due to the rather flexible structure of the polymer in solution and the equilibrated diffusion process of free dye. From the autocorrelation curve the presence of polymer/silica/dye particles of the diffusion time about 1ms can be verified for both systems (PMETAI and PDMAEMA). In conclusion, polymer/silica nanoparticles have the ability to encapsulate a fluorescent dye, which can be conveniently studied by FCS and fluorescence microscopy.

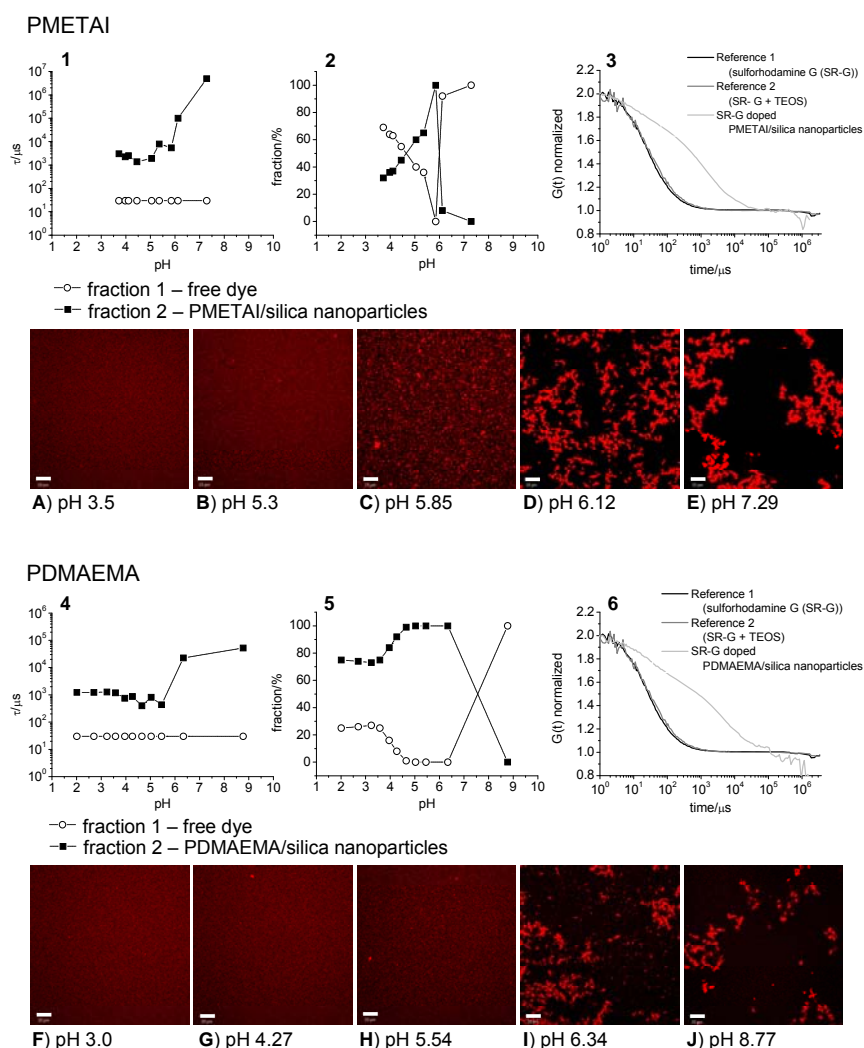


Figure 24: FCS measurements of PMETAI and PDMAEMA silica nanoparticles. Diffusion time of the two fractions (free dye and polymer/silica nanoparticles) obtained from PMETAI and PDMAEMA/silica nanoparticles plotted versus pH (panels 1 and 4). The magnitude of the fractions (in %) plotted versus pH (panel 2 and 5). Normalized autocorrelation curves plotted versus time (panels 3 and 6). Additionally, confocal microscopy images were acquired at different pH values of the PMETAI/silica nanoparticles (panels A - E), and of the PDMAEMA/silica nanoparticles (panel F - J); scale bar: 20 μm .

To further study the properties of the star-shaped polymer/silica systems concerning encapsulation of substances, pH dependent FCS measurements and confocal fluorescence images were acquired. The pH of the initially prepared polymer/silica nanoparticle solution was adjusted stepwise from 3 to 9 with 10 mM NaOH. Fraction 1 in Figure 24 represents the free dye (diffusion time: 30 μ s) and fraction 2 shows the second existing species in the system.

Dye/PMETA/silica nanoparticles at pH 5.5

In Figure 24 (panel 1) the FCS measurements on PMETA/silica nanoparticles demonstrate an increase for fraction 2 with increasing pH whereas fraction 1 represents the diffusion time of the free dye and stays constant. The increase is more significant starting from pH 6 (Figure 24; panel 1). Figure 24 (panel 2) shows a decrease in the percentage of fraction 1 (free dye) with increasing pH and consequently the behavior of fraction 2 is opposite. That means the particles start to aggregate with increasing pH and the remaining free dye from the solution is associated to the growing aggregates. At pH 6, precipitation seems to take place which is also supported by confocal microscopy images (panels A to E). The precipitates change the status of the overall system due to their inertia from dynamic to static. This is indicated by the strong decrease of fraction 2 and a simultaneous rise of fraction 1 (Figure 24; panel 2)). The precipitates are considerable immobile in comparison to the freely diffusing dye or the fluorescent silica nanoparticles, which means that the precipitates are in principle invisible to FCS. Consequently, to determine the relative fraction of fluorescently labeled polymer and/or free dye in this precipitates is not really possible.

Dye/PDMAEMA/silica nanoparticles at pH 3

The same behavior is apparent in the PDMAEMA/silica system. Also here the diffusion time rises with increasing pH. The trend in the relative values of fraction 2 (corresponding to the particles) and of fraction 1 (corresponding to the free dye) are similar to that of the PMETA/silica system (Figure 24; panels 4 and 5). The critical aggregation-precipitation area is likewise reached with pH 6, for the reasons explained above. However, it has to be noted that a transition domain was detected at pH 4.2 for both fractions (Figure 24; panel 5). In that area the diffusion time for fraction 2 stays rather constant and no significant aggregates are detected by

confocal fluorescence microscopy. The only explanation for that phenomenon is the adsorption of remaining free dye to the particles. Results from both FCS and confocal fluorescence microscopy show that sulforhodamine G does not interact with silica indicating that the absorption is due to the PDMAEMA. Based on the predictions that the polymer is covered by a silica shell, the dye has the possibility to diffuse through the silica layer to the polymer.

As PDMAEMA is pH sensitive, in contrast to the quaternized amine in PMETA1, dye release was expected in the former system, which could be a very interesting concept for further biomedical applications. In conclusion, it is clearly visible that the assumed dye release from the polymer/silica particles does not take place at the short time scale investigated here. However these experiments have shown that the star-shaped/silica nanoparticles have the potential to constantly trap and enclose a negatively charged compound in the silica shell over a broad pH range. Possible future applications include fluorescence imaging, catalysis or implementations in the biological area where biomolecules need to be trapped in a protective environment.

5.3.1.2 *Trapping of metal complexes in the polymer/silica nanoparticles*

To prove the encapsulation potential of polymer/silica core-shell structures for metal complexes we applied electron paramagnetic resonance (EPR) studies. With this method it is possible to characterize the first coordination sphere around a paramagnetic metal ion with regard to the geometry, and identification of nuclei with a non-zero spin. For example, in the case of copper(II) ion, which exhibits labile stereochemistry, the values of Spin Hamiltonian parameters can be related to the various distortions of the metal environment, and thus permit to identify different metal coordination zones in the presence of complex polymer systems. Due to its property of allowing fluxional stereochemistry and variable coordination numbers between 4 and 6, the Cu(II) ion is well known to accommodate a large variety of geometrical arrangements in its first coordination sphere. This influences the interactions with the ligand atoms and consequently its physicochemical properties and behavior.

In our study copper(II) trifluoromethanesulfonate ($\text{Cu}(\text{OTf})_2$), also known as copper triflate, was used because of the easy exchange of the triflate with other

ligands in solution and the high affinity of copper to nitrogen^{142,143}. Thereby, the different complex binding forms can be distinguished and conclusions can be drawn from the trapping potential of the polymer towards the metal salt.

Analogously to the fluorescent dye trapping method discussed above the copper salt was mixed with the polymer and subsequently TEOS was added to initiate the silica shell formation.

Metal/PDMAEMA/silica nanoparticles at pH 3

The results from metal complex/PDMAEMA/silica nanoparticles at pH 3 are presented in Table 1 and in Figure 25.

Because the magnetic field in EPR is applied in z-direction decisive conclusions can be made by comparing the z-gyromagnetic tensors as well as the z-hyperfine interactions. Changes in gyromagnetic tensors correlate also with changes in the symmetry.

Sample	System	g			A [mT]		
		g_{xx}	g_{yy}	g_{zz}	A_{xx}	A_{yy}	A_{zz}
A1	PDMAEMA + Cu(OTf) ₂	2.048	2.074	2.362	2.3	2.6	14.5
A2	Cu(OTf) ₂ /PDMAEMA/silica nanopart.	2.077	2.077	2.375	0.5	0.5	14.3
A3	Cu(OTf) ₂ + TEOS	2.079	2.079	2.381	0.5	0.5	13.6
A4	Cu(OTf) ₂	2.078	2.078	2.381	0.5	0.5	13.6

Table 1: Spin Hamiltonian parameters of the Cu(II) paramagnetic species formed by the addition of Cu(OTf)₂ in acidic aqueous solution (pH 3). A1) PDMAEMA + Cu(OTf)₂; A2) previously mixing of PDMAEMA Cu(OTf)₂ and subsequent addition of TEOS to form the metal/polymer/silicacore-shell nanoparticles; A3) silica precursor (TEOS) + Cu(OTf)₂; A4) Cu(OTf)₂. Each sample was prepared in acidic solution pH 3. (g) is the gyromagnetic tensor and (A) is the hyperfine interaction.

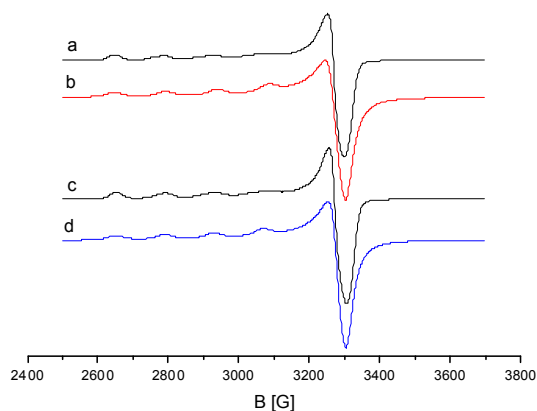


Figure 25: EPR spectrum of copper in the Cu(OTf)₂/PDMAEMA/silica nanoparticles system (a) (sample A2 in Table 1), and its simulated spectra (b). For comparison, the spectrum of Cu(OTf)₂ is shown in (c), together with its simulation (d).

The comparison of the Spin Hamiltonian parameters obtained for the metal salt at pH 3 when mixed with TEOS (A3) indicates that TEOS neither complexes the metal, nor changes the geometry of copper triflate arrangement, compared to the $\text{Cu}(\text{OTf})_2$ in solution (A4, Table 1). However, when the metal salt is added to the star-shaped PDMAEMA alone (A1, Table 1), there is a change of the gyromagnetic tensor (values and symmetry), and a slight increase in the hyperfine coupling constants. The slight change in the geometry of the metal environment together with the increase in the hyperfine interaction leads to the supposition that the metal is trapped in the polymer system.

In conclusion, the results indicate that the geometry of the metal complex trapped inside the polymer system is not disturbed when the polymer/silica nanoparticles form. In order to monitor the first deviation of absorption, the double integrals of the EPR spectra were calculated. Integral A4 shows the complete paramagnetic species $\text{Cu}(\text{OTf})_2$ in aqueous solution whereas the increasing integrals (from A3 to A1) presents the appearance of a silent $\text{Cu}(\text{I})$ specie which is not detectable in EPR and therefore lower the integral height. The change of $\text{Cu}(\text{II})$ to $\text{Cu}(\text{I})$ species can be due to the presents of PDMAEMA which means that the copper salt is trapped by the polymer (Figure 26).

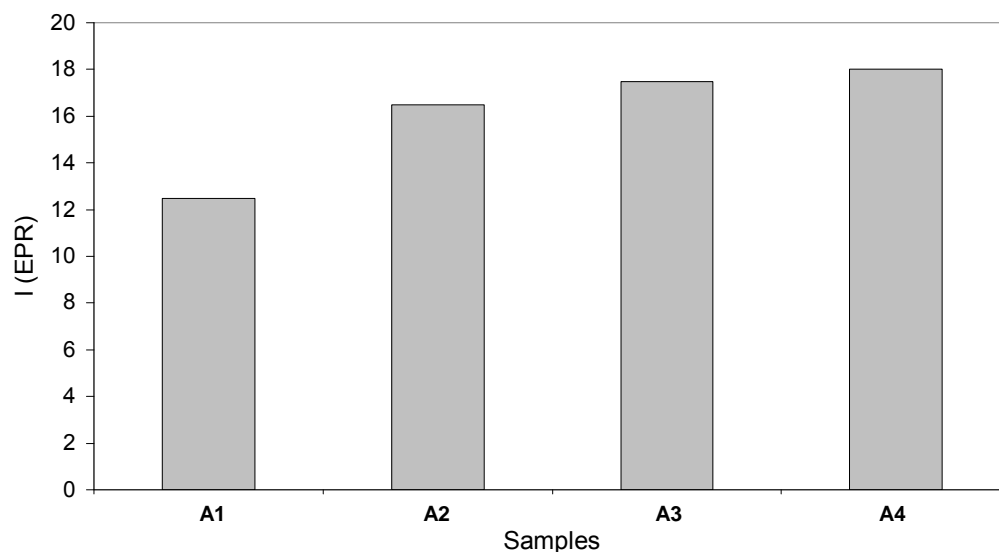


Figure 26: Integrals of the EPR spectra for different PDMAEMA-based systems. Denotation A1 – A4 is the same as in Table 1.

Metal/PMETA/silica nanoparticles at pH 5.5

The results from metal/PMETA/silica nanoparticles at pH 5.5 are presented in Table 2 and in Figure 27.

Here also, the z-gyromagnetic tensors as well as the z-hyperfine interactions were compared.

Sample species	System	g			A [mT]		
		g_{xx}	g_{yy}	g_{zz}	A_{xx}	A_{yy}	A_{zz}
B1	PMETA + Cu(OTf) ₂	2.077	2.077	2.375	2.2	2.2	13.7
B2 X Y	Cu(OTf) ₂ /PMETA/silica nanopart.	2.083	2.083	2.375	0.5	0.5	13.5
		2.083	2.083	2.427	0.7	0.7	11.0
B3 X Y	Cu(OTf) ₂ + TEOS	2.081	2.081	2.381	1.5	1.5	14.0
		2.084	2.084	2.426	1.8	1.8	11.2
B4	Cu(OTf) ₂	2.129			-	-	-

Table 2: Spin Hamiltonian parameters of the Cu(II) paramagnetic species formed by the addition of Cu(OTf)₂ in aqueous solution (pH 5.5). B1) PMETA + Cu(OTf)₂; B2) PMETA/silica nanoparticles previously mixed with Cu(OTf)₂ before silicification; B3) silica precursor (TEOS) + Cu(OTf)₂; B4) Cu(OTf)₂ in aqueous solution (pH 5.5). (g) is the gyromagnetic tensor and (A) is the hyperfine interaction.

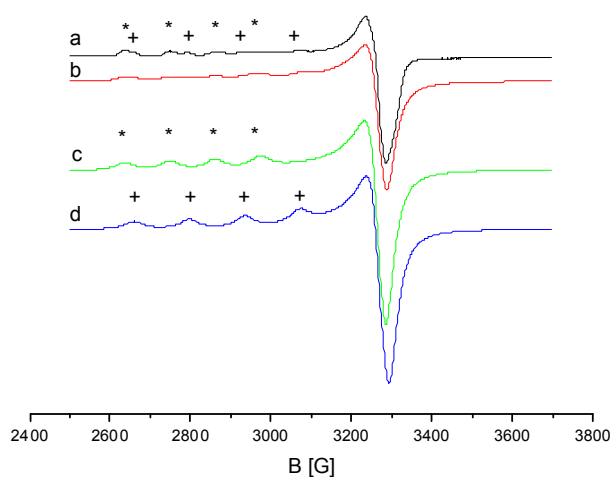


Figure 27: EPR spectrum of copper in the Cu(OTf)₂/PMETA/silica nanoparticles system (a) (sample B2 in Table 2), together with its simulated spectra (b), based on simultaneous presence of two paramagnetic species: X (c) and Y (d). * indicates the peaks from X species in the parallel region of EPR spectrum. + indicates the peaks from Y species in the parallel region of EPR spectrum.

EPR spectrum obtained from the metal salt in water compared to that one in pH 3, is very broad and without a resolved hyperfine pattern associated to the interaction between the unpaired electron and the metal center (B4, Table 2). In this respect only the isotropic gyromagnetic factor can be calculated, and its value shows that copper is surrounded by water molecules, as expected due to the strong coordination character of water molecules compared to that of triflate. When the metal salt was mixed with TEOS in acidic solution, a very different EPR spectrum was obtained, with an overall shape indicating the presence of two paramagnetic species (B3: X and Y). While the Y species has EPR parameters indicating water coordination around the metal, and thus corresponds to a completely hydrated metal, the EPR parameters of the X species are different. That means in acidic solution a small fraction of the metal complex associates with TEOS.

When the metal salt is added to a solution of polymer (B1), there is only one paramagnetic species, with slightly different EPR parameters compared to the X and Y species in the reference system B3. When metal/PMETAI/silica nanoparticles (B2) are measured, the overall shape of the EPR spectrum indicates the presence of two paramagnetic species. One of them being the one with water in the coordination sphere of the metal and the other one announce the coordination of the copper to the polymer. The slight change in the geometry of the metal environment together with the increase in the hyperfine interaction leads to the supposition that the metal is trapped in the polymer system, but differently than with PDMAEMA.

In conclusion, the formation of PMETAI/silica nanoparticles implicates only a partial ability of complexing and trapping the metal inside the polymer system. As the quaternized ammonium, with iodide as a counter-ion, has a different chemical surrounding compared to the tertiary amine in PDMAEMA, suggestions can be made that the complexing of copper by the quaternized amine is disabled. A different complexing process could take place, related to the presence of ester groups in the polymer (Scheme 2). This would explain the presence of the second species (besides that one where water is coordinated), which are also different from the paramagnetic species in the PDMAEMA system. In the latter, the protonated tertiary amine group is available, not connected to a counter-ion and is highly attracted to copper. The ester groups in that case are the minor points. In the PMETAI polymer the quaternized amine is not that attractive to copper also because of sterical

features of the iodide. Additionally, the ester group becomes predominant in that system, as copper can also coordinate here. Another possibility can be the reaction of the counter-ion iodide with copper(II) salt, resulting in the silent copper(I) iodide.

The descriptive use of the double integral of the EPR spectra in the case of PMETA1 is not really appropriate due to the presence of two paramagnetic species in some of the stages (B2 and B3). Moreover, the overall shape of the free metal salt in water (pH5.5) compared to that one in pH3 (Figure 26), is extremely broad. Therefore, only a very rough comparison will be presented in Figure 28. B2 together with the control samples B1 and B3 are presented in order to show the total intensity of the spectra of polymer/silica nanoparticles,

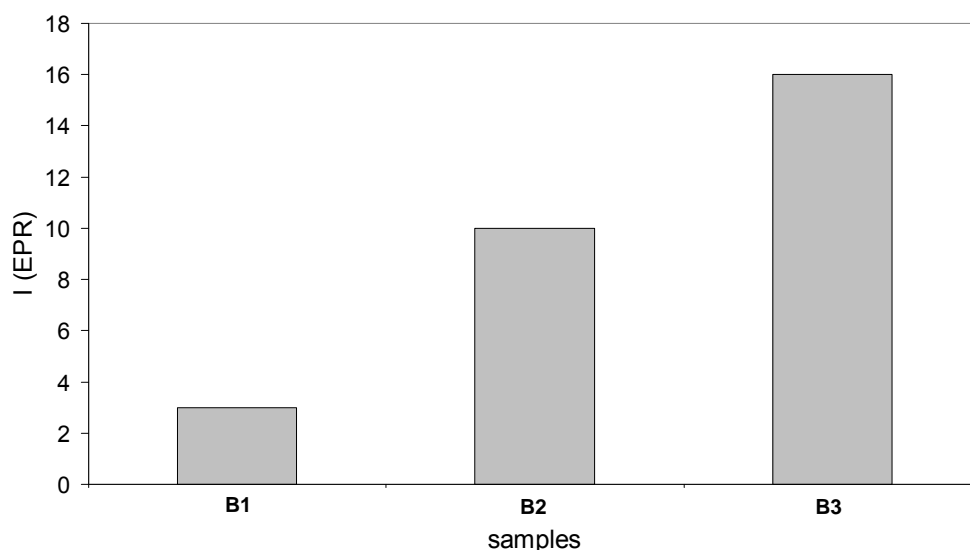


Figure 28: Integrals of the EPR spectra for the different PMETA1-based systems. Denotation B1 – B4 are the same as in Table 2

Even if the comparison is not quantitative, it is possible to see that in the case of the free polymer system the intensity of the EPR spectrum decreases significantly, therefore the change of Cu(II) to Cu(I) is more significant than in the case of the first polymer type (PDMAEMA). However, this change can be caused by the coordination of the copper to the polymer (either quaternized amine or ester group) and therefore the copper will be also encapsulated in the silica system. But most probably there is a reaction of copper (II) salt and the polymer counter-ion iodide taking place, resulting in copper (I) iodide. In that case the copper will not be coordinated to the polymer and consequently is not encapsulated in the silica shell.

5.3.1.3 Trapping of hemoglobin in the polymer/silica nanoparticles

The following experiments were performed to test the encapsulation capabilities of polymer/silica systems with regard to large molecules, e.g. biomolecules. The model protein used here was hemoglobin.

Hemoglobin consists of four polypeptide subunits (two pairs of α and β subunits), each subunit has one non-covalently bound heme prosthetic group which comprises an iron atom (Figure 29).

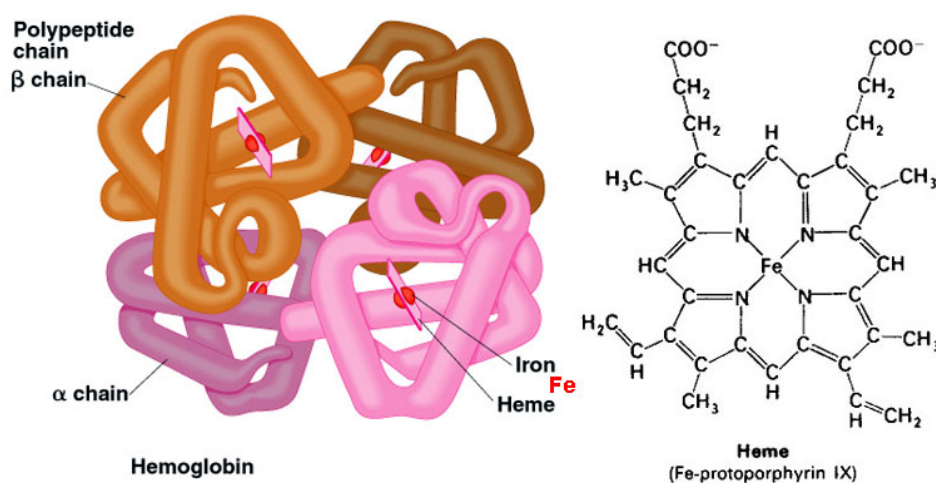


Figure 29: Scheme of hemoglobin ¹⁴⁴

Hemoglobin is an interesting biomolecule from the protein-folding point of view, with regard to the proper folding and assembly of the subunits to form the appropriate quaternary structure, necessary for the native hemoglobin. It has a general slightly negative net charge. It is an easily available complex protein with a general slightly negative net charge ¹⁴⁵ and was chosen to investigate the encapsulation capacity of our polymer/silica systems.

In order to observe whether hemoglobin is incorporated in the polymer/silica nanoparticle, the protein was labeled with 5(6)-carboxyfluorescein N-hydroxysuccinimide ester (6-FAM), and the fraction of incorporated protein was determined using FCS.

Labeling of hemoglobin

Hemoglobin was labeled with fluorescein according to the protocol of Molecular Probes™ 146. The labeling efficiency was detected by UV-Vis and was calculated at 1.109 moles dye per mole hemoglobin.

Similarly to the measurements with the fluorescent dye sulforhodamine G and the metal salt Cu(OTf)₂, the star-shaped polymer was previously mixed with the fluorescein-labeled hemoglobin (Hem-(6-FAM)), and subsequently the silicification was started with the addition of TEOS.

For the encapsulation process, different pH conditions for the star-shaped polymers were chosen. Concerning PMETA1, the synthesis was performed in aqueous neutral conditions (pH 5.5) whereas the synthesis with PDMAEMA was carried out starting with the solution pH of 3 (similarly to the conditions of sulforhodamine G and metal salt encapsulation; Chapter 5.3.1.2 and 5.3.1.3)

Hemoglobin/PMETA1/silica nanoparticles at pH 5.5

In the neutral (pH 5.5) environment, the free Hem-(6-FAM) (Table 3 (C1)) has a diffusion time τ_D of 186 μ s, which corresponds to a hydrodynamic radius of 3.0 nm. This is in good agreement with the theoretical radius of hemoglobin (64500 kDa) of 2.8 nm.

	Sample
C1	Hem-(6-FAM)
C2	Hem-(6-FAM) + TEOS
C3	PMETA1 + Hem-(6-FAM)
C4	Hem-(6-FAM)/PMETA1/silica nanoparticles

Table 3: Reference systems and samples measured by FCS (star-shaped polymer PMETA1).

If Hem-(6-FAM) is measured in the presence of TEOS (C2), there are two populations present. According to the fit of the autocorrelation function, the first population is the fraction of free, labelled protein (as a major component), and the second one shows a significantly higher diffusion time ($\tau_D = 7.5$ ms), but the fraction percentage is less than 6%. This represents the fraction of unspecifically bound Hem-(6-FAM) to TEOS, reflected by the presence of aggregates (Figure 30 (C2))

No free hemoglobin was detected in the reference sample consisting of Hem-(6-FAM) and PMETA1 without any addition of TEOS (C3). Here also two populations of aggregates are present: small aggregates ($\tau_D \approx 10.2$ ms) as a major component, and big aggregates ($\tau_D \approx 89.2$ ms), not more than 10% as shown in Figure 30 (C3).

When Hem-(6-FAM) had been previously mixed with the star-shaped polymer (PMETAI) and afterwards TEOS was added, initiating the silica shell formation (C4), there is no free Hem-(6-FAM) detected, but likewise the two populations of aggregates are present: small aggregates ($\tau_D \approx 5.2$ ms), and big aggregates ($\tau_D \approx 39.2$ ms). They are present in different proportions, but the population of small aggregates is still the major component as shown in Figure 30 (C4).

We considered the PMETAI/silica core-shell nanoparticles as spheres with a diameter of $\sim 40 - 50$ nm. The diffusion time of $\tau_D \approx 5.2$ ms can be calculated to a diameter of approximately 160 nm, which leads to the conclusion that the solution contains quite monodisperse polymer/silica nanoparticles (perhaps 4 aggregated particles) with trapped haemoglobin. The smaller fraction represents bigger aggregates of particles in that sample volume. However, we cannot exclude the presence of hemoglobin on the outer silica shell of the particles even if this proportion will be rather small based on the control measurements (Figure 30 (C2)). Explicit proof has to be obtained by other methods.

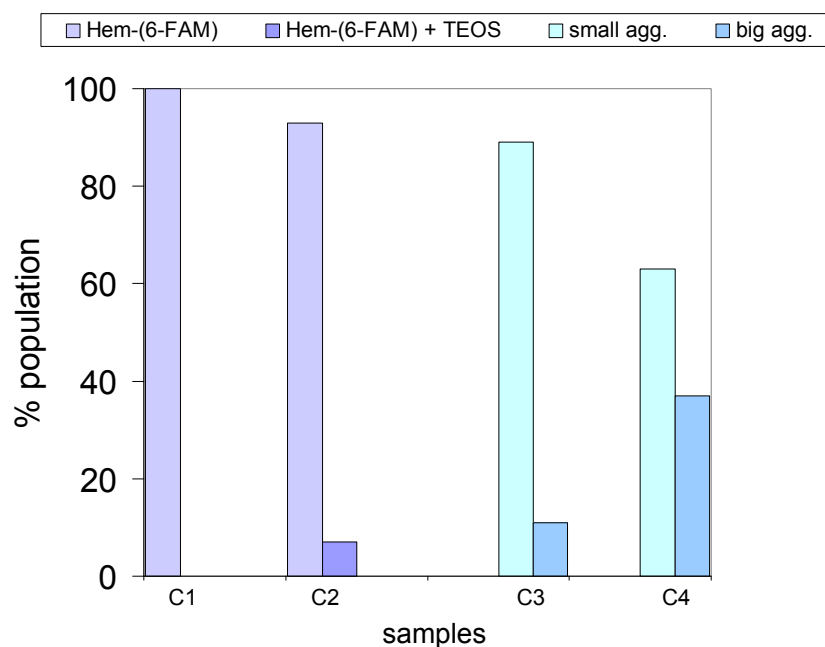


Figure 30: Encapsulation of hemoglobin in polymer/silica particles: (Hem-(6-FAM)) (C1) in water (pH 5.5); Hem-(6-FAM) with the silica precursor (TEOS) (C2); Hem-(6-FAM) with the star-shaped polymer (PMETAI) (C3); and the Hem-(6-FAM)/PMETAI/silica nanoparticle system (C4)

Hemoglobin/PDMAEMA/silica nanoparticles at pH 3

The Hem-(6-FAM) encapsulated PDMAEMA/silica nanoparticles were prepared in acidic conditions (pH 3). In the presence of Hem-(6-FAM) mixed with TEOS (D2), two populations are determined. According to the fit of the autocorrelation function, a small fraction of free protein, and a second major population (approx 72 %) with a significantly higher diffusion time ($\tau_D = 7.2$ ms) are present in the sample. This indicates that in acidic pH the interaction of the partially protonated hemoglobin with TEOS is predominant and complicates the interpretation of the data (Figure 31 (D2)).

	Sample
D1	Hem-(6-FAM)
D2	Hem-(6-FAM) + TEOS
D3	PDMAEMA + Hem-(6-FAM)
D4	Hem-(6-FAM)/PDMAEMA/silica nanoparticles

Table 4: Reference systems and samples measured by FCS (star-shaped polymer PDMAEMA).

If Hem-(6-FAM) is mixed with the star-shaped PDMAEMA without the addition of TEOS two populations exist: one represents free hemoglobin (major component, Figure 31 (D3)), and the second one represents small aggregates ($\tau_D \approx 3.6$ ms). This leads to the conclusion that the association of hemoglobin to the polymer accounts only for 10-20%, contrary to the PMETA polymer where all the protein is trapped inside the aggregates formed together with the polymer.

When hemoglobin is incorporated in the PDMAEMA/silica nanoparticles, there is still free hemoglobin present but in a low proportion. The second major population of small aggregates ($\tau_D \approx 2.1$ ms) is shown in Figure 31 (D4).

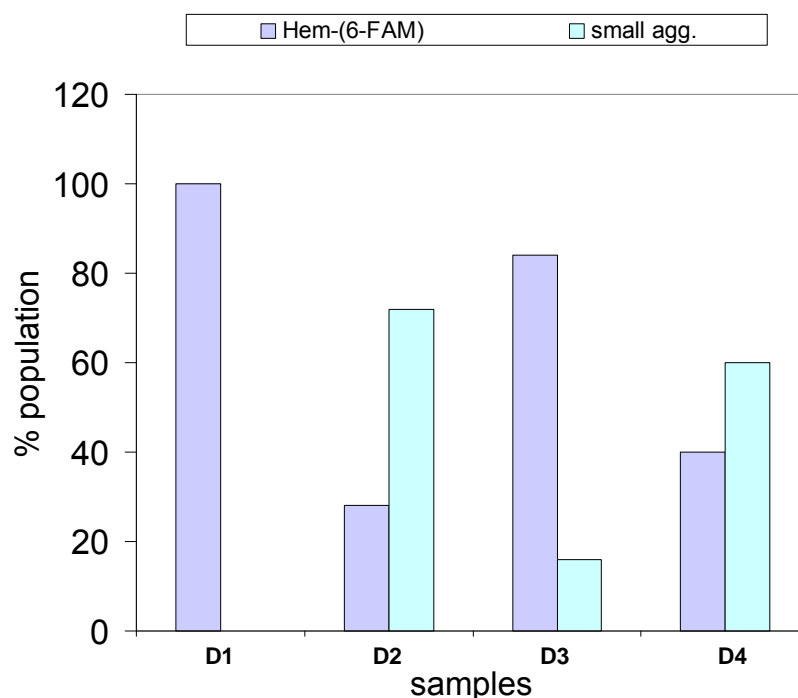


Figure 31: Encapsulation of labeled hemoglobin in polymer/silica particles: (Hem-(6-FAM)) (D1) in water (pH 3); Hem-(6-FAM) with the silica precursor (TEOS) (D2); Hem-(6-FAM) with the star-shaped polymer (PDMAEMA) (D3); and the Hem-(6-FAM)/PDMAEMA/silica nanoparticle system (D4)

Based on the approximate diameter of 15 – 25 nm of the PDMAEMA/silica core-shell nanoparticles, the diffusion time of the small aggregates ($\tau_D \approx 3.6$ ms) represents a diameter of ~ 120 nm and predicts a number of about 6 aggregated PDMAEMA/silica nanoparticles containing hemoglobin. Also here we cannot exclude the presence of hemoglobin on the outer silica shell, because the protein comprises amino groups which can catalyze, independently from the polymer the silica-shell formation. However, no particular structures are visible by TEM (Figure 32 (A)). On the other hand, the Hem/PMETA/silica system showed bloated spherically shaped nanoparticles in TEM (Figure 32 (B)). The suggestion is that encapsulated hemoglobin caused these changes in shape and in size, compared to star-like aggregates obtained without hemoglobin.

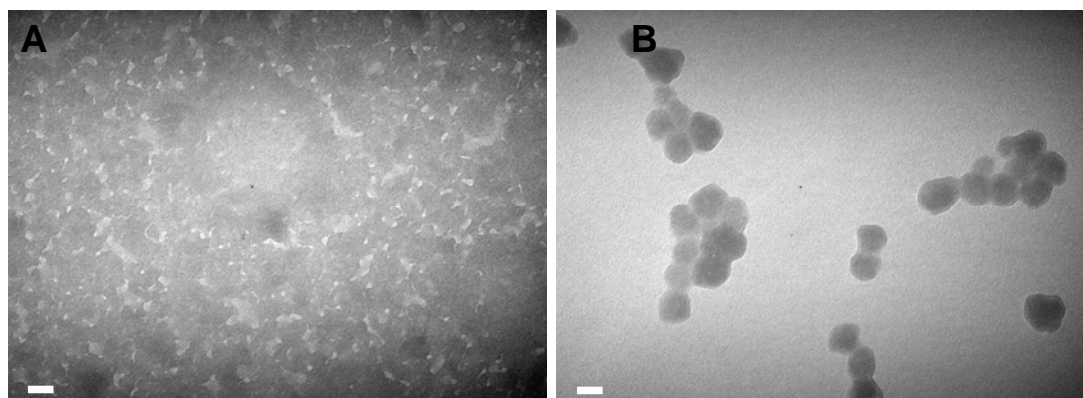


Figure 32: TEM micrographs of (A) hemoglobin reacted with TEOS. (B) Hem/PMETA/silica core-shell nanoparticles. The scale bar is 50 nm.

Comparing the two Hem-(6-FAM)/polymer/silica systems the aggregation in samples with the star-shaped PDMAEMA is in general smaller than with the PMETA system.

The examination of both polymer/silica systems on the basis of hemoglobin encapsulation, points out that PMETA is able to trap completely the hemoglobin amount inside two different aggregate populations, while in the case of PDMAEMA free hemoglobin still remains in solution (approximately 40%).

This is contrary to the results obtained from metal-encapsulating polymer/silica systems. Here, the tendency of completely trapping the metal in the silica surrounding was observed with the PDMAEMA/silica nanoparticles. On the other hand, in the PMETA/silica system some metal was complexed to water or the iodide (free existence in solution). According to that observation we can offer two polymer/silica systems, which can trap different substances most probably due to their difference in charge composition (tertiary or quaternary amines).

5.3.1.4 *Activity test of the trapped hemoglobin in polymer/silica nanoparticles*

To verify if the hemoglobin is encapsulated and protected from the silica shell, digesting experiments were performed by applying the enzyme trypsin to the hemoglobin-containing polymer/silica nanoparticles in solution.

Additionally activity tests were done by UV-Vis measurements. The substrates, potassium cyanide and carbon monoxide are known to bind to the active site of hemoglobin and thus change the conformation of the iron. By observing the

changes in UV-Vis conclusions can be drawn on the activity of hemoglobin in the polymer/silica environment.

Trypsin induced digesting experiments with the hemoglobin/polymer/silica system

Figure 33 shows the UV-Vis measurements of the references hemoglobin alone in solution (A1/B1), hemoglobin after the addition of trypsin (A2/B2), and the hemoglobin-encapsulating polymer/silica system in the presence of trypsin (A3/B3). It is clearly visible that the polymer/silica system with PMETA1 (Figure 33 (A3)) reflects no shift in the wavelength as it would occur with non-protected hemoglobin (A2). This indicates the protection and encapsulation of hemoglobin in the polymer/silica nanoparticles and further demonstrates the diffusion barrier of the silica shell towards larger molecules, like enzymes.

On the other hand, the Hem/PDMAEMA/silica system shows a slight shift in the UV-Vis spectra (Figure 33 B), which indicates that some hemoglobin molecules are accessible to the enzyme. It was shown by FCS measurements with the fluorescein-labeled hemoglobin, that the encapsulation efficiency was decreased compared to the PMETA1 system, and additionally it was detected that hemoglobin builds aggregated structures with TEOS. In conclusion, the protein can be free in solution, attached to the silica surface or partially encapsulated in silica but accessible to enzymes. However the shift in wavelength is not that pronounced like in the reference B3, which leads to the argumentation of hemoglobin still trapped inside the Hem/PDMAEMA/silica nanoparticles.

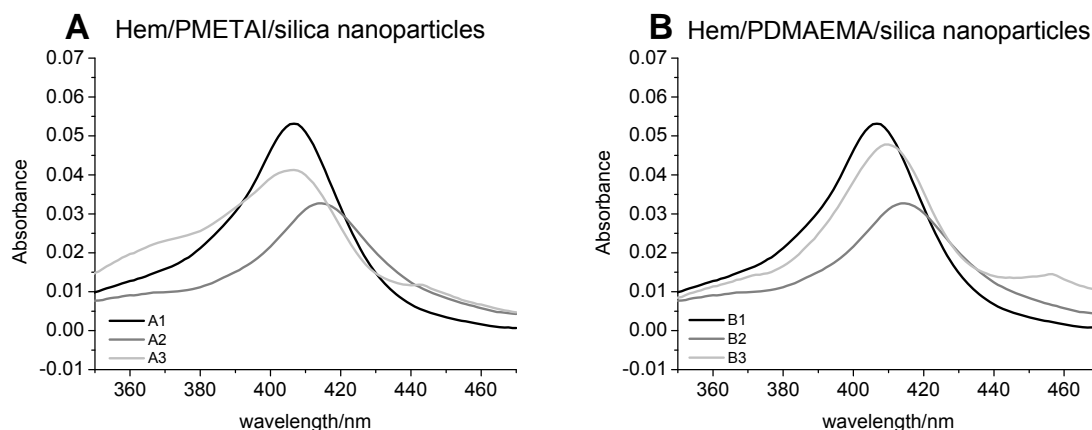


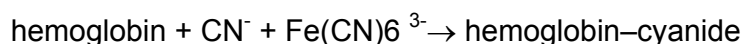
Figure 33: UV-Vis measurements of the trypsin digestion. (A) Hem/PMETA1/silica nanoparticles incubated with trypsin; (A1) hemoglobin; (A2) hemoglobin + trypsin; (A3) Hem/PMETA1/silica nanoparticles + trypsin. (B) Hem/PDMAEMA/silica nanoparticles incubated with trypsin; (B1) hemoglobin; (B2) hemoglobin + trypsin; (B3) Hem/PDMAEMA/silica nanoparticles + trypsin

Activity test by applying potassium cyanide to the Hem/polymer/silica system

Protein conformational motions play a central role in biological processes and provide a dramatic example of the structure-function relationship in proteins. One of the procedures used for the classification and the characterization of the conformational states in hemoglobin relies on determining the binding properties of ligands, such as O₂, CO, CN and NO to the heme iron¹⁴⁷.

Hemoglobin has remarkable oxygen transportation properties, due to the fact that it can change its conformation to accept oxygen (oxyhemoglobin). This process can be inhibited by carbon monoxide, which has 200 times larger affinity to hemoglobin (carboxyhemoglobin) than oxygen. Hemoglobin possesses an iron atom core in its ferrous (Fe²⁺) state. If the iron is oxidized to its ferric (Fe³⁺) state, its oxygen transport capabilities are diminished and the molecule is called methemoglobin (metHb).

Total hemoglobin can be quantified by performing a reaction of hemoglobin with potassium cyanide to form a hemoglobin–cyanide complex.



In our studies we used commercially available human hemoglobin, which is in the state of methemoglobin. The methemoglobin shows maximum UV-Vis signal at 404 nm, which can be shown in the reference sample in Figure 34. If hemoglobin reacts with the cyanide ion, there is a peak shift towards higher wavelength (418 nm). The reference of hemoglobin alone in the solution after addition of cyanide ions shows this shift, as well as the Hem/polymer/silica nanoparticle samples with both polymers (Figure 34). However the shift of the reference sample (hemoglobin + CN⁻ (C2)) in pH 5.5 is not that perfect as the shift of the sample D2, which was measured in pH 3. It seems that the coordination to CN⁻ to the native protein is additionally pH dependent.

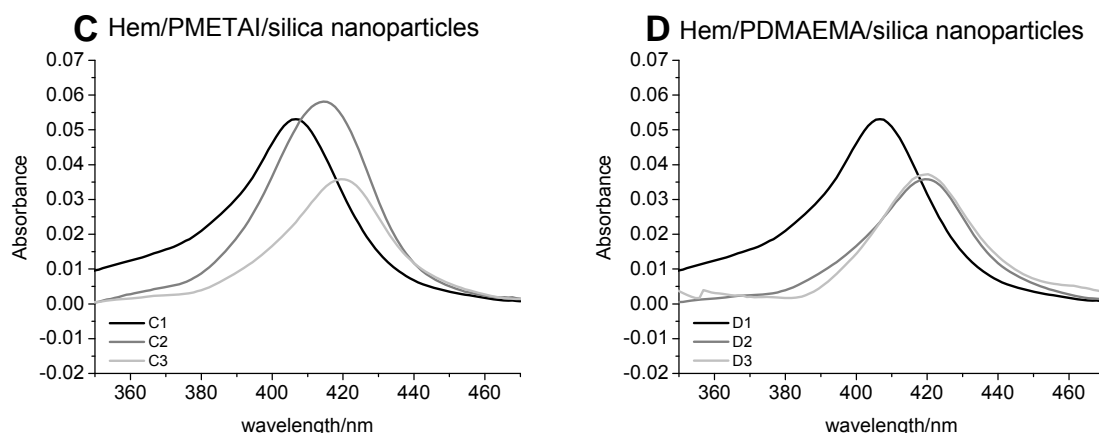


Figure 34: UV-Vis measurements of the Hem/polymer/silica nanoparticles after addition of potassium cyanide. (C) Hem/PMETA/silica nanoparticles + KCN; (C1) hemoglobin; (C2) hemoglobin + KCN; (C3) Hem/PMETA/silica nanoparticles + KCN. (D) Hem/PDMAEMA/silica nanoparticles + KCN; (D1) hemoglobin; (D2) hemoglobin + KCN; (D3) Hem/PDMAEMA/silica nanoparticles + KCN

In conclusion, we showed the access of cyanide ions to the iron site of hemoglobin when encapsulated in the polymer/silica nanoparticles. This demonstrates that the protein remains active inside the particles, even after silicification and independent from the pH.

Activity test by applying CO to the Hem/polymer/silica system

Because CN^- can coordinate to the hemoglobin in the ferrous and the ferric state, the activity concerning the oxygen or CO affinity is not completely proved. Oxygen or CO can only complex to the reduced iron (Fe^{2+}) which implicates the full activity of the protein.

As already mentioned, CO has a 200 times larger affinity to the heme-iron complex as oxygen. In order to test the activity of the encapsulated and trapped protein, reduction process of Fe^{3+} to Fe^{2+} has to be performed before testing the system with CO. For reduction, sodium hydrosulfite (dithionate) was used. The reduction can be monitored by eye because the initially brownish solution changes the color to purple red. By bubbling CO gas through the samples, CO will bind to the reduced iron (Fe^{2+}) in hemoglobin. This process was detected by UV-Vis, where carboxyhemoglobin appears as the maximum at 419 nm.

State of protein	Absorption maxima (nm)			
methemoglobin	404	500	540	576
reduced hemoglobin	428		555	
CN-hemoglobin	418		546	
CO-hemoglobin	419		539	568

Table 5: Optical absorption characteristics of hemeoglobin ¹⁴⁷

Regarding the Hem/PMETA/silica system (Figure 35(E)) as well as the Hem/PDMAEMA/silica system (Figure 35 (F)) the difference in the absorption peak from methemoglobin/polymer/silica nanoparticles (~ 404 nm (Table 5)) and the reduced (Fe^{2+})-Hem/polymer/silica particles (~ 428 nm (Table 5)) is clearly detectable. After bubbling CO gas through the samples hemoglobin encapsulated in both polymer/silica systems (PDMAEMA as well as PMETA) demonstrate the typical absorption spectra of CO bound hemoglobin (~ 419 nm and additionally the double peaks at 539 and 568 nm (Table 5))

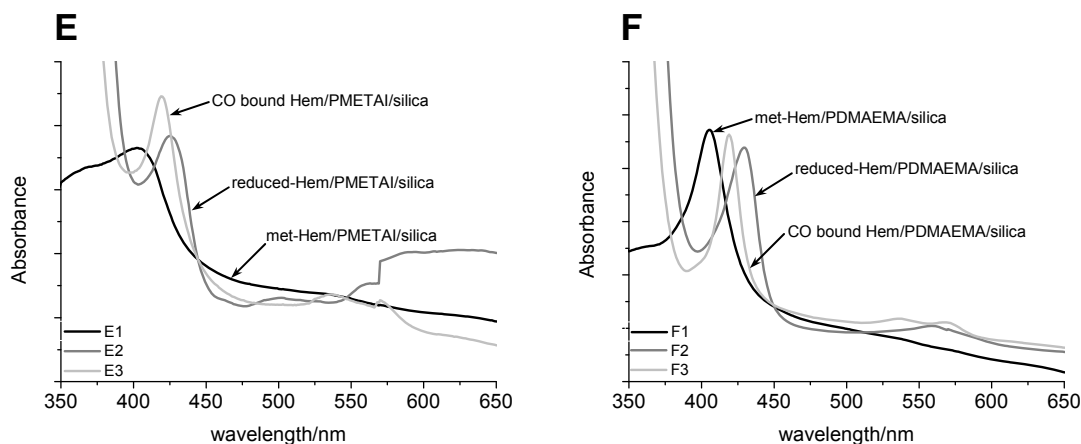


Figure 35: UV-Vis measurements of the Hem/polymer/silica nanoparticles after CO bubbling (E) Hem/PMETA/silica nanoparticles + CO; (E1) Hem/PMETA/silica nanoparticles; (E2) Hem/PMETA/silica nanoparticles + CO. (F) Hem/PDMAEMA/silica nanoparticles + CO; (F1) Hem/PDMAEMA/silica nanoparticles; (F2) Hem/PDMAEMA/silica nanoparticles + CO.

In summary, hemoglobin has been encapsulated and trapped in the polymer/silica nanoparticles and showed to be not hindered concerning the protein folding and therefore retains its activity towards CN^- and CO even when encapsulated in a protective silica shell.

5.4 Silica surface functionalization

Surface modification is usually used to obtain reactive groups on silica nanoparticle surfaces. Most of the recent functionalization reactions concerning surface modifications are based on surface grafting of organosilanes onto silica.

In this thesis, the functionalization was performed by first generating the silica shell with TEOS, and by subsequent addition of a TEOS/APTMS mixture, amine-functionalization was introduced in a post-synthetic step. This synthesis was done in a one-pot reaction step. The advantage of the one-pot reaction is that unnecessary washing and centrifugation steps, which cause aggregation, will be excluded.

As a reference system, bare silica nanoparticles manufactured from inverse microemulsion approach were used for the functionalization. The non-functionalized silica nanoparticles show a homogeneous size distribution ($d \approx 90\text{nm}$) (Figure 36)

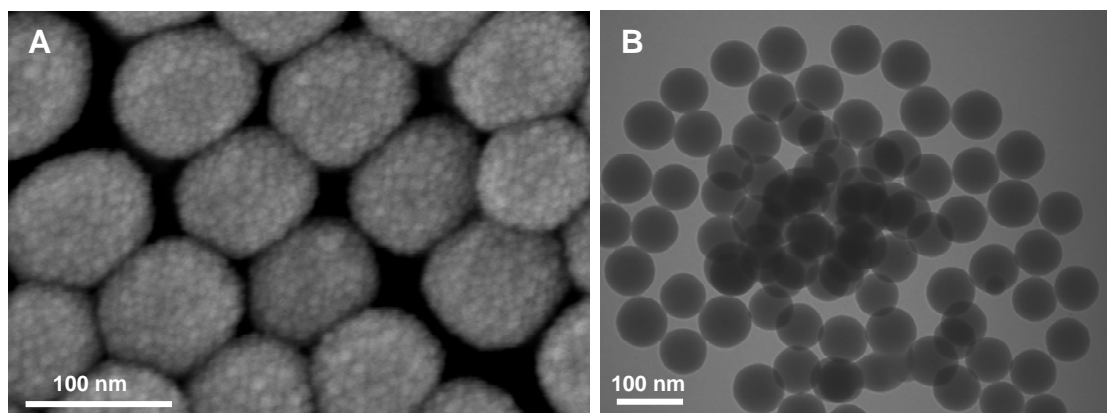


Figure 36: Non-functionalized silica nanoparticles generated from inverse microemulsion. (A) SEM micrograph; (B) TEM micrograph.

PDMAEMA/ and PMETA/silica nanoparticles were functionalized as mentioned above in a post synthetic step with a mixture of TEOS/APTMS. The non-functionalized and functionalized particles were analyzed by elemental analysis. The results are summarized in Table 6.

Sample	Content in %		
	C	H	N
A) SiO ₂ nanoparticles from microemulsion	2.38	1.45	< 0.1
B) NH ₂ -SiO ₂ nanoparticles from microemulsion	9.51	2.51	1.55
C) PDMAEMA/silica nanoparticles	14.05	2.94	1.77
D) NH ₂ -(PDMAEMA/silica) nanoparticles	20.80	3.66	2.96
E) PMETA/silica nanoparticles	8.26	2.33	1.0
F) NH ₂ -(PMETA/silica) nanoparticles	12.99	2.87	1.97

Table 6: Elemental analysis of the non-functionalized nanoparticles (A/C/E) and the amine-functionalized nanoparticles (B/D/F).

It is clearly seen that the amine-functionalized particles show an increase of the C, H, and N content. This leads to the assumption that the particles are covered with propylamine groups, exhibiting the possibility to connect the particles via this amine groups to, e.g. surfaces, or opens the feasibility of further functionalization (e.g. receptors, polymers).

This surface functionalization approach completes the idea of complex multifunctional template-based polymer/silica nanoparticles, assembled according to the LEGOTM brick system approach (Figure 2)

6 Conclusion and Outlook

The current thesis presents a facile route to nano-sized polymer/silica core-shell particles utilizing star-shaped polyelectrolytes and block copolymers as templates. It could be demonstrated that secondary, tertiary and quaternary amines catalyze the hydrolysis and condensation reaction of silicon alkoxide precursors to form a shell embedding the templates. Besides the polymer morphology, it could be shown that also the chemistry of the polymer has an influence on the overall shape of the resulting polymer/silica systems. More complex polymer assemblies, obtained either by a covalent linkage or by the self-assembly approach, can lead to more complex polymer/silica structures.

The naturally occurring diatoms represent the most complex silica structure so far. In order to mimic these structures using the template directed synthetic approach described in this thesis, more research has to be performed in the future towards higher organized supramolecular templated structures. Synthetic PEIs resemble closely the naturally occurring linear polyamines and can serve as ideal candidates to synthesize complex biomimetic silica structures.

Beside the intention to generate complex silica morphologies the polymer template directed synthesis offers the opportunity to utilize the functionality of the polymer for more sophisticated applications.

The advantage of utilizing the silicification process catalyzed by the polymer templates at ambient conditions, offers the opportunity to apply the system to sensitive biological arrangements. The star-shaped polymers allow the entrapment of various compounds like fluorescent dyes, metal complexes or biomolecules by electrostatic interactions. The encapsulation of the polymer/compound composition into a silica shell leads to a protective enclosure of the embedded compound.

For imaging applications, dye-doped nanoparticles containing encapsulated dyes are particularly attractive. The brightness of the fluorescence signal from such imaging probes can be controlled by the number of encapsulated dye molecules per nanoparticle, with the maximum dye density limited only by self-quenching. Dye-doped nanoparticles show often enhanced stability of the encapsulated dye towards bleaching, due to the protective shell.

The encapsulation of transition metal complexes into silica systems offers an attractive method to utilize these systems in catalysis. The provided porosity of the silica shell allows the diffusion of small substrates into the catalytic area. At the same time the entrapped catalysts can be excluded from the reaction solution by simple centrifugation steps.

The advantage to protect encapsulated biomolecules with a silica shell from the unwanted effects of the environment (e.g. digesting by enzymes) plays an important role in biological applications. As mentioned already, above, the silica shell is porous and only small molecules (substrates), can diffuse into the interior of the particles, whereas the encapsulated biomolecule is protected from degradation and can preserve its natural functionality.

In addition to the encapsulation and protection, the use of silica as a shell assembly also opens up the possibility to consecutively further chemically functionalize the outer surface of the silica structures. Depending on the chemical nature of the functionalization, the aggregation of particles can be avoided. Furthermore, other functionalities, e.g. targeting moieties can be attached to the surface to generate highly functional silica shell structures with encapsulated molecules. This opens up a broad range of applications in chemistry and medicine.

In conclusion the polymer template directed synthesis of silica structures offers a broad range of possibilities concerning the functionality and applications.

7 Materials and Methods

7.1 Materials

Star-shaped PDMAEMA and PMETAI

The synthesis and characterization of the templates was reported before ⁹¹. Here we used a star-shaped poly(*N,N*-dimethylaminoethyl) methacrylate (PDMAEMA) and poly[2-(methacryloyloxy)ethyl] trimethylammonium iodide (PMETAI).

Ultrapure water (resistivity of 18 MΩ/cm) from a Millipore water purification system was used in all experiments. For pH adjustments, 0.01 M HCl and 0.01 M NaOH were used.

	M_n [g/mol]	f_n	PDI (in f_n distribution)	P_n	PDI (of arms)
(PMETAI ₂₄₀) ₂₄	$1.8 \cdot 10^6$	24	~ 1.4	240	~ 1.3
(PDMAEMA ₂₄₀) ₂₄	$9.5 \cdot 10^5$	24	~ 1.4	240	~ 1.3

Table 7: poly[2-(methacryloyloxy)ethyl] trimethylammonium iodide (PMETAI) and poly(*N,N*-dimethylaminoethyl) methacrylate (PDMAEMA). M_n : molecular weight; f_n : average number of arms; P_n : degree of polymerization; PDI: polydispersity index

PEG₅₀₀₀-*b*-PEI₅₀₀₀

The polymer was provided by A. Shkilnyy (Prof. A. Taubert; University of Potsdam; germany).

The linear polyethylene imine (PEI) was prepared by ring opening reaction of methyloxazoline and cationic polymerization ¹⁴⁸ resulting in poly(2-methyl-2-oxazoline) (PMOXA). PEG-(tosylate) was added in dry acetonitrile and the reaction was stirred for 24 hrs at 60 - 80°C. The diblock copolymer PEG-*b*-PMOXA was isolated and transferred to HCl-solution (reflux) to obtain the PEG-*b*-PEI hydrochloride.

For a detailed list of materials see Annex 8.1

7.2 Methods

7.2.1 Nanoparticle synthesis

7.2.1.1 *PDMAEMA and PMETA/silica nanoparticles*

A) PDMAEMA/silica nanoparticles

1 mg of PDMAEMA star-shaped polymer was dissolved in 1 mL of water at pH 3. Then 5, 10, or 20 μL (22.4, 44.8, or 89.6 mM) of TEOS were added. The reaction mixture was stirred at room temperature for 72 hrs (3 days) in the general protocol and for 170 hrs (7 days) for the kinetic studies (ζ -potential versus pH measurements). The resulting transparent suspensions were directly used for further analysis.

B) PMETA/silica nanoparticles

1 mg of PMETA star-shaped polymer was dissolved in 1 mL of water at pH 5.5. Then 5, 10, or 20 μL (22.4, 44.8, or 89.6 mM) of TEOS were added. The reaction mixture was stirred at room temperature for 72 hrs (3 days) in the general protocol and for 170 hrs (7 days) for the kinetic studies (ζ -potential versus pH measurements). The resulting transparent suspensions were directly used for further analysis.

C) Amino functionalized polymer/silica nanoparticles

The polymer/silica particles were prepared as described above in A or B: 1mg of the respective star-shaped polymer was dissolved in 1 mL of water at the desired pH. After the addition of 5 μL (22.4 mM) TEOS the solution was stirred for 24 hrs (1 day) at room temperature. The functionalization was started by addition of a mixture of (1 μL APTMS and 4 μL TEOS) in the same reaction solution (one-pot synthesis). The reaction was stopped after 48 hrs and the resulting suspension was lyophilized for the elemental analysis.

7.2.1.2 *PEG-b-PEI/silica nanoparticles*

1 mg of the block copolymer (PEG-*b*-PEI) was dissolved in 1 mL methanol, sonicated and dialyzed (CE, 1000 Da cutoff) three times against 1L of bistilled. H₂O. Then 10 μL (44.8 mM) of TEOS were added. The reaction mixture was stirred at room temperature for 72h (3 days). The resulting transparent suspensions were directly used for further analysis.

7.2.1.3 *SiO₂ nanoparticles from inverse microemulsion*

A) SiO₂ nanoparticles

7.5 mL n-hexane (573 mmol), 1.6 mL (12.6 mmol) n-hexanol and 1.77 mL (3 mmol) Triton® X-100 was mixed at room temperature in a 1 L Erlenmeyer flask by vigorous stirring (700 rpm) for 10 minutes with a magnetic stirrer. Subsequently, 400 μL (22.2 mmol) ultra pure H₂O was added and again stirred for 30 minutes under the same conditions. The solution should be clear. After the addition of 100 μL (3 mmol) tetraethyl-orthosilicate (TEOS) and 60 μL (1.5 mmol) ammonium hydroxide solution (26%) the solution was stirred for 48h (2 days) at room temperature.

B) Work-up procedure:

By addition of 10 mL ethanol to the reaction the particles precipitate. Centrifugation was carried out for 20 minutes at room temperature at 13500 rpm. The pellet was washed three times with ethanol and subsequently resuspended in H₂O. The suspension was directly used for further analysis.

C) Amino functionalized SiO₂ nanoparticles

The microemulsion was prepared as described above. In place of 100 μL (3 mmol) TEOS, 80 μL (2.4 mmol) TEOS was added together with the constant amount of ammonium hydroxide solution (60 μL (1.5 mmol)). After 24 hrs stirring, a mixture of (4 μL APTMS and 16 μL TEOS) was added and the suspension was stirred for 24 hrs.

After the work up procedure (see 7.2.1.3 (B)) the resulting suspension was lyophilized for the elemental analysis.

7.2.2 pH measurements

The pH versus the reaction time was determined with a Mettler Toledo MP 220 pH meter with an InLab 423 electrode. The pH meter was calibrated with standard buffer solutions of pH 4, 7, and 10.

7.2.3 ζ -potential and size measurements

ζ -potentials and hydrodynamic diameters were measured on a Malvern Instruments Zetasizer Nano ZS with a 4 mW He-Ne laser (633 nm) and a detection angle of 173°. Size distributions were determined by fitting the experimental correlation curve to a multi-exponential using the CONTIN algorithm. ζ -potentials were calculated via the Smoluchowski equation¹⁴⁹.

7.2.4 Atomic force microscopy (AFM)

Tapping-mode AFM was performed using a Molecular Imaging PicoLE system with Super Sharp Silicon SFM-Sensors (SSS-NCHR-10, Nanosensor) with a tip radius of 2 nm, spring constant of 10-130 N/m, and resonance frequency of 204-497 kHz (values given by the manufacturer). All measurements were performed at very soft tapping conditions to minimize structural changes of the previously deposited star-shaped polymer. Additionally, imaging was done at low scan speeds (0.1-1 Hz) to minimize lateral forces exerted by the SFM tip on the sample. Samples were prepared from 0.01 wt% solutions in ultrapure H₂O on mica.

7.2.5 Scanning electron microscopy (SEM)

Particle suspensions were diluted 100- fold with ultrapure H₂O and deposited on a mica substrate. The dry samples were coated with platinum (4 nm) in a BalTec MED 020. Samples were imaged on a Hitachi S-4800 with a field emission source at 5 kV.

7.2.6 Transmission electron microscopy (TEM)

Particle suspensions were diluted 100-fold with ultrapure H₂O. 5 μL of the suspension were deposited on a carbon-coated 300 mesh copper grid. After 1 minute, the remaining liquid was removed and samples were imaged with a Philips Morgani 268D with a tungsten source operated at 80 kV.

7.2.7 Cryogenic transmission electron microscopy (cryo-TEM)

Particle suspensions were diluted 100-fold with ultrapure H₂O. 5 μL of the suspension were deposited on a lacey carbon-coated 300 mesh copper grid. Most of the drop was removed with blotting paper. Subsequently, the samples were shock-frozen in liquid ethane and held at approximately 90 K by a temperature-controlled freezing unit. Cryo-TEM experiments were done using a Zeiss 912 Omega Microscope operated at 120 kV.

7.2.8 3D transmission electron microscopy (3D-TEM)

Samples were prepared as above. The tilt series for 3D analysis were acquired in bright-field mode on a Tecnai F20 operated at 200 kV with a 0.23 nm point-to-point resolution and a high-tilt sample holder. Several series of images were recorded on a 2048 pixels x 2048 pixels cooled CDD array detector in different locations of the grid containing the structures of interest. Samples were tilted from -65° to 65°, with an image recorded every 2° between -40 and 40° and 1° elsewhere. During the acquisition, TEM parameters like defocusing, horizontal specimen shift, and specimen tilt were controlled automatically. Calibrated 5 nm diameter gold nanoparticles were added on the grid before acquisition to simplify data analysis.

The Imod software¹⁵⁰ was used for data processing, including alignment of all projections, corrections related to the geometry of the acquisition, calculation of the volume from the series of projections using a back-projection technique¹⁵¹ which leads to a 3D volume image of the sample. ImageJ^{152,153} was used for further data filtering and data reduction. Slicer¹⁵⁴ was used to surface-render the tomograms.

7.2.9 Small angle X-ray scattering (SAXS)

SAXS curves were recorded at room temperature with a Nonius rotating anode instrument (4 kW, Cu K α radiation) with pinhole collimation and a MARCCD detector (pixel size: 79). The distance between sample and detector was 74 cm, covering a range of the scattering vector $s = 2/\lambda \sin \theta = 0.04 - 0.7 \text{ nm}^{-1}$ ($\theta =$ scattering angle, $\lambda = 0.154 \text{ nm}$). 2D diffraction patterns were transformed into a 1D radial average of the scattering intensity. For measurements, samples were placed in quartz Mark tubes (Hilgenberg) with 1 mm in diameter and 10 μm wall thickness. Tubes were sealed before measurement. Concentrations of all samples were 2 mg/mL in water.

7.2.10 Fluorescence correlation spectroscopy (FCS)

Studies were performed with a Zeiss 510 Confocor 2 setup equipped with an argon-ion laser (maximum power 30 mW). 488-nm line of the argon-ion laser was used for the excitation of the 6-FAM (5(6)-carboxyfluorescein N-hydroxysuccinimide ester) and 510 nm line of the argon-ion laser was used for the excitation of the Sulforhodamine G. FCS autocorrelation curves were obtained by exciting a small amount (5 μl) of sample, which was applied to a rigid sample holder (Lab-Tek, NUNC). Improvement of signal to noise ratio of autocorrelation curves was achieved by averaging 5 measurements, each 10 seconds long. The dye concentration used in the trapping procedure was 10nM. The samples (1 mg/ml polymer) were diluted 10 times.

7.2.11 Electron paramagnetic resonance (EPR)

EPR spectra were recorded at 123 K with a CW Bruker ElexSys500 X-band spectrometer, equipped with a helium temperature control system ER4112HV. All measurements were taken using 2 mW microwave power. The modulation frequency was 100 kHz and the modulation amplitude was 0.4 mT; other spectral parameters were adjusted for each spectrum individually. The 3rd-order polynomial averaging was used for subsequent noise reduction. Gaussian line shapes were assumed with

the line-width adjusted for each spectrum. The g -values were referenced to diphenylpicrylhydrazyl (DPPH) ($g = 2.0036$) as an external standard.

7.2.12 UV-Vis spectroscopy

UV-Vis measurements were carried out on a Varian Cary 5000 UV-Vis NIR spectrophotometer (200 – 800 nm) in a 1mL quartz cuvette.

8 Annex

8.1 Materials

8.1.1 Chemicals

(PDMAEMA₂₄₀)₂₄; Prof. A. Müller; University Bayreuth; Germany

(PMETA₁₂₄₀)₂₄; Prof. A. Müller; University Bayreuth; Germany

(PEG₁₁₃)-*b*-(PEI₁₁₃); M_w of each block: 5000 g/mol; Prof A. Taubert; University Potsdam; Germany

Methanol; purum; Schweizerhalle; CAS 67-56-1

Ethanol; puriss, 96%; Schweizerhalle; CAS 64-17-5

n-Hexane; purum, ≥98.0% (GC); Fluka; CAS 110-54-3

Hexanol; puriss, ≥99.0% (GC); Fluka; CAS 111-27-3

Triton[®]X-100; for molecular biology; Fluka; CAS 9002-93-1

Ammonium hydroxide solution (26%); Sigma-Aldrich; CAS 1336-21-6

TEOS; puriss, 99% (GC); Fluka; CAS 70-10-4

APTMS; purum, ≥97.0% (NT); Fluka; CAS 13822-56-5

Sodium hydrosulfite (dithionate); BioChemika, ≥82% (RT); Sigma-Aldrich

6-FAM; BioChemika, for fluorescence, ≥85% (HPLC); Fluka

Copper(II)triflate; 98%; Sigma-Aldrich; CAS 34946-82-2

Hemoglobin human; lyophilized powder; Sigma-Aldrich; CAS 9008-02-0

Suforhodamine G; sye content 60%; Sigma-Aldrich; CAS 5873-16-5

NaOH; BioChemika, 1.0 M; Fluka; CAS 1310-73-2

HCl; BioChemika, ~0.1 M; Fluka ; CAS 7647-01-0

9 References

- 1 <http://www.bhikku.net/archives/03/img/diatoms>.
- 2 <http://www.artinsteel.co.uk/>.
- 3 <http://www.bgbm.org/bgbm/garden/bereiche/areas/hortsic.htm>.
- 4 <http://esp.cr.usgs.gov/info/lacs/diatom.htm>.
- 5 Round, F. E., Mann, D. G., and Crawford, R. M., *The diatoms biology & morphology of the genera*. (Cambridge Univ. Press, Cambridge [u.a.], 1996).
- 6 <http://botit.botany.wisc.edu/>.
- 7 Tréguer, P., Nelson, D. M., Bennekom, A. J. V. et al., *Science* **268** (5209), 375 (1995).
- 8 Falciatore, A. and Bowler, C., *Annu. Rev. Plant Biol.* **53** (1), 109 (2002).
- 9 Roberts, K., Granum, E., Leegood, R. C. et al., *Plant Physiology* **145** (1), 230 (2007).
- 10 Xu, M., Gratson, G. M., Duoss, E. B. et al., *Soft Matter* **2** (3), 205 (2006).
- 11 Parkinson, J. and Gordon, R., *Trends in Biotechnology* **17** (5), 190 (1999).
- 12 Morse, D. E., *Trends in Biotechnology* **17** (6), 230 (1999).
- 13 Losic, D., Mitchell, J. G., Lal, R. et al., *Adv. Func. Mater.* **17** (14), 2439 (2007).
- 14 Parkinson, J., Brechet, Y., and Gordon, R., *Biochimica et Biophysica Acta (BBA) - Molecular Cell Research* **1452** (1), 89 (1999).
- 15 Kröger, N., Lehmann, G., Rachel, R. et al., *European Journal of Biochemistry* **250** (1), 99 (1997).
- 16 Iler, R. K., *The Chemistry of Silica: Solubility, Polymerization, Colloid and Surface Properties, and Biochemistry*. (John Wiley & Sons, NewYork, 1979).
- 17 Bergna, H. E. and Roberts, W. O., *Colloidal Silica*. (CRC Press, Boca Raton, FL, 2006).
- 18 Brott, L. L., Naik, R. R., Pikas, D. J. et al., *Nature* **413** (6853), 291 (2001).
- 19 Shimizu, K., Del Amo, Y., Brzezinski, M. A. et al., *Chemistry & Biology* **8** (11), 1051 (2001).
- 20 Kröger, N., Deutzmann, R., and Sumper, M., *Science* **286** (5442), 1129 (1999).
- 21 Kroger, N., Deutzmann, R., and Sumper, M., *The Journal of Biological Chemistry* **276** (28), 26066 (2001).

- 22 Poulsen, N., Sumper, M., and Kröger, N., *Proceedings of the National Academy of Science* **100** (21), 12075 (2003).
- 23 Marnier, W. D., Shaikh, A. S., Muller, S. J. et al., *Biomacromolecules* **9** (1), 1 (2008).
- 24 Kent, M. S., Murton, J. K., Zendejas, F. J. et al., *Langmuir Article ASAP* (doi:10.1021/la801794e) (2008).
- 25 Hildebrand, M., Volcani, B. E., Gassmann, W. et al., *Nature* **385** (6618), 688 (1997).
- 26 Kröger, N., Bergsdorf, C., and Sumper, M., *EMBO Journal* **13** (19), 4676 (1994).
- 27 Moran, I. W., Briseno, A. L., Loser, S. et al., *Chemistry of Materials* **20** (14), 4595 (2008).
- 28 Lu, J., Yuan, D., Liu, J. et al., *Nano Letters* **8** (10), 3325 (2008).
- 29 Menon, R., Patel, A., Gil, D. et al., *Materials Today* **8** (2), 26 (2005).
- 30 Tseng, A. A., *Journal of Micromechanics and Microengineering* **14** (4), R15 (2004).
- 31 Zhang, L. B., Shi, J. X., Yuan, J. L. et al., *Materials Science Forum* **471 - 472**, 353 (2004).
- 32 Alexe, M. and Hesse, D., *Journal of Materials Science* **41** (1), 1 (2006).
- 33 Jeffryes, C., Gutu, T., Jiao, J. et al., *ACS Nano* **2** (10), 2103 (2008).
- 34 Srinivasan, S., Praveen, V. K., Philip, R. et al., *Angewandte Chemie International Edition* **47** (31), 5750 (2008).
- 35 Syms, R. R. A., Yeatman, E. M., Bright, V. M. et al., *Microelectromechanical Systems, Journal of* **12** (4), 387 (2003).
- 36 Sandhage, K. H., USA (2006).
- 37 Shian, S., Cai, Y., Weatherspoon, M. R. et al., *Journal of American Ceramic Society* **89** (2), 694 (2006).
- 38 Cai, Y., Allan, S. M., Sandhage, K. H. et al., *Journal of American Ceramic Society* **88** (7), 2005 (2005).
- 39 Unocic, R. R., Zalar, F. M., Sarosi, P. M. et al., *Chemical Communications* (7), 796 (2004).
- 40 Dudley, S., Kalem, T., and Akinc, M., *Journal of American Ceramic Society* **89** (8), 2434 (2006).

- 41 Weatherspoon, M. R., Allan, S. M., Hunt, E. et al., *Chemical Communications* (5), 651 (2005).
- 42 Jia, Y., Han, W., Xiong, G. et al., *Journal of Colloid and Interface Science* **323** (2), 326 (2008).
- 43 Zhao, J., Gaddis, C. S., Cai, Y. et al., *Journal of Material Research* **20** (2), 282 (2005).
- 44 Weatherspoon, M. R., Haluska, M. S., Cai, Y. et al., *Journal of The Electrochemical Society* **153** (2), H34 (2006).
- 45 Cai, Y., Dickerson, M. B., Haluska, M. S. et al., *Journal of American Ceramic Society* **90** (4), 1304 (2007).
- 46 Cai, Y. and Sandhage, K. H., *Physica Status Solidi A* **202** (10), R105 (2005).
- 47 Rosi, N. L., Thaxton, C. S., and Mirkin, C. A., *Angewandte Chemie International Edition* **43** (41), 5500 (2004).
- 48 Sandhage, K. H., Allan, S. M., Dickerson, M. B. et al., in *Handbook of Biomineralization*, edited by Peter Behrens and E. Bäuerlein (WILEY-VCH Verlag GmbH & Co. KGaA, Weinheim, 2007), pp. 235
- 49 Cai, X., Zhu, G., Zhang, W. et al., *European Journal of Inorganic Chemistry* (18), 3641 (2006).
- 50 Holmes, S. M., Graniel-Garcia, B. E., Foran, P. et al., *Chemical Communications* (25), 2662 (2006).
- 51 Losic, D., Mitchell, J. G., and Voelcker, N. H., *New Journal of Chemistry* **30** (6), 908 (2006).
- 52 Bao, Z., Weatherspoon, M. R., Shian, S. et al., *Nature* **446** (7132), 172 (2007).
- 53 Lettieri, S., Setaro, A., De Stefano, L. et al., *Advanced Functional Materials* **18** (8), 1257 (2008).
- 54 Wu, J., Yang, Y. S., and Lin, J., *Journal of Hazardous Materials* **127** (1-3), 196 (2005).
- 55 Xiong, W. and Peng, J., *Water Research* **42** (19), 4869 (2008).
- 56 Korunic, Z., *Journal of Stored Products Research* **34** (2-3), 87 (1998).
- 57 Burns, D. E., Baumann, E. R., and Oulman, C. S., *Journal of American Water Works Association* **62**, 121 (1970).
- 58 Wang, L. K., Wang, M. H., and Kao, J.-F., *Water, Air, & Soil Pollution* **9** (3), 337 (1978).

- 59 Kiwi-Minsker, L., Bulushev, D. A., and Renken, A., *Catalysis Today* **110** (3-4), 191 (2005).
- 60 Parker, A. R. and Townley, H. E., *Nature Nanotechnology* **2** (6), 347 (2007).
- 61 Baeumner, A., *Analytical and Bioanalytical Chemistry* **377** (3), 434 (2003).
- 62 Hildebrand, M., *Chemical Reviews* **108** (11), 4855 (2008).
- 63 Ahn, B. Y., Seok, S. I., Baek, I. C. et al., *Chemical Communications* (2), 189 (2006).
- 64 Behrens, P. and Menzel, H., in *Handbook of Biomineralization*, edited by Peter Behrens and E. Bäuerlein (WILEY-VCH Verlag GmbH & Co. KGaA, Weinheim, 2007).
- 65 Schmid, A., Tonnar, J., and Arms, S. P., *Advanced Materials* **20**, 3331 (2008).
- 66 Wu, C., Szymanski, C., and McNeill, J., *Langmuir* **22**, 2956 (2006).
- 67 Nann, T. and Mulvaney, P., *Angewandte Chemie International Edition* **43** (40), 5393 (2004).
- 68 Stöber, W. and Fink, A., *Journal of Colloid and Interface Science* **26**, 62 (1968).
- 69 Darbandi, M., Thomann, R., and Nann, T., *Chemistry of Materials* **17** (23), 5720 (2005).
- 70 Förster, S., in *Topics in Current Chemistry* (Springer, Heidelberg, 2003), Vol. 223, pp. 1.
- 71 Malinova, V., Kind, L., Grzelakowski, M. et al., in *Polymer-based nanostructures: Medical Applications*, edited by Pavel Proz (RCS, in press).
- 72 Förster, S. and Plantenberg, T., *Angewandte Chemie International Edition* **41** (5), 688 (2002).
- 73 Whitesides, G. M. and Grzybowski, B., *Science* **295**, 2418 (2002).
- 74 Hamley, I. W., in *Developments in Block Copolymer*, edited by Hamley I. W. (Wiley 2004).
- 75 M. Antonietti, S. F., *Advanced Materials* **15** (16), 1323 (2003).
- 76 Caruso, F., Caruso, R. A., and Möhwald, H., *Science* **282** (5391), 1111 (1998).
- 77 Liufu, S.-C., Xiao, H.-N., and Li, Y.-P., *Journal of Colloid and Interface Science* **285** (1), 33 (2005).
- 78 Fleming, M. S., Mandal, T. K., and Walt, D. R., *Chemistry of Materials* **13**, 2210 (2001).

- 79 Ghannam, L., Parvole, J., Laruelle, G. et al., *Polymer International* **55** (10), 1199 (2006).
- 80 Kraft, A., Arrighi, V., and Grima, N., *Polymeric Materials: Science & Engineering* **98**, 349 (2008).
- 81 Chang, J. H. and Kim, K. J., *Journal of Sol-Gel Science and Technology* **33** (1), 15 (2005).
- 82 Barrer, R. M. ed., *The Hydrothermal Chemistry of Zeolites*. (Academic Press, London, 1982).
- 83 Nakamura, M., Kumazawa, T., and Eriko, K., Japan (1987).
- 84 Kresge, C. T., Leonowicz, M. E., Roth, W. J. et al., *Nature* **359** (6397), 710 (1992).
- 85 Yuan, J.-J., Mykhaylyk, O. O., Ryan, A. J. et al., *Journal of American Chemical Society* **129** (6), 1717 (2007).
- 86 Percy, M. J., Barthet, C., Lobb, J. C. et al., *Langmuir* **16** (17), 6913 (2000).
- 87 Neofotistou, E. and Demadis, K. D., *Colloids and Surfaces A: Physicochem. Eng. Aspects* **242**, 213 (2004).
- 88 Knecht, M. R. and Wright, D. W., *Langmuir* **20** (11), 4728 (2004).
- 89 Knecht, M. R., Sewell, S. L., and Wright, D. W., *Langmuir* **21** (5), 2058 (2005).
- 90 Khanal, A., Inoue, Y., Yada, M. et al., *Journal of American Chemical Society Communication* **129**, 1534 (2007).
- 91 Plamper, F. A., Schmalz, A., Penott-Chang, E. et al., *Macromolecules* **40** (16), 5689 (2007).
- 92 Xiaoguang Qiao, M. C. J. Z. L. W., *Journal of Polymer Science Part A: Polymer Chemistry* **45** (6), 1028 (2007).
- 93 Chen, M., Zhou, S., You, B. et al., *Macromolecules* **38** (15), 6411 (2005).
- 94 Qian, Z., Zhang, Z., Song, L. et al., *Journal of Materials Chemistry* **19** (9), 1297 (2009).
- 95 Plamper, F., University Bayreuth, 2007.
- 96 Braunecker, W. A. and Matyjaszewski, K., *Progress in Polymer Science* **32** (1), 93 (2007).
- 97 Wang, J.-S. and Matyjaszewski, K., *Macromolecules* **28** (22), 7572 (1995).
- 98 Muthukrishnan, S., Plamper, F., Mori, H. et al., *Macromolecules* **38** (26), 10631 (2005).

- 99 Kircheis, R., Wightman, L., and Wagner, E., *Advanced Drug Delivery Reviews* **53** (3), 341 (2001).
- 100 Brissault, B., Kichler, A., Guis, C. et al., *Bioconjugate Chemistry* **14** (3), 581 (2003).
- 101 Park, I.-K., von Recum, H. A., Jiang, S. et al., *Langmuir* **22** (20), 8478 (2006).
- 102 Bai, Y., Koh, C. G., Boreman, M. et al., *Langmuir* **22** (22), 9458 (2006).
- 103 Ungaro, F., De Rosa, G., Miro, A. et al., *Journal of Pharmaceutical and Biomedical Analysis* **31** (1), 143 (2003).
- 104 Ochietti, B., Guerin, N., Vinogradov, S. V. et al., *Journal of Drug Targeting* **10** (2), 113 (2002).
- 105 Vinogradov, S. V., Bronich, T. K., and Kabanov, A. V., *Advanced Drug Delivery Reviews* **54** (1), 135 (2002).
- 106 Yowell, S. L. and Blackwell, S., *Cancer Treat. Rev.* **28 (Suppl. A)**, 3 (2002).
- 107 Lee, M. and Kim, S. W., *Pharmaceutical Research* **22** (1), 1 (2005).
- 108 Mehvar, R., *J. Pharm. Pharmaceut. Sci.* **3** (1), 125 (2000).
- 109 Sirsi, S. R., Schray, R. C., Guan, X. et al., *Human Gene Therapy* **19**, 795 (2008).
- 110 Shkilnyy, A., Friedrich, A., Tiersch, B. et al., *Langmuir* **24** (5), 2102 (2008).
- 111 Shkilnyy, A., Gräf, R., Hiebl, B. et al., *Macromolecular Bioscience* **9** (2), 179 (2009).
- 112 Huang, H., Tang, G., Wang, Q. et al., *Chemical Communications*, 2382 (2006).
- 113 Murcia, M. J. and Naumann, C. A., in *Nanotechnologies for the Life Sciences*, edited by Challa Kumar, S. S. R. (WILEY-VCH Verlag GmbH & Co. KGaA, Weinheim, 2005), pp. 1
- 114 Rossi, L. M., Shi, L., Quina, F. H. et al., *Langmuir* **21** (10), 4277 (2005).
- 115 Finnie, K. S., Bartlett, J. R., Barbe, C. J. A. et al., *Langmuir* **23** (6), 3017 (2007).
- 116 Thorek, D., Chen, A., Czupryna, J. et al., *Annals of Biomedical Engineering* **34** (1), 23 (2006).
- 117 López-Quintela, M. A., Tojo, C., Blanco, M. C. et al., *Current Opinion in Colloid & Interface Science* **9** (3-4), 264 (2004).

- 118 Prasad, P. N. ed., *Introduction to Biophotonics*. (John Wiley & Sons, Inc., New
Jersey, 2004).
- 119 Lichtman, J. W. and Conchello, J.-A., *Nature Methods* **2**, 910 (2005).
- 120 Ntziachristos, V., *Annual Review of Biomedical Engineering* **8** (1), 1 (2006).
- 121 Haugland, R. P. ed., *Handbook of Fluorescent Probes and Research
Products*, 9th ed. (Molecular Probes Inc., Eugene, Oregon, 2002).
- 122 Bagwe, R. P., Zhao, X., and Tan, W., *Journal of dispersion science and
technology* **24**, 355 (2003).
- 123 Avnir, D., Coradin, T., Lev, O. et al., *Journal of Material Chemistry* **16** (11),
1013 (2006).
- 124 Zhuravlev, L. T., *Colloids and Surfaces A: Physicochemical and Engineering
Aspects* **74** (1), 71 (1993).
- 125 Yoshitake, H., Yokoi, T., and Tatsumi, T., *Chemistry of Materials* **14** (11),
4603 (2002).
- 126 Yokoi, T., Yoshitake, H., and Tatsumi, T., *Journal of Materials Chemistry* **14**
(6), 951 (2004).
- 127 Cao, W., Zhang, H., and Yuan, Y., *Catalysis Letters* **91** (3), 243 (2003).
- 128 Bitterwolf, T. E., David Newell, J., Carver, C. T. et al., *Inorganica Chimica Acta*
357 (10), 3001 (2004).
- 129 Pérez, C., Pérez, S., Fuentes, G. A. et al., *Journal of Molecular Catalysis A:
Chemical* **197** (1-2), 275 (2003).
- 130 Alcón, M. J., Corma, A., Iglesias, M. et al., *Journal of Molecular Catalysis A:
Chemical* **194** (1-2), 137 (2003).
- 131 Macquarrie, D. J., Jackson, D. B., Tailland, S. et al., *Journal of Material
Chemistry* **11** (7), 1843 (2001).
- 132 Kubota, Y., Nishizaki, Y., Ikeya, H. et al., *Microporous and Mesoporous
Materials* **70** (1-3), 135 (2004).
- 133 Corrie, S. R., Lawrie, G. A., and Trau, M., *Langmuir* **22** (6), 2731 (2006).
- 134 Sadasivan, S., Khushalani, D., and Mann, S., *Journal of Materials Chemistry*
13, 1023 (2003).
- 135 Plamper, F. A., Walther, A., Muller, A. H. E. et al., *Nano Letters* **7** (1), 167
(2007).

- 136 Schiffelers, R. M. and Storm, G., *Expert Opinion in Drug Delivery* **3** (3), 445
(2006).
- 137 Casse, O., PhD Thesis; University of Basel, in progress.
- 138 Kang, S. M., Lee, K.-B., Kim, D. J. et al., *Nanotechnology* **17**, 4719 (2006).
- 139 Pham, K. N., Fullston, D., and Sagoe-Crentsil, K., *Journal of Colloid and
Interface Science* **315**, 123 (2007).
- 140 Kohlrausch, R., *Pogg. Ann.* **12** (353) (1847).
- 141 Williams, G. and Watts, D. C., *Trans. Faraday Soc.* **66**, 80 (1970).
- 142 Tamura, O., Mitsuya, T., and Ishibashi, H., *Chemical Communications* (10),
1128 (2002).
- 143 Cox, C., Ferraris, D., Murthy, N. N. et al., *Journal of American Ceramic
Society* **118**, 5332 (1996).
- 144 <http://porpax.bio.miami.edu/~cmallery/150/chemistry/hemoglobin.jpg>.
- 145 Gros, G., Rollema, H. S., Jelkmann, W. et al., *J. Gen. Physiol.* **72**, 765 (1978).
- 146 <http://probes.invitrogen.com/media/pis/mp00143.pdf>, I. M. P., Amine-Reactive
Probes.
- 147 Lan, E. H., Dave, B. C., Fukyto, J. M. et al., *J. Mater. Chem.* **9**, 45 (1999).
- 148 Menzel, H., Horstmann, S., Behrens, P. et al., *Chem. Commun.* (24), 2994
(2003).
- 149 Hunter, R. J. ed., *Zeta Potential in Colloid Science*. (Academic Press, New
York, 1981).
- 150 Kremer, J. R., Mastronarde, D. N., and McIntosh, J. R., *J. Struc. Biol.* **116**, 71
(1996).
- 151 Weyland, M., *Topics in Catalysis* **21** (4), 175 (2002).
- 152 Rasband, W. S., Available at <http://rsb.info.nih.gov/ij/>, (1997 - 2004).
- 153 Messaoudil, C., Boudier, T., Sorzano, C. O. S. et al., *BMC Bioinformatics* **8**,
288 (2007).
- 154 2, S. v., Available at www.slicer.org.

10 Curriculum vitae

Personal Details

Name	Lucy Kind
Date and place of birth	03.07.1974, Duisburg, Germany
Nationality	german

Education

- 2005 - 2009 **Ph.D. in Physical Chemistry, University of Basel, Switzerland**
- *Project:* Template directed synthesis of highly organized functional biomimetic silica nanostructures
 - *Supervisor:* Prof. Dr. Wolfgang Meier (University of Basel, Basel, Switzerland)
Prof. Dr. Uwe Pieleles (University of Life Sciences, MuttENZ, Switzerland)
Prof. Dr. Andreas Taubert (University of Potsdam, Golm, Germany)
- 2004 - 2005 **Master of Science in Chemistry, University of Basel, Switzerland**
- *Project:* ABA Triblock Copolymer Vesicles with integrated Na⁺/K⁺ ATPase
 - *Supervisor:* Prof. Dr. Wolfgang Meier (University of Basel, Basel, Switzerland)
- 2003 - 2004 **Diploma in Chemistry, Swiss Tropical Institute, Basel, Switzerland**
- *Project:* Application and Evaluation of a Micro Array Based SNP Analysis System for Drug Resistance Markers of Malaria
 - *Supervisor:* Prof. Dr. Hans-Peter (STI, Department of Molecular Parasitology – Epidemiology, Basel, Switzerland)

Prof. Dr. Uwe Pieles (University of Applied Sciences, Muttenz, Switzerland)

1999 - 2004 **Student in Chemistry, University of Applied Sciences, Department of Chemistry and Biotechnology, Muttenz, Switzerland**

- Diploma in Chemistry, FH

1997 - 1999 **Part-time postgraduate program in Chemistry, evening school for technician, Gewerblich-Technische Unterrichtsanstalt, Mülheim an der Ruhr, Germany**

1993 - 1997 **Apprenticeship, Chemical Labassistant, Max-Planck Institute für Kohleforschung, Mülheim an der Ruhr, Germany**

- Chemical Labassistant

Research and Practical Experience

2005 - 2009 **Assistant, University of Basel, Switzerland**

- Practical training for students in organic chemistry

2004 **Scientific Assistant, University of Applied Sciences, Muttenz, Switzerland (6 months)**

- Nanotechnology, Microarrays

2000 - 2004 **Data Entry for medical studies, Analytica (IMOR), Lörrach, Germany**

Sep. 2002 **Practical training, Syngenta, Bracknell Berkshire, Great Britain**

(1 month)

- Biokinetics

Sep. 2000 **Practical training, Polyphor Allschwil, Switzerland (3 weeks)**

- Organic fundamental chemistry

1997 - 1999 **Biological Technical Assistant, Academic Medical Center, Essen, Germany**

- Department of cell biology (cancer research)

- 1997 **Chemical Labassistant, Max-Planck Institute für Kohleforschung, Mülheim an der Ruhr, Germany (6 months)**
- Polymer chemistry

Technical Skills

<i>Cell Biology:</i>	Cell culturing; Confocal laser microscopy
<i>Immunology:</i>	ELISA; Microarray (gene analytically)
<i>Molecular Biology:</i>	DNA extraction and analysis (restriction digestion, sequencing, PCR)
<i>Analytic:</i>	GC; CE; HPLC; Light Scattering (dynamic, static)
<i>Imaging:</i>	TEM; SEM; AFM;
<i>Molecular modeling:</i>	molecular dynamics simulations, Quasar
<i>Medical studies:</i>	Data base system SAS

Collaboration Projects

- Prof. A. Taubert, Institut for Supramolecular Chemistry, University of Potsdam, Germany
- Dr. Thomas Graule, KTI Project: Nanolacquer, EMPA, Dübendorf, Switzerland
- Dr. Rainer Kneuer, Novartis Institutes for Biomedical Research
Discovery Technologies / Analytical and Imaging Sciences, Basel, Switzerland
- Prof. A. Müller, Makromolekular Chemistry, University of Bayreuth, Germany
- Prof.U.Pieles, University of Life Science, Department of Chemistry and Bioanalytic,
Muttenz, Switzerland

Municipal Engagement

Project leader: "Rearrangement of Klybeckstrasse" in Kleinbasel,
Projectcoordination: Integrale Aufwertung Kleinbasel (IAK); (2002-2006)

Member of the organisation committee for the „Kulturfest – Begegnung in der Klybeckstrasse“

Department: Communication and Advertisement; (2003/2004)

Poster and Conferences

- **PILS Meeting, Basel, Switzerland, Sep. 2008**
Poster: “Stimuli responsive core-shell silica nanoparticles”
Lucy Kind, Per Rigler, Andreas Taubert, Uwe Pieleles, Axel Müller, Wolfgang Meier,
- **Biezenmortel, Netherlands, Sep. /Oct. 2007**
Polyamphi Summer School, Polyelectrolytes in solutions and at interfaces: synthesis, theory, applications
- **SCS Fall meeting, Lausanne, France, September 2007**
Poster: “Responsive core-shell silica nanoparticles”
Lucy Kind, Axel Müller, Andreas Taubert, Uwe Pieleles, Wolfgang Meier
- **Biosurf IIV, Zürich, Switzerland, Aug. 2007**
Poster: “Stimuli responsive core-shell silica nanoparticles”
Lucy Kind, Per Rigler, Andreas Taubert, Uwe Pieleles, Axel Müller, Wolfgang Meier
- **Club Emulsion, Strassburg, France, Sep. 2006**
Poster: “Tunable Delivery Systems Based on Hollow Silica Nanoparticles”
Lucy Kind, Sayed Mohammady, Andreas Taubert, Amina Wirth, Uwe Pieleles, Wolfgang Meier
- **PILS Meeting, Murten, Switzerland, Apr. 2006**
Poster: “Amphiphilic Triblock Copolymer Vesicles with integrated Na⁺/K⁺ ATPase”
Lucy Kind, Caroline Fraysse, Wolfgang Meier,

Publications

in progress

Silica nanoshells by templating with degradable poly(ethylene oxide)-block-poly(valerolactone) diblock copolymer micelles

Kind, Lucy; Senti, Alexander; Meier, Wolfgang; Taubert, Andreas

in progress

Poly(ethylene oxide)/poly(ethylene imine) di- and triblock copolymers as templated and catalysts for the formation of highly monodisperse silica nanoparticles

Kind, Lucy; Shkilnyy, Andriy; Meier, Wolfgang; Taubert, Andreas

Submitted to Langmuir

A one-pot approach to functional polyelectrolyte-based core-shell silica nanoparticles

Kind, Lucy; Plamper, Felix; Manton, Alexandre; Weber, Jens; Göbel, Ronald; Müller, Axel H. E.; Taubert, Andreas; Pieles, Uwe; Meier, Wolfgang

New Journal of Chemistry, 32(4), 588-593 (2008).

Controlling silica nanoparticle properties for biomedical applications through surface modification.

Legrand, Sebastien; Catheline, Amelie; **Kind, Lucy**; Constable, Edwin C.; Housecroft, Catherine E.; Landmann, Lukas; Banse, Petra; Pieles, Uwe; Wirth-Heller, Amina

Biological Chemistry, 383(11), 1691-1700 (2002).

Evidence for haploinsufficiency of the human HNF1 α gene revealed by functional characterization of MODY3-associated mutations.

Thomas, Heike; Badenberg, Britta; Bulman, Michael; Lemm, Ira; Lausen, Jorn; **Kind, Lucy**; Roosen, Simone; Ellard, Sian; Hattersley, Andrew T.; Ryffel, Gerhart U.

Book chapter, in press

Polymer-based nanostructures. Medical Applications; Royal Society of Chemistry

Strategies for triggered release from polymer-based nanostructures

Violeta Malinova, **Lucy Kind**, Mariusz Grzelakowski, Wolfgang Meier;

References

Prof. Dr. Wolfgang P. Meier
University of Basel
Institute of Physical Chemistry
Basel, Switzerland
Tel.: +41 (0)61 2673802
wolfgang.meier@unibas.ch

Prof. Dr. A. Taubert
University of Potsdam
Department: Supramolecular Chemistry
Golm, Germany
Tel.: +49 (0)331 977 5773
ataubert@uni-potsdam.de

Prof. Dr. U. Pieleles
University of Life Science
Department: Nanotechnology
MuttENZ, Switzerland
Tel.: +41 (0)61 4674453
uwe.pieleles@fhnw.ch

Prof. Dr. rer. nat. H.-P. Beck
Swiss Tropical Institute
Basel, Switzerland
Tel.: +41 (0)61 2848116
Hans-Peter.Beck@unibas.ch